Design Synthesis Exercise Autumn 2012 Group 10

Final Report - SCALAIR
Scalable Aircraft Model

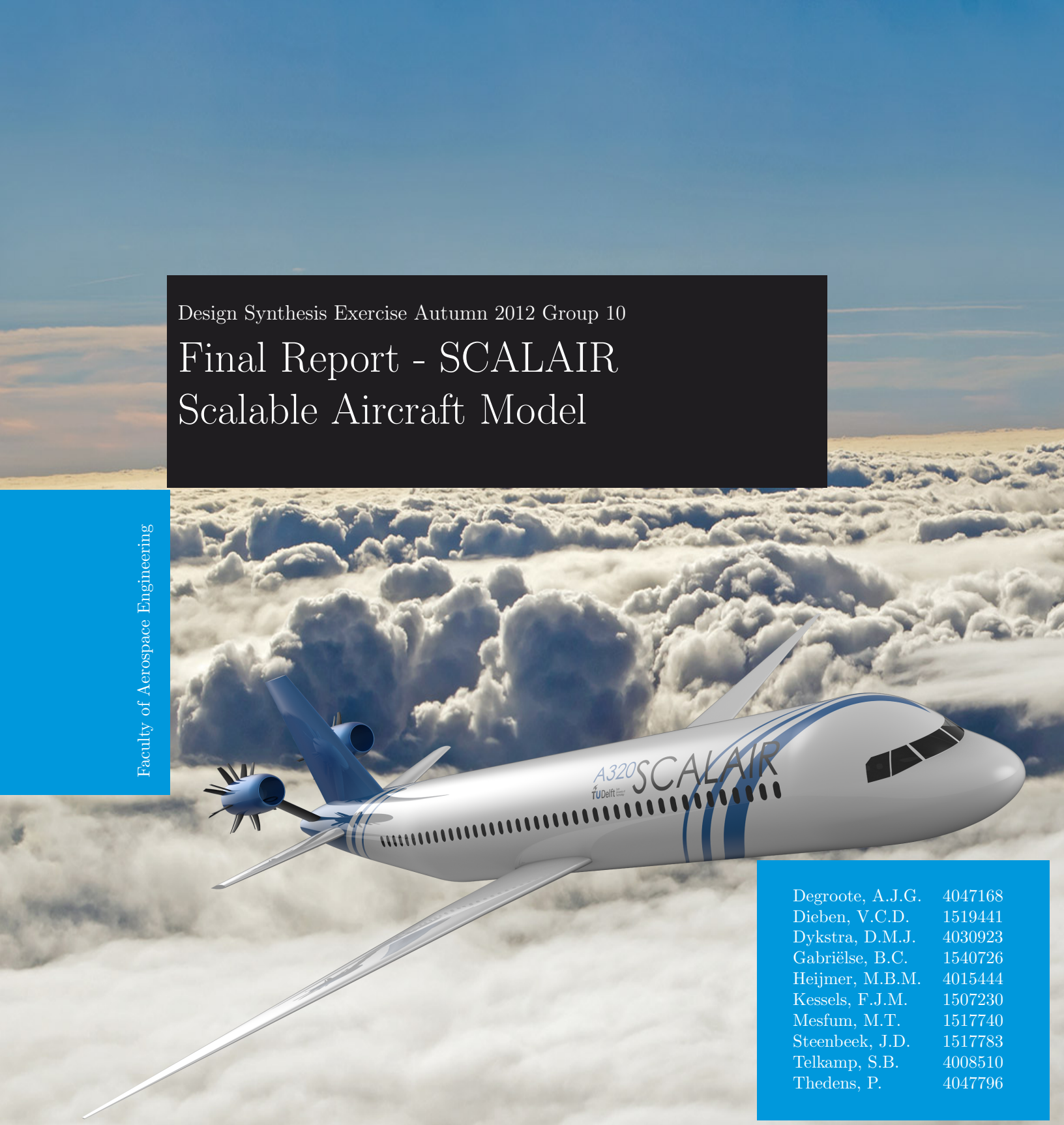

Faculty of Aerospace Engineering

Degroote, A.J.G.	4047168
Dieben, V.C.D.	1519441
Dykstra, D.M.J.	4030923
Gabriëlse, B.C.	1540726
Heijmer, M.B.M.	4015444
Kessels, F.J.M.	1507230
Mesfum, M.T.	1517740
Steenbeek, J.D.	1517783
Telkamp, S.B.	4008510
Thedens, P.	4047796

TU Delft Delft University of Technology

Challenge the future

Revisions

Version	Date	Performed by	Chapters affected	Brief description of change
1.0.0	22-01-2013	All	All	Basic report set up
1.0.1	23-01-2013	Stefan	Aerodynamics	Textual changes, repairing references
1.0.2	24-01-2013	Arne	Performance	Table, Figure and Text repairing
1.0.3	24-01-2013	Arne	Engine Characteristics	Text and Equation repairing
1.0.4	24-01-2013	Arne	Final Design	Stall Propagation added
1.0.5	24-01-2013	David	Performance	Table changed
1.0.6	24-01-2013	Arne	Model	Chapter added
1.0.7	25-01-2013	Paul	Final Design	Spelling, grammar, and content improvements. Figure added
1.0.8	25-01-2013	Stefan	Abbreviations	List updated
1.0.9	25-01-2013	Stefan	Sustainable development strategy	Textual changes
1.1.0	25-01-2013	Stefan	Introduction	Requirements added
1.1.1	26-01-2013	Arne, Benjamin	All	Layout repairing and squeezing
1.1.2	27-01-2013	Benjamin	All	Wrapping text around figures
2.0.0	28-01-2013	All	All	Draft Report
2.0.1	28-01-2013	Fleur	Market Analysis & Summary	Updated with feedback.
2.0.2	29-01-2013	Arne	Sustainable, Performance and Engine characteristics	Updated with feedback.
2.0.3	29-01-2013	Michal	Technical Risk Assessment	Feedback implemented
2.0.4	29-01-2013	Johannes	Final Design	Feedback implemented
2.0.5	29-01-2013	David	Structural Design	Structural Design chapter rewritten
2.0.6	29-01-2013	Johannes	Structural Design	Feedback implemented
2.0.7	29-01-2013	Paul/Fleur	Stability & Control	Updated with feedback and discussion.
2.0.8	29-01-2013	Michal	Final Design; Aerodynamics	controllabillity and stall calculations; taper limitation
2.0.9	29-01-2013	Johannes	Structural Design Appendix	Own feedback
2.1.0	29-01-2013	Fleur	Summary, Conclusion & Recommendations	Updated for new design and grammar
2.1.1	29-01-2013	All	All	All feedback inserted
3.0.0	29-01-2013	Benjamin	All	Wrap up to Final Report

Preface

This report is part of the Design Synthesis Exercise (DSE), which is part of the Aerospace Engineering bachelor's curriculum of the Delft University of Technology. To complete the DSE this group was assigned to develop a scalable aircraft model and utilize this to redesign an existing aircraft into an efficient medium size transport aircraft with larger aspect ratio wings and propeller propulsion.

We would like to express our gratitude to our tutors Dr. ir. L.L.M. Veldhuis, Dr. ir. B.W. van Oudheusden, Prof. dr. A. Rothwell and Ir. J.A. Melkert for their guidance and help during the project. Furthermore, we would like to show our appreciation to Dr. ir. E. Mooij and Dr. ir. M. Snellen for supervising the DSE. Finally, we would like to thank the Delft University of Technology that provided us with the facilities and data needed for our research.

DSE-Group 10, autumn 2012:

Arne J.G. Degroote
Victor C.D. Dieben
David M.J. Dykstra
Benjamin C. Gabriëlse
Michaël B.M. Heijmer
Fleur J.M. Kessels
Medhany T. Mesfum
Jorden D. Steenbeek
Stefan B. Telkamp
Paul Thedens

Summary

Ever more stringent environmental regulations on e.g. NO_X emissions and the constantly increasing fuel prices strongly drive the demand for more efficient green-technology aircraft. This leads not only to changes in market demand but also to changes with respect to the choices made for designing next generation aircraft. More importantly, it leads to changes in the need for more efficient and innovative aircraft design processes. As a large degree of resemblance is to be found when comparing the geometrical lay-outs of conventional transport aircraft, it is definitely tempting to make use of existing knowledge to arrive at a new design.

The mission of the SCALAIR project is to develop a more time and cost efficient aircraft design method for medium-size, medium-range passenger aircraft with lower Direct Operating Costs (DOC) through lower fuel consumption. This method can then be utilised to redesign an existing medium-size transport aircraft into a more efficient aircraft with large aspect ratio wings and propeller propulsion. Fundamental to the new design method and the resulting computational model is the scaling of an existing aircraft, while keeping an equivalent topology to maximise the use of existing knowledge and experience. The scaling is based on scaling laws that are derived from analytical relations, trends and empirical data.

From the market analysis it follows that the forecast for the air traffic market - and in particular the demand for narrow-body aircraft - is promising. The emerging economies are found to be the main drivers of economic growth and demand in air traffic (4.7-5.0 % growth rate), and single-aisle aircraft amount to 68-70 % of the total passenger aircraft market. Furthermore, the demand for turboprops is expected to increase as well over the next few years since their (by definition) higher efficiency becomes more and more relevant.

The use of next generation propulsion technology, such as open rotor propulsion is still a concept under development. From a sustainable point of view these engines are expected to be very beneficial, given the higher propulsive efficiency and the fact that the resulting increase in fuel efficiency can be linked to a reduction in pollutant emissions. So, when focusing on environmental regulations Contra-Rotating Open Rotor (CROR) engines are a good choice.

Regarding the model, the use of a scaling approach based on existing knowledge has multiple advantages in reducing the ecological footprint of aviation, since it reduces the time and cost required for the design- and manufacturing phase. Allowing for e.g. quickly replacing the ageing fleet with more fuel efficient aircraft.

In the developed computational model the wing structure is modelled analytically based on the aerodynamic analysis. The aerodynamic wing loading and performance characteristics are acquired by means of a Vortex Lattice Method (VLM). Here the spanwise loading is of particular interest because of its interdependency with the structural analysis. By iterating certain geometric wing parameters, trends are obtained which describe the effect on the lift to drag ratio. For the structural module scaling laws are found and implemented based on the analytical model. From the combination of the two analyses, scaling laws are obtained which indicate what the optimum combinations - i.e. to minimize DOC - of the geometric parameters are. Note that fuselage dimensions remain constant and that the external structure is scaled based on changing load distributions.

For the performance analysis loading diagrams and CS25 regulations have been used to determine the load factors driving the design configuration. Furthermore, fuel estimations were made to be able to evaluate the fuel efficiency of the new design with respect to the A320. The scaling laws that

were derived for the fuel were always within a 0.32 % margin of the A320 data. It is to be noted, however, that the module should only be used for the engine design speeds. The engine used for the new design is the General Electric UDF. Mainly due to this change in engine from turbofan to open rotor the flight speed has been decreased from 0.78 Mach for the A320 to 0.72 Mach for the new design. In the model the engine mass is scalable with respect to the thrust, to account for changes in the maximum take-off mass.

Subsequently, the stability and control characteristics are addressed by means of the longitudinal X-plot for the horizontal tail sizing and 'fast vertical tail sizing for directional stability of fuselage-mounted engines aircraft' approach for the vertical tail sizing. These methods do not take into consideration the interaction of the fuselage-mounted engine with the tail surfaces, which changes the tail size considerably. With the aforementioned methods scaling laws were obtained regarding tail size and wing position to optimise for stability and controllability.

The Direct Operating Costs per block hour are calculated both for the A320 and the newly designed aircraft. Direct Operating Costs are defined as the costs which have to be made to operate the aircraft, and are dependent on the type of aircraft. For this, the method presented by Liebeck [1] is used. It was determined that the DOC is reduced significantly, where this change is mainly the result of a decrease in fuel consumption. The fraction of the fuel costs are reduced from 27 % to 18 % of the DOC. Also, the economic effects of a lower flight speed are considered. These effects are not incorporated in the DOC, and are therefore determined separately.

A complete model containing the previous technical analyses has been created which allows the range, sweep, taper, aspect ratio and the engine type and location (two options) to be varied within certain ranges, restricted by the design space. The program is split up into the following modules: wing, fuselage, tail, engine/performance, fuel/weights and a calling routine for Athena Vortex Lattice (AVL). Scaling laws describing the effects of range, sweep, Mach and the new engine were obtained by using this complete model. For the range it was found that the new engine is considerably more efficient than the A320 at larger ranges. A sensitivity analysis has shown that there is a snowball effect in the model where an increase in the input of the initial mass results in a chain reaction in the structural mass.

The following categories are taken into account with respect to risk awareness and risk handling: general design process risks, scaling law risks, computer program risks, verification and validation risks, feasibility of the computer program, feasibility of a typical scaled aircraft from the SCALAIR project and approval of a typical scaled aircraft from the SCALAIR project. The severity and likelihood of the risks were qualitatively estimated.

Utilising the new design method, the redesigned, scaled A320 with fuselage-mounted GE36 Unducted Fan engines features a low taper ratio of 0.25, an aspect ratio of 11.4 and a sweep angle of 17 degrees. Performance-wise the lift to drag ratio is increased by 12.2 % and there is a 15.2 % decline in maximum take off mass. Also, the operational empty mass is reduced by 11.0 %. The design complies with the same payload and range requirements as those for the A320, but with a 35.8 % reduction in fuel consumption and thus reduced DOC. The DOC is reduced by 8 %, from $ 7485 to $ 6890 per block hour. Also noteworthy is that there is 38.1 % less CO_2 emissions per year for the new design, when compared with the original A320.

Contents

Nomenclature

Symbols

b	*Wing span*	[m]
c	*Chord length*	[m]
e	*Oswald factor*	[-]
h	*Hours*	[-]
l	*Length or Moment arm*	[m]
m	*Mass*	[Kg]
n	*Loading factor*	[-]
p	*Pressure*	[Pa]
AR	*Wing aspect ratio*	[-]
C_D	*Drag coefficient*	[-]
C_{D_I}	*Induced drag coefficient*	[-]
C_{D_0}	*Parasite drag coefficient*	[-]
C_L	*Lift coefficient*	[-]
C_{n_β}	*Stability derivative, Z-axis*	[-]
C_{m_α}	*Stability derivative, Y-axis*	[-]
D	*Drag*	[N]
K	*Load allevation factor*	[-]
L	*Lift*	[N]
M	*Mach number*	[-]
M_{eff}	*Effective Mach number*	[-]
M_∞	*Free stream Mach number*	[-]
P	*Power*	[kW]
S	*Wing surface area*	[m^2]
S_h	*Horizontal tail surface area*	[m^2]
T	*Thrust*	[N]
V	*Aircraft velocity*	[m/s]
Λ	*Sweep angle*	[°]
ρ	*Air density*	[kg/m^3]
λ	*Taper ratio*	[-]
η	*Efficiency*	[-]

Abbreviations

AOA	*Angle of Attack*
AR	*Aspect Ratio*
AHP	*Analytical Hierarchy Process*

APU	*Auxilary Power Unit*
ASK	*Available Seat Kilometer*
ASM	*Aerospace Materials department*
ATC	*Air Traffic Control*
AVL	*Athena Vortex Lattice*
CBS	*Cost Breakdown Structure*
CFD	*Computational Fluid Dynamics*
CG	*Center of Gravity*
COMFD	*Communication Flow Diagram*
CROR	*Counter Rotating Open Rotor*
DLR	*Deutsches Centrum fr Luft- und Raumfahrt*
DOC	*Direct Operating Cost*
DSE	*Design Synthesis Exercise*
EASA	*European Aviation Safety Agency*
EPNdB	*Effective Perceived Noise in dB*
FAA	*Federal Aviation Administration*
FFD	*Functional Flow Diagram*
FR	*Final Report*
GUI	*Graphical User Interface*
GWP	*Global Warming Potential*
ICAO	*International Civil Aviation Organization*
IEA	*International Energy Agency*
IOC	*Indirect Operating Cost*
IPCC	*Intergovernmental Panel on Climate Change*
LEMAC	*Leading Edge Mean Aerodynamic Chord*
LTO	*Landing-Takeoff*
MAC	*Mean Aerodynamic Chord*
MEM	*Manufacturer Empty Mass*
MTOM	*Maximum Take-off Mass*
MTOW	*Maximum Take-off Weight*
MTR	*Midterm Report*
NLR	*Nationaal Lucht- en Ruimtevaartlaboratorium*
NEO	*New Engine Option*
OEM	*Operating Empty Mass*
OEW	*Operating Empty Weight*
RF	*Radiative Forcing*
RFI	*Radiative Forcing Index*
RPK	*Revenue Passenger Kilometer*
SWOT	*Strengths, Weaknesses, Opportunities and Threats*
SFC	*Specific Fuel Consumption*
SNASA	*Secret National Aeronautics and Spce Administration*
TSFC	*Thrust Specific Fuel Consumption*
UDF	*Unducted Fan*
UHB	*Ultra High Bypass*
VLM	*Vortex Lattice Method*
VMS	*Von Misses Stress*
WBS	*Work Breakdown Structure*
WFD	*Work Flow Diagram*

VMS	*Von Mises Stress*
VMS_{fail}	*Allowable Von Mises Stress*
W	*Weight*
WHO	*World Health Organisation*

Chapter 1

Introduction

With the increase of current fuel prices the demand for more fuel efficient aircraft is on the rise. While traditional turbofan engines are reaching their limit on fuel efficiency, the industry is trying to improve using different technologies. The usage of propeller aircraft which provide a lower fuel consumption has declined in the past decades due to their relatively low flight speed and noise pollution. A possible alternative is the Unducted Fan which combines a low fuel consumption with higher cruise speeds than conventional turboprops and the potential of reducing its noise level. A cheap method to further improve already existing aircraft is a scalable computational model which makes the whole cumbersome conceptual design phase obsolete. Combining the use of an efficient engine with a scalable aircraft computer model, provides a cheap and simple method to improve aircraft, such as the A320.

The mission of the SCALAIR project is to develop a more time and cost efficient aircraft design method for medium-size, medium-range passenger aircraft. The second goal is to use this method to redesign an existing medium-size, medium range transport aircraft into a more efficient aircraft with lower direct operating cost through lower fuel consumption.

The purpose of the final report is to state the results of the whole project, obtained during the last nine weeks. The results consist of scaling laws, optimal design parameters for the most efficient aircraft model and further recommendations on how to improve the model in the future.

Requirements for the project consists of the design of a mathematical description of an aircraft and the evaluation of scaling laws for all relevant aspects of it. The scaling laws should be validated and used to redesign a medium-size aircraft based on the Airbus A320. The new aircraft should have large aspect ratio wings, propeller propulsion and lower direct operating costs through a reduction in fuel consumption of at least 30% [2].

The scaling laws will be derived from empirical data, analytical approaches and simulations which determine trend lines incorporated in the program. The attained scaling laws will be used to redesign and optimise a new aircraft within certain constraints. It will be optimised for fuel consumption in order to achieve the required reduction in fuel consumption and direct operating Cost.

With the attained scaling laws the designed aircraft is optimised within its constraints to achieve the reduced direct operating Cost.

Basic limitations occurring in the project are constraints given by time, experience and miscommunication induced by risks within the project. These limitations require assumptions and simplifications of the model and methods used, and a structured project execution.

The report consists of fourteen chapters, which can be split over three parts. The first part is about project management and includes Chapter 2 and Chapter 3.

The second part of the report consists of the simulation. This part describes the core of the project. It discusses how the model is created and how it used to create a final design. The technical categories, consisting of the aerodynamics, structural design, performance, engine characteristics and stability and control are considered in Chapters 4 to 8 respectively. After that, the model characteristics are discussed in Chapter 9, including the sensitivity analysis. The risk management

can be found in Chapter 10 followed by the aspects dealing with the final design in Chapter 11 and the Direct Operating Costs in Chapter 12.

The third part of the report discusses the post-DSE phase. This part consists of the post-DSE planning presented in Chapter 13. The cost break-down is discussed in the same chapter. Finally, the report ends with Chapter 14 which includes the conclusions and recommendations.

Chapter 2

Market Analysis

The current chapter describes the market analysis for the developed product. The aim of the project is to design a software model that scales a medium-sized aircraft type based on the A320 as a reference aircraft. Ultimately, this model should be sold to a manufacturer. Therefore, it is very advisable to find a market area where a demand for the product exists.

The market analysis is structured as follows. First, the trends of air traffic, aircraft demand and aircraft design processes are analysed in order to locate and narrow down the area of interest, and to estimate possible demands and market shares. Next, the macro environment and the stakeholders are identified and described. Finally, the Strengths, Weaknesses, Opportunities and Threats (SWOT) analysis is done in order to provide a good overview of the company's internal and external environment. In this case the company is the team developing the model.

2.1 General and emerging trends in air traffic and aircraft demand

Over the past few decades the demand for air traffic, and thus also for aircraft, has increased considerably. From Airbus' Global Market Forecast [3] and Boeing's Current Market Outlook [4] it follows that not only did the total air traffic demand these last twelve years increased with a stunning 53 %, it also turns out to be resilient to external economic shocks (e.g. major crises) [5, 4]. Figure 2.1 shows that over the course of these crises no significant decline in demand was to be noted. On the contrary, the demand for air traffic has consistently been on the way up.

In their forecast, Airbus foresees a worldwide growth in air traffic demand of approximately 4.7 %, mainly driven by the expanding regions (i.e. the emerging economies: Brazil, Russia, India and China) [3]. Embraer also notes in the 2012 Market Outlook that the strong pace of growth in the emerging markets is one of the main drivers impacting the global air travel industry and they conclude on a growth of 5.0 % in the Revenue Passenger Kilometer (RPK) [6]. The latter is in accordance with Boeing's 5.0 % expected increase in airline traffic [4].

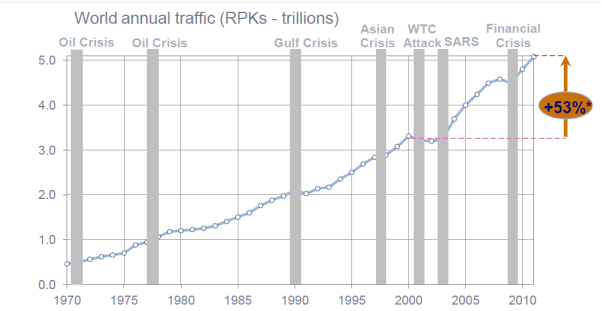

Figure 2.1: Word annual traffic, * 53% increase from 2000-2012 [5]

The consensus is thus that the emphasis is on the emerging economies and that growth levels between 4.7 and 5.0 % are to be expected. The increasing contribution of these expanding regions can also be deducted from the economic growth depicted in Figure 2.2.

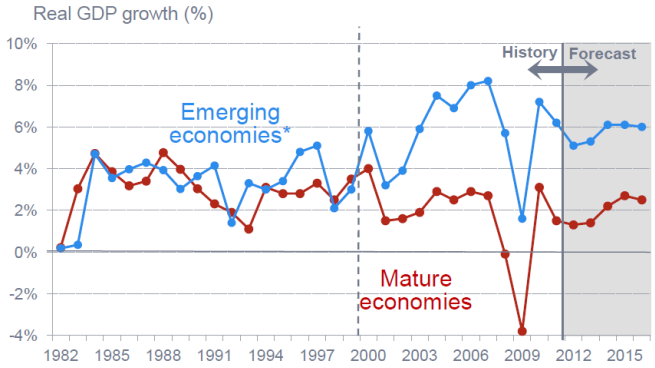

Figure 2.2: Real growth in Gross Domestic Product [5]

Extrapolating the growth in air traffic demand to the resulting need for aircraft, Airbus concludes that in the coming 20 years over 27,000 passenger aircraft will be needed to provide for the market's needs. Including freight aircraft this even results in a staggering 28,200 aircraft, or in other words, a total value of 3.14 trillion Euro is at stake [3]. According to Embraer, the total market value might even amount to 3.6 trillion euros [6]. Here it is to be taken into account that the largest contribution to the growth will come from the emerging economies.

2.1.1 Narrow-body aircraft demand

The aircraft market is typically segmented into narrow- and wide-body types of aircraft (e.g. A320 vs. A380) where narrow-body or single aisle aircraft take over two thirds of the sold types according to Boeing [7], resulting in a high demand. Given that the currently developed methodology is to be applied to narrow-body, medium-haul types of aircraft, this market analysis focuses on the narrow-body niche. Currently, the major players in this particular field are [8, 4]:

- Airbus with the A320 Family
- AVIC with the ARJ-900
- Boeing with the 737 Family
- Bombardier with the CSeries/CRJ-1000
- Embraer with the 190/195
- Tupolev with the Tu-204/Tu-214

And the following aircraft are due to enter the market within the next five years [8, 4]:

- Comac with the C919 (planned for 2014)
- Irkut with the MC-21 (planned for 2016)

Noteworthy is that, competition-wise, the narrow-body market appears to be deviating from the well-known Boeing-Airbus duopoly, with a partnership between Bombardier and COMAC posing the biggest threat to their usually so confident market leadership. As indicated by Glennon Harrison in his report for the Congressial Research Service: *the importance of narrow-body aircraft to both companies cannot be overstated* [9]. Hence, their dedication to this particular market segment is such that they intend to saturate the market's demand. However, given their current choices it might be that they are not be able to provide for the forecasted increase in demand [9]. Thereby paving the way for new entrants to the market, and thus a more competitive and innovative environment [10, 11].

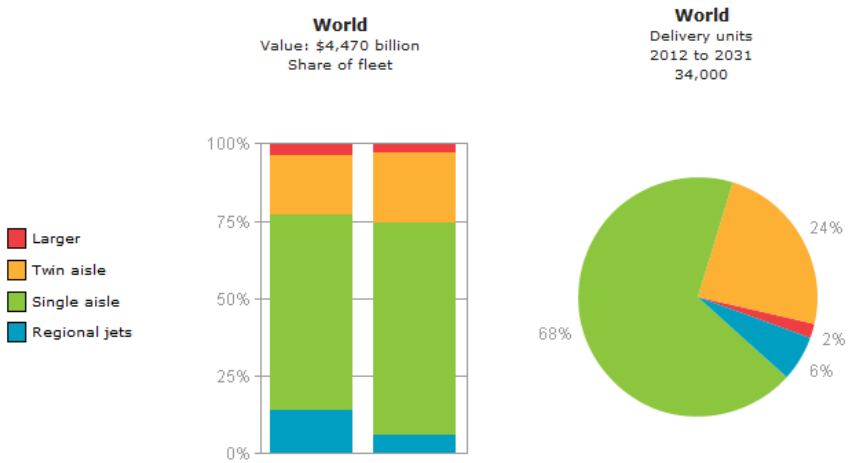

Figure 2.3: Global market forecast for passenger aircraft [4]

With respect to the trends in narrow-body demand it is found in Boeing's Current Market Outlook that the single-aisle segment amounts to 68 % of the world's total aircraft demand, see also Figure 2.3 [4]. Or, as indicated in the table in Figure 2.4, a total of 23,240 aircraft. Embraer, on the other hand, even foresees a dominating 70 % market share for single-aisle aircraft deliveries with 120+ seats. Furthermore, Airbus' forecast settles right in between those two figures with a single-aisle contribution of 69 % and 19,518 new passenger aircraft deliveries by 2031.

WORLD

New airplane deliveries 2012 to 2031	New deliveries	Market share by size (%)	Fleet in 2011	Fleet in 2031
Large	790	2	790	1,030
Twin aisle	7,950	24	3,710	9,110
Single aisle	23,240	68	12,610	27,430
Regional jets	2,020	6	2,780	2,210
Total	34,000	100	19,890	39,780

Figure 2.4: Global market forecast for passenger aircraft [4]

More specifically, from Boeing's current market outlook it follows that for A320 type of aircraft (single-aisle) in the 90 - 175 seats sector a demand of 21,880 single-aisle aircraft is to be expected in 2031, 18,580 units of which are new deliveries, as indicated in Figures 2.5 and 2.6 [4]. Besides, in the narrow-body niche it is to be noted that the main growth is introduced by an increase in the contribution of the emerging economies.

The Airbus A320 is in the 90 to 175 seats single aisle sector. Data is for the 90 to 175 seats single aisle sector NOT the airplane type.

90 TO 175 SEATS SINGLE AISLE

Region	Fleet in 2011	Fleet in 2031	New deliveries	Market value (2011 $B) 2012-2031
Asia-Pacific	2,780	7,010	5,940	500
China	1,290	3,210	2,710	213
Oceania (Australasia)	330	570	520	50
Northeast Asia	260	400	410	30
Southeast Asia	590	1,640	1,290	110
South Asia	310	1,190	1,010	100
North America	2,980	4,650	4,030	340
Europe	2,720	5,010	4,830	420
Middle East	430	1,160	920	73
Latin America	990	2,540	1,810	150
Africa	390	760	510	40
C.I.S.	550	750	540	35
World	10,840	21,880	18,580	1,550

Figure 2.5: Single-aisle market segment forecast [4]

90 TO 175 SEATS SINGLE AISLE

Region	Share of Fleet in 2011 (%)	Share of Fleet in 2031 (%)	Share of New deliveries (%)	Market value Share (%)
Asia-Pacific	26	32	32	32
China	12	15	15	14
Oceania (Australasia)	3	3	3	3
Northeast Asia	2	2	2	2
Southeast Asia	5	7	7	7
South Asia	3	5	5	6
North America	27	21	22	22
Europe	25	23	26	27
Middle East	4	5	5	5
Latin America	9	12	10	10
Africa	4	3	3	3
C.I.S.	5	3	3	2
World	100	100	100	100

Figure 2.6: Single-aisle market segment forecast [4]

2.1.2 Turboprop demand

Environmental issues and stringent environmental regulations force industry to improve the aging fleet with green-technology aircraft [6]. It is because of this high need for 'greener' aircraft that turboprop engines are back on the rise.

Where turboprop engines are generally used in the short-range market, chances are that their use might expand into the medium-haul segment following the trend of turboprop-driven aircraft increasing in size [12]. An example of this tendency towards larger aircraft is the Bombardier Q series, where only the Q400 (the largest) is still in production. Besides that, the observed trend is also supported by Embraer's explorations into designing a turboprop 100-seater. In the narrow-body segment, Embraer does however expect that jets will still prevail due to their high productivity and overall operational efficiency [6].

The total demand for turboprop-driven aircraft as forecasted by Embraer is depicted in Figure 2.7.

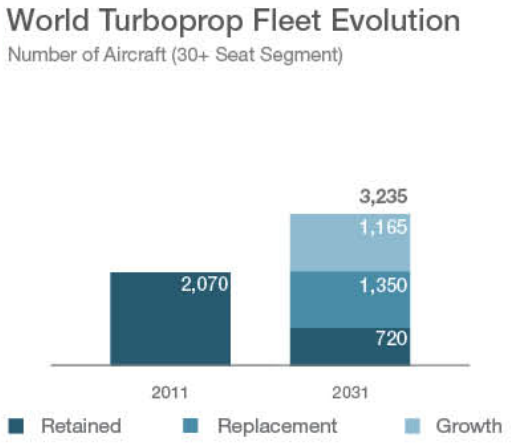

Figure 2.7: World turboprop fleet evolution for 30+ passengers segment [6]

2.1.3 Expected market share

From the previous analyses it can be concluded that the forecast for the air traffic market, and in particular the demand for narrow-body aircraft, is promising. The emerging economies are found to be the main drivers of economic growth and demand in air traffic (4.7-5.0 %), and single-aisle aircraft amount to 68-70 % of the total passenger aircraft market. Furthermore, the demand for turboprops is expected to increase as well over the next few years. So, there is definitely sufficient demand for medium-size, medium range aircraft the coming two decades.

It is to be noted, however, that the software model that is developed is very specific and will only be able to be implemented in the narrow-body niche with only a small number of potential buyers (see section 2.1.1)). Therefore, the aim is to have a considerably high market share within that niche. It is however to be expected that a buyer will request exclusivity, hereby constraining the market share opportunities significantly.

2.2 General and emerging trends in aircraft design processes

Aircraft design is an elaborate, cumbersome process if it is to be conducted from scratch (i.e. an ab initio design approach). Therefore, all manufacturers strive to make the process as cost and time

efficient as possible. Especially for the bigger companies like Airbus and Boeing with their design projects running for over several years, efficiency is of the utmost importance. A lot of resources are therefore used to improve current processes and or come up with new ones. The last few years the focus of the manufacturers has increasingly shifted from the actual testing of aircraft (parts) to the use of simulations. Something Airbus' credo confirms: *More simulation, less testing.* A well-known example of this drive to improve efficiency by means of simulations is the DLR tau-code [13]. This particular code has been used as a CFD-tool by Airbus and its development took place not only internally, but also through collaborative national, European and university projects [13]. These developments indicate that the field of software-based design methodology is definitely on the rise.

Moreover, in economic recessive times the profit rates decline, hereby inducing an increase in labour productivity growth to make up for the losses [11]. Ergo, more time and resources will have to be spent on making processes as efficient and as innovative as possible. Therefore, it is to be expected that future markets will also appreciate innovative, cost and time efficient design methodologies.

2.3 Macro environment and stakeholders

The development of new tools in for example design processes does not only change the methodology itself. In the immediate, competitive environment, the resulting product and its effect on the buyer (and supplier) are obviously to be taken into account as well. Besides that, the new tool will influence the demand for the products of rivals and the demand for substitute products. Not to mention the fact that the new 'design climate' will shape the behaviour of potential new entrants to the market. Consequently, the efficiency and demand that come with the new design tool define the behaviour and confidence of the company's (hypothetical) shareholders.

The changes in the immediate environment ultimately influence the macro environment, and vice versa. An increase in demand for aircraft, for example, leads to changes in the labour market with lower unemployment and thus a stronger bargaining position for the unions. Ergo, the economic and political environment are affected too. Furthermore, altered immediate environments could lead to modified legislation and regulations.

Noteworthy, if people are willing and able to travel and fly more, it eventually culminates in a completely different lifestyle and coverage of the globe. Thus, a higher demand for aircraft changes society, both in its demography and in terms of lifestyle. Finally, note that fluctuations in competitive positions strongly influence the development of new technology, as competitors will want to catch up with their rivals.

Note that the current analysis has been conducted from the point of view of the company. Obviously, the environment has a great impact on the company too. Hence, in *reality* the arrows would point both ways.

The above is summarised in the stakeholders alliance in Figure 2.8.

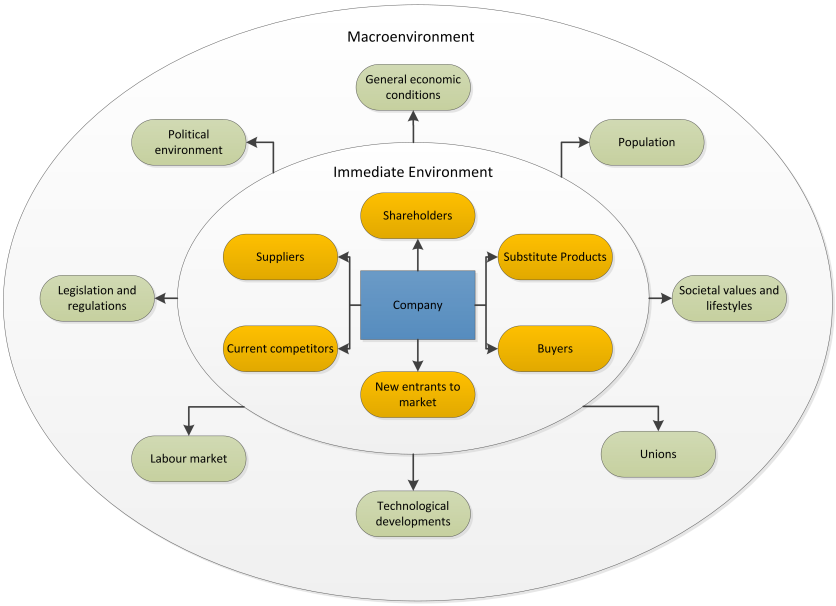

Figure 2.8: Stakeholder alliance with a subdivision in immediate and macro environment. Adapted from [10, 14]

2.4 Competitive analysis and SWOT analysis

In order to assure a market share for the developed product it is crucial to determine the company's resources and competences. First, the valuable resources (not only physical but e.g. intellectual capital) need to be identified and compared with possible competition. In this case, the uniqueness of the developed program, the people working on it and even TU Delft which provides room and support can be defined as resources. Next, the determination of competitive power needs to be done. Is the resource rare, hard to copy or substituted by another resource? Those factors state how rivals might react on the introduction of the developed product. Finally, the company's competences need to be refined. Especially distinctive competences which give an advantage over rivals are important to find and analyse. In Table 2.1 weighted competences with their resulting advantages can be found.

Table 2.1: Distinctive competences

Competence	**Weight**	**Resulting advantage**
Use of existing know-how	high	low development costs
Use of a single program	medium	simple end product
TU Delft as sponsor	low	brand name and possible support by employees

The overall situation of a company can easily be described using a SWOT analysis [10]. It is a simple but powerful tool for displaying the internal resource strengths and competitive deficiencies, its external market opportunities and threats. Table 2.2 provides a good overview of the future well-being of the company.

Table 2.2: SWOT Analysis

Strengths	Weaknesses
• Technology based on existing knowledge, thus more efficient use of time and resources • Mathematical analysis is simplified by keeping topology constant (i.e. shape optimisation) • Due to modular approach simple to add features	• Limitations given: medium size and range types of aircraft • MATLAB is used which is relatively slow and requires license • Manufacturing follow-up not incorporated
Opportunities	**Threats**
• *Blue ocean* strategy (new market development) [10] • Niche market solutions • Licensing of technology	• Open sourcing of the utilised design approach • Competitor/manufacturer does similar research and/or shows copycat behaviour • New generation aircraft with extremely different topology is developed

Chapter 3

Sustainable Development Strategy

Air transport is one of the fastest-growing transportation modes, and it is expected to hold on to that trend in the near future [15]. However in order for this growth to be sustainable aircraft manufacturers are working on reducing fuel consumption and making aviation more available to everyone. This results in the following trends: The growth in global jet fuel consumption has paled in comparison with the growth in traffic[5]. As in general aviation has become more fuel and cost efficient in the past decades and it is expected that this trend will continue at least for another two decades (this trend holds for fossil fuel propulsion systems)[16].

In order to further improve sustainability for air transport and aviation, a certain level of awareness should be present in aviation products and their design methods or approaches. This should lead to the capacity to support, and steadily improve quality of life for everyone and everything on our planet, now and in the future.

The SCALAIR project has a sustainability vision concerning several topics [17]. However, the largest contributors on the path to a more green aircraft are the change in propulsive system and the change in design method.

3.1 Open Rotor Propulsion

When using open rotor propulsion instead of a turbofan, several important aspect with respect to sustainability come in mind. Mainly: fuel consumption reduction, pollutant emission reduction and noise of the open rotor.

3.1.1 Fuel and Emissions

Open rotor propulsion has a higher propulsive efficiency, this leads to a lower Thrust Specific Fuel Consumption (TSFC), meaning a reduction in fuel consumption. The reason why this open rotor technology is more efficient is mainly due to the fact that a turboprop takes a larger mass of air and gives that mass a smaller velocity increase, compared to a turbofan.

$$\eta_{Propulsive} = \frac{2}{1 + \frac{V_{jet}}{V_\infty}} \tag{3.1}$$

Using Equation 3.1 it can be shown that if $V_{jet_{CROR}} < V_{jet_{TURBOFAN}}$ the $\eta_{Propulsive_{CROR}} > \eta_{Propulsive_{TURBOFAN}}$. The only drawback is that due to this fact, the turboprop is more limited in its top speed. As of the moment the produced jet velocity, $V_{jet_{CROR}}$, is equal to the free stream velocity, V_∞, the thrust equals zero. This jet velocity depends on the lift produced by the blades, this lift is proportional to the freestream velocity of the blade which again depends on both the freestream velocity of the aircraft and the velocity induced by the rotational speed. So the jet velocvity is limited by the rotational speed of the propeller which in turn is limited by the Mach number reached at the tips of the propeller blades. By using multiple blades—$8 - -12$—the overall rotor diameter can be reduced leading to a lower tip speed, however this also leads to an increase in blade loading. The CROR system can attain higher airspeeds, with an equal or higher propulsive efficiency than regular turboprop systems. The velocity can range up to Mach 0.9 but the zone of interest for this project

is Mach $0.67 - 0.73$ [18]. A comparison between several propulsive systems with respect to their optimal flight speed can be seen in Figure 3.1. Higher disk loading, however, leads to a stronger swirl. By using a second contra-rotating propeller the flow can be proportionally de-swirled leading to some additional propulsive efficiency increase. Which is another advantage of the CROR with respect to the propulsive efficiency. This ultimately results in 35.8% fuel consumption reduction of the UDF compared to the engines used on the A320 at this moment, see Chapter 11.

This reduction in fuel consumption is directly linked to a reduction in pollutant emissions which is very beneficial for the environment, as aviation contributes for approximately two to five per cent to air pollution. This is on one hand by producing pollutant emissions and on the other hand by secondary effects like the formation of contrails. Therefore the actual effect of air transport on the climate is much larger than would be expected. This can be quantified by means of the Radiative Forcing (RF) or Radiative Forcing Index (RFI), i.e. the relative ratio of the RF to that of CO_2 emissions alone. The RFI was determined to be 2.7 for aircraft [20]. Which says as much as the climate change due to aircraft is 2.7 times larger than the climate change of aircraft solely due to burning fossil fuels and thereby producing CO_2.

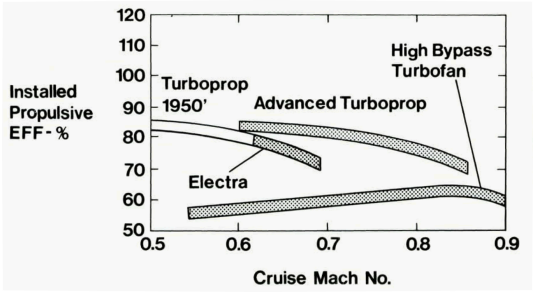

Figure 3.1: Installed propulsive efficiency vs cruise Mach number of several propulsion systems [19]

CO_2 is quantitatively the largest of all engine emissions. With exception of H_2O, CO_2 is a factor 1000 larger than other emissions [21]. The aviation induced CO_2 contribution with respect to all other man made CO_2 is a reasonable 2% [15]. According to the International Energy Agency (IEA), aviation is responsible for 11% of all transport energy used (in 2006)[15]. Which means that CO_2 cannot be left out of the engine design process, as CO_2 is a quite important emission factor. Also, CO_2 is linearly dependent on the aircraft fuel consumption. Meaning that by reducing the fuel consumption by 35.8%, the CO_2 emission will be reduced by 35.8%.

Of course CO_2 is not the only emission to be reduced, NO_X also takes up a substantial part in polluting the air. Especially when looking at the relative importance of emissions to global warming according to the IPCC. This gives rise to the term Global Warming Potential (GWP), which also takes the life time of a pollutant into account. The GWP is a ratio between the global warming caused by a given mass pollutant, compared to the warming of a similar mass CO_2. According to the IPCC the GWP value of NO_X is significantly higher than that of CO_2, in the order of 300. Besides that, taking into account that altitude has an effect on the severity of NO_X emission, i.e. the higher NO_X is injected in the atmosphere the larger effect it has on the environment [21]. Thus making it safe to say that aircraft NO_X emissions should definitely be reduced in order to prevent or limit global warming.

NO_X emissions are mainly produced in internal combustion engines due to high flame temperatures and long reaction times. Another mechanism to produce NO_X is Fuel-NO formation, which is based on oxidation of nitrogenous compounds. Kerosine, however, does not contain a lot of fuel-bound nitrogen, so this mechanism is negligible in gas turbines [21]. In order to reduce NO_X formation the flame temperature should be reduced, which lowers the thermodynamic efficiency. There are also other measure to reduce NO_X, like : redesigning the combustor, optimising the engine stoichiometric operating zone,i.e. leaner mixture, injecting ammonia to control NO_X formation and using a catalytic filter system. However, the details of this matter are beyond the scope of this project.

By using an open rotor system the NO_X level will certainly be reduced. In 2011, NASA presented results concerning the NO_X emission of their UDF engine [22]. As a result of a higher propulsive efficiency and an advanced lean combustor, the UDF emits less NO_X during all flight phases, compared to a turbofan engine. These findings are depicted in Table 3.1. From this it can be concluded that the NO_X emission of aircraft using open rotor technology are reduced significantly during the take off role, which means as much as aircraft emissions can be reduced significantly in and around airports. Landing-Takeoff (LTO) NO_X values are also present in Table 3.1, where a

reduction of approximately 80% compared to the reference turbofan could even be realised. The reduction in LTO NO_X is mainly accredited to the reduction in fuel flow, and a smaller part due to a low NO_X combustor.

Table 3.1: NASA Engine Model Results [22]

	A320 Engine Model	**UDF Engine Model**
	LTO Fuel Flow [kg/s]	
Take off	1.053	0.452
Climb out	0.880	0.369
Approach	0.319	0.119
Idle	0.128	0.043
	NO_X Emission Index [g/kg]	
Take off	26.5	11.1
Climb out	22.3	6.9
Approach	8.9	9.0
Idle	4.7	5.0
LTO NO_X D_p/F_∞ [g/kN]	56.2	11.57

Up to today it is still a concept under development, but it is regaining attention, since the oil prices are high and will probably keep rising. Several authorities are currently doing extensive research with respect to the problems of open rotor propulsion that have been discovered during the '80s. These major problems are expected to be solved within a reasonable amount of time and the engine can then be used for commercial applications. This is because the knowledge concerning materials still grows every year, and by using a simulation based design approach acoustic, vibration and fatigue or safety problems can be solved properly and more rapid. As such, these open fan propulsive systems should be applicable in the near future.

3.1.2 Noise

As is already apparent from the definition of noise, it is an unwanted and subjective phenomenon that leaves its marks on the environment. Therefore, it is not just about the excessive sound levels, but also about the impact on the environment that comes with it. As such, noise is the main limiting factor on growth for commercial airports, like Schiphol [23]. Not in the last place due to the effect it has on the people living or working in the airport's vicinity. It has been shown that the number of complaints has gone up, whereas the number of complainants has reduced over the last few years [23]. Thereby implying that the level of unwantedness has increased considerably.

With noise being the main limiting factor for the growth of airports, it is of importance to evaluate the noise footprint taken up by aircraft and by propeller driven aircraft in particular.

Noise has a definite impact on the environment, and especially on the communities near airports. The obvious consequence here is of course annoyance, but also the health impact and the devaluation of property are to be taken into account [23]. Not to mention the quality of life [24], both for humans and for animals. Moreover, noise is a driving factor in the health- and quality of life impact discussed in the report of the World Health Organisation (WHO) on environmental health inequalities in Europe [25]. So, in terms of pollution there are several factors to be considered.

An additional note on the discomfort due to noise is the fact that the sensation level does not vary linearly with the magnitude of the actual physical stimulus. Rather, it increases in an exponential way (Stevens' power law).

Because of the experienced nuisance near airports, there are several efforts to mitigate noise. As for example indicated by NASA's goal in Figure 3.2. These efforts can be made at different levels: aircraft level, aircraft operation level or aircraft design/planning level [23]. Examples applicable for the SCALAIR project are at an aircraft level: the reduction of engine noise and its interaction with the airframe (e.g. by manipulating the engine positioning). Or at the aircraft operational level: the effect of the design time (as discussed in section 3.2.1) on the phasing out of older aircraft.

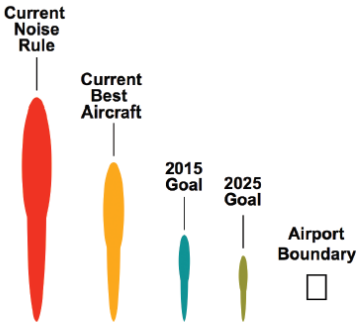

Looking to the future, the ultimate goal is to confine any objectionable noise within the boundaries of an airport. *Source: NASA*

Figure 3.2: The intention of NASA with respect to shrinking nuisance noise footprint [24]

3.1.2.1 Noise Footprint

The way to quantitatively and qualitatively lessen the impact on the community is by minimising the noise footprint. This footprint is defined by the noise levels in a radius from the runway threshold, as depicted in Figure 3.3. Obviously, this also encompasses the approach and take-off. Current efforts to minimise the footprint for the approach and take-off phases (i.e. at operational level), amongst others, include the increased use of continuous decent approaches.

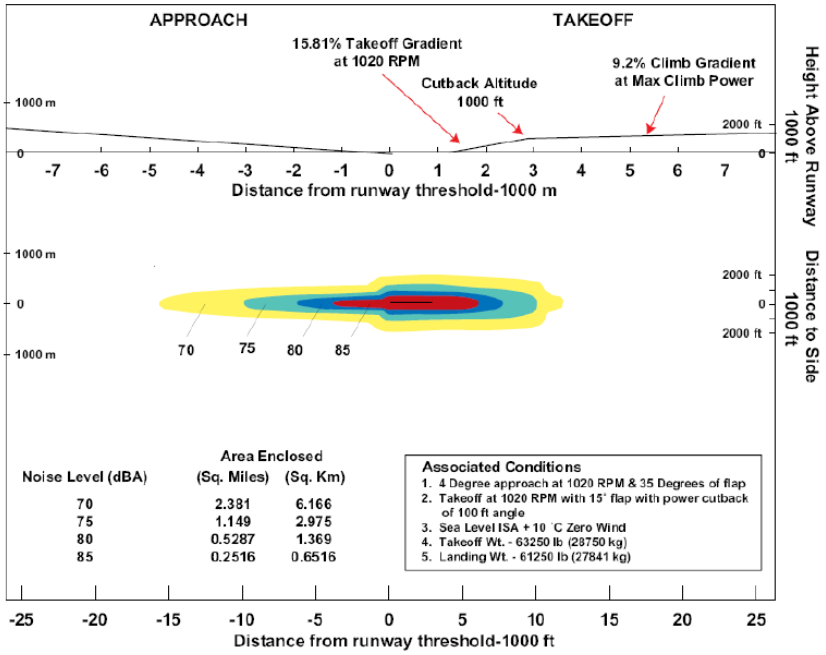

Figure 3.3: Example of Noise footprint for standard L-TO procedure [26]

3.1.2.2 Contribution to Noise by Propulsive System

One of the main contributors to aircraft noise is of course the engine (with the other being the aerodynamic contribution). Given the change from turbofan propulsion to the use of turboprop/open rotor types of engine, it is important to assess what this change would mean in terms of noise generation.

Compared to turbofan engines, the total sound levels of turboprop engines are similar, as follows from research by Bombardier and the DLR (Figure 3.4) [26, 27]. Unfortunately, the magnitude of this total level comes eeringly close to the speech interference level (of the passengers), for both types of engine. It is noteworthy, however, that the noise patterns produced by turboprops and jet engines are completely different. Jets generate higher broadband noise and turboprops generate

strong tones due to the blade rotation and its interference with the fuselage. Thus the equivalent total noise is not equal to the equivalent perception [26].

Location wise, the lowest frequencies are experienced for an aft rotor and for front rotors the highest peak levels and highest frequencies are acquired [28].

The major factor in the noise generation of open rotor engines appears to be the fact that there is no nacelle shielding the rotor to prevent excessive acoustic propagation. Therefore, there is not only the propagation of the engine sound levels itself, but also an increased interaction effect between the engine and other airframe elements. The excessive acoustic propagation is especially true for pusher configurations at low-speed take-off and approach [27].

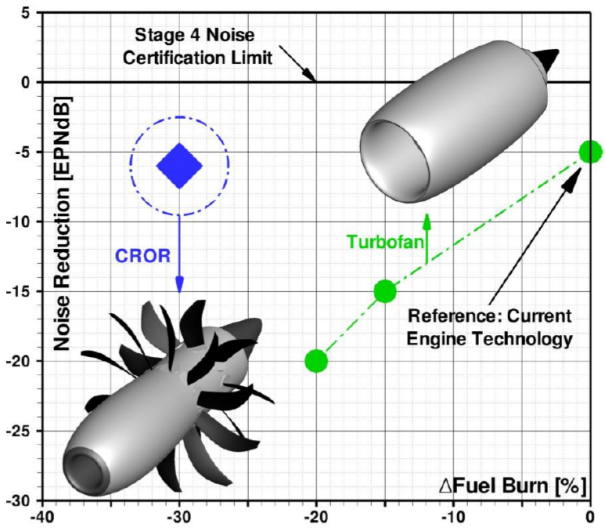

Figure 3.4: Noise reduction vs. fuel reduction for turbofan and turboprop engines[27]

To determine the rotor effect in an analytical manner, the NLR conducted an investigation into the noise radiation of propellers [29]. This research allows for evaluation of the tones to be expected, the effects of spanwise source distributions and the directivity of individual noise components. As such it provides a basis for new studies into the reduction of the noise generated by rotor configurations.

Further elaboration on the actual noise characteristics of the UDF as well as approaches to reducing the rotor noise can be found in Chapter 7.

A word of precaution should also be included concerning the numbers given on the fuel reduction. The analysis that was performed and used in this project is based on an 80's UDF engine technology. This technology is compared to the engine technology used on the A320 at this moment. Off course the future A320, i.e. the A320 NEO (New Engine Option), will feature an ultra high bypass turbofan or a geared turbofan. According to recent research performed by the NASA, the advanced propfan of the future should be able to compete against those advanced turbofan [30]. The results of this research can be found in Table 3.2.

As can be seen in Table 3.2 the Propfan is still expected to have the fuel efficiency benefit. At top of climb the advanced geared propfan has a TSFC of approximately 13% lower than the advanced geared turbofan and up to approximately 30% when compared to the current A320 engine. The reason that this is not 36% as mentioned earlier is that the open rotor engine used here is a geared open rotor, to achieve even higher cruise mach number, unfortunately this higher mach number comes with a small loss in efficiency.

Table 3.2: NASA Advanced Engine Model Results [30]

	A320 Engine Model	**Advanced Geared Turbofan**	**Advanced Geared Propfan**
T_{static}	111kN	104kN	121kN
TSFC (M=0.78, 35000ft)	17.28g/kNs	13.99g/kNs	12.12g/kNs
T/W (M=0.78, 35000ft)	0.72	0.74	0.54
	LTO Fuel Flow [kg/s]		
Take off	1.053	0.728	0.521
Climb out	0.880	0.602	0.427
Approach	0.319	0.192	0.139
Idle	0.128	0.067	0.046
	NO_X Emission Index [g/kg]		
Take off	26.5	16.5	14.0
Climb out	22.3	10.7	9.0
Approach	8.9	9.0	9.0
Idle	4.7	5.0	5.0
LTO NO_X D_p/F_∞ [g/kN]	56.2	22.00	12.15

The reduction in TSFC during take off is even higher with respect to the other two engines. This trend can also be observed in Table 3.1. However there is one drawback visible in Table 3.1. It can be seen that the T/W is approximately 30% lower. This drawback is however counteracted by the fuel efficiency.

3.1.3 Positioning of Propulsive System

By placing the engine on the end of the aircraft fuselage, it is possible to obtain a clean wing. That is, a laminar or smooth wing. Such a wing reduces the aerodynamic drag for for given wing lift, and increases the overall lift-to-drag ratio. The increase in the lift-to-drag ratio has a positive effect on the fuel efficiency. If the increased lift-to-drag ratio is coupled with a lower aircraft empty weight, resulting from a more efficient propulsive system, the total efficiency of the aircraft will be even higher.

3.1.4 Conclusion

Up to today, open rotor propulsion is still a concept under development, but it is regaining attention, since the oil prices are high and will probably keep rising. Several authorities are currently doing extensive research with respect to the problems of open rotor propulsion that have been discovered during the '80s. These major problems are expected to be solved within a reasonable amount of time and the engine can then be used for commercial applications. This is because the knowledge concerning materials still grows every year, and by using a simulation based design approach acoustic, vibration and fatigue or safety problems can be solved properly and more rapid. As such, these open fan propulsive systems should be applicable in the near future. So it can be concluded that the CROR is a reasonable choice as next generation propulsion technology. Especially when focusing on environmental regulations, like NO_X regulations and Noise regulations. As at this moment the UDF could pass all these certifications regulations to the highest standard with proper margin. However, it would be beneficial if the CROR technology would arrive at noise levels, normally associated with advanced geared turbofan engines. Finally, a prediction concerning the actual reduction in fuel with respect to the different aircraft groups can be seen in Table 3.3.

Table 3.3: Future aircraft fuel intensity reduction potential to today's aircraft[15]

Type of improvement	Percentage fuel intensity reduction
Airframe aerodynamics	20-30%
Airframe light-weighting	20-30%
Engine technologies	15-25%
ATM and operations	7-12%
Total	40-50%

3.2 Effects of the Scaling Design Methodology

It is strived for to further reduce the fuel consumption by appropriately scaling the aircraft elements (such as the wings), while keeping the topology constant (i.e. shape optimisation). Some of the aspects that were analysed and optimised during this synthesis are for example the wing sweep, aspect ratio and type of engine.

Noteworthy is also that the scaling approach has multiple advantages when it comes to reducing the ecological footprint by aviation. Namely, the scaling methodology reduces the time and cost required for the design- and manufacturing phase.

3.2.1 Design Time and Cost

The reduction in design time and cost is a result of the fact that most of the components of the aircraft have already been designed. Or in other words, the eventual design is based on existing knowledge. Therefore, the first phase (planning and conceptual design phase) of the aircraft life cycle does not have to be accounted for. This phase is responsible for a large part of the design phase of an aircraft which is cumbersome and expensive. Note, that for the final optimisation process, time and resources still need to be taken into account. For a more thorough discussion of matters concerning the design life cycle costs the reader is referred to section 2.4 of the Baseline Report [31].

This reduction in design time is directly coupled to a reduction in energy as well as a reduction in design resources, e.g. computers, facilities, printers, etc.

3.2.2 Manufacturing Cost

By using a scaling approach, aircraft parts keep their original shape with an eventual in- or decrease in length, thickness or height. Since no completely new parts are designed, the manufacturing facility of the original A320 can be used, incorporating minor changes. The same procedure is applied for the whole aircraft family of Airbus where parts have different scales (e.g. A320 and A319). By using the same facility and experienced labourers, resources can be saved. Besides resources a lot of energy can be saved. Also if the diversity of the parts decreases, the fabrication process could be optimised in terms of energy, cost, and time which will also lead to a decrease in ecological footprint.

Another beneficial aspect of using less diversity in parts is that this makes the aircraft recycling less complex. And as with the fabrication the end of life recycling could also be optimised.

Chapter 4

Aerodynamics

In order to arrive at aerodynamic scaling laws a few approaches can be used. These approaches differ in the method of obtaining the data that is used to generate a trend. The data can either be obtained by statistics or can be based on empirical data. The three main approaches all have the same goal, i.e. try to produce and visualise the general trend between the different parameters, and set-up a polynomial function which serves as a trend line. This trend line can then be used as a scaling law, although it should only be used under specified conditions. That is, there is a limited range where all parameters should be positioned.For this project the computational approach is used, and the empirical data serves as validation data. In this chapter the sweep angle, angle of attack(AOA), taper and aspect ratios, wing twist are referred to as the geometrical parameters.

The first Section, Section 4.1, describes the performed processes by the aerodynamic Matlab model. This is followed by Section 4.2 in which the geometric lay-out of the wing, the derivation of the sweep angle and the aerodynamic methods are described. Section 4.3 presents the first result of varying one of the geometrical parameters on the spanwise lift and drag distributions. These result are then expressed in Section 4.4 the form of a scaling law for lift and drag coefficients, span efficiency factor and lift to drag ratios. In Section 4.5 the result for the lift to drag ratio with two varying parameters are presented and analysed on trends. This is followed by the verification and validation of the model and the obtained results in Section 4.6 and Section 4.7, respectively. Finally the scaling laws are discussed and their potentials are analysed in Section 4.8

4.1 Model Methodology

The computational method used in this a Vortex Lattice Method (VLM) and is executed by by Athena Vortex Lattice Method (AVL). This method is selected as it can derive aerodynamic aspect of specific wing geometries as specified by the user. Compared to a method which is based on statistical data, AVL is a fast method to analyse many different wings and obtain trend lines and scaling laws. The limitations of AVL and the theory behind VLM can be found in Appendix A.

AVL however is a Fortran based program, this is not practical if large data sets need to be ran through the program. Therefore a Matlab based interface was created to control AVL via batch input.

One of the important setting for AVL is the vortex panel distribution. As the size and shape of panels, which are constrained at the corners by vortices, influences the accuracy and sensitivity of the result. It is important to define the shape of the panels properly. The panels in the chordwise direction are distributed in a cosinusoidal matter with decreasing panel size towards the leading and trailing edge. In the spanwise direction the wing is divided in two sections. Section one is constrained by the root and kink and has a sinusoidal distribution of the panels with decreasing size towards the root. The second section is constrained by the kink and tip and has also a sinusoidal distribution but with decreasing panel size towards the tip. The number of chordwise panels equals 30 and the spanwise number of panels per section equals 20.

The following data provided by AVL is used:

- Spanwise lift, moment and induced drag coefficients

- Total lift and induced drag coefficient incl Prandt Glauert corrections
- Span efficiency factor
- Average and local chord lengths

Further performed aerodynamic computations are described in Section 4.2.

The run file serves as batch entry for the program, so it is actually a chronological list of input commands for the program. The main commands are; loading the geometry, define and save the case, run the analysis and save the results. This run file is created through a loop in Matlab, where the geometry and case file change every iteration. The case is described in the run file by simple commands. It consists of the environmental parameters and flight state parameters like angle of attack (AOA), free-stream velocity, density, etc.

The AVL output files are then read by Matlab and the required computations are performed before the trends and scaling laws can be produced. In Section 4.2 the computations and methods used by the program are described.

4.2 Design Methodology

Appendix A contains a description of flow simplifications used to make the aerodynamic computations. AVL does take the Prandtl Glauert compressibility effect up to a Mach number of 0.7 in to account, this is applicable to unswept wing and can increase as the wing sweep increases. For the Scalair project the accuracy of AVL will be sufficient w.r.t compressibility effect but a more advanced method like CFD would be preffered.

4.2.1 A320 Wing Geometry

Spanwise wing twist is incorporated in the wing design based on reference data from a Boeing 737, as there was no information found regrading the A320 design. The twist from root location to kink location decreases by two degrees and the twist from kink location to the tip decreases by five degrees. Due to safety requirements with respect to the controllability of the aircraft in case of wing stall the total change of wing twist from root to tip is set constant at seven degrees. Furthermore, it is assumed that the spanwise twist changes linearly between the previous specified locations. This assumption of linear change does differ from reality in which the twist changes in a more precise and efficient matter. Therefore, a change in outcome and decrease in performance can be expected with respect to the reference aircraft.

The wing's planform geometry as used in the aerodynamic analysis is represented in Figure 4.1. The black dashed horizontal line indicates where the fuselage wall is located. It can be seen that the leading edge of the wing is expected to continue inside the fuselage with the same sweep angle. Also the trailing edge is expected to continue its path inside the fuselage. When the planform is changed as a result of a change in input these assumptions are retained. It is further noted that the length from root till kink is a ratio of the the total span length and is equal to the A320.

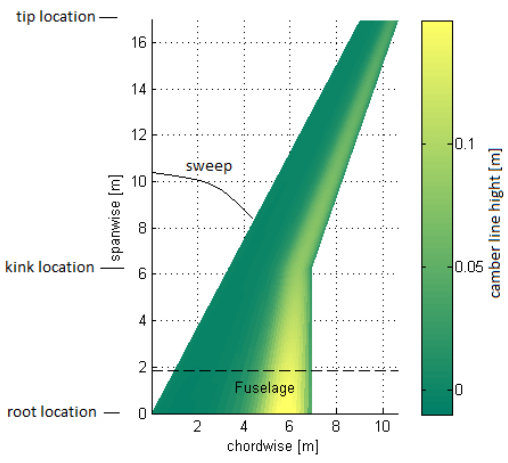

Figure 4.1: Wing planform geometry

The geometric parameters for the A320 are listed in Table 4.1. It is indicated whether these parameters are obtained from reference data known or derived have been derived to comply with the A320.

Table 4.1: Geometrical Parameters

Parameter	value	Unit	Obtained
Sweep	28	degree	Reference
Aspect ratio	9.39	-	Reference
Taper ratio	0.24	-	Reference
Root twist	3	degree	Derived
Kink twist	1	degree	Derived
tip twist	-4	degree	Derived
AOA cruise	1	degree	Derived
Wing area	122.4	m^2	Reference
Kink location	0.37	-	Derived

4.2.2 Airfoil

The critical Mach number of an airfoil indicates at which free stream velocity the flow over the airfoil becomes sonic for the first time. At this point, a shockwave forms over the wing which increases drag. When the Mach number is increased further, this wave drag is increased. At the Mach number for drag divergence, the drag rise is so significant that flying beyond it is not possible with the available thrust. This number is unique for every airfoil and much research is dedicated to increasing this number. A special class of airfoils, the supercritical airfoils, is designed to delay the pressure recovery over the airfoil so that a small shockwave is present, rather than a very large one. This delays the drag divergence Mach number and therefore allows higher cruising speeds. Modern airliners are equipped with these supercritical airfoils to be able to fly between the critical Mach number and the drag divergence Mach number without excessive drag penalties.

The first step is to determine the critical mach number for the airfoil. The airfoil which is selected in this case to represent the A320's is illustrated in Figure 4.2 and was taken from the University of Illinois database [32]. Since there was no representative information available for the A320, this somewhat standard supercritical airfoil was chosen. This airfoil is used over the complete span of the wing. However, the use of only one airfoil is not a realistic representation of a wing, hence influences in the outcome can be expected with respect to reference data of existing wings. This airfoil was analysed with JavaFoil, a free online program for airfoil analysis. This program is very simple to use, and accurate, off course, up to a certain point. It uses a Karman Tsien compressibility correction, which is more accurate than the Prandtl-Glauert correction. However, limitations are that JavaFoil is not capable of computing laminar separation bubbles and flow separation. The flow separation at stall is modeled by some empirical relations, but going far beyond stall will lead to incorrect results.

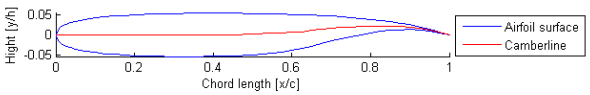

Figure 4.2: NASA/Langley Whitcomb integral supercritical airfoil

4.2.3 Wing sweep

Since the new engines for the improved design dictate a different flight speed of Mach 0.72, several components of the aircraft are influenced by this. The most important parts, the wings, are off course affected by a change in airspeed. Since the airfoil remains constant for the sake of simplicity, this change can be facilitated by a variation of the sweep angle. The role of the critical Mach number is first explained, followed by a description of the effects of wing sweep and its relation with tail sweep.The purpose of swept wings is mainly to increase the critical mach number of the airplane in order to cruise faster, or allow for a thicker airfoil for a given cruise speed. This is achieved by the decrease in the perpendicular component of the oncoming flow on the airfoil. This decrease is

proportional to the cosine of the sweep angle, which is measured at the leading edge.

Consequently, the spanwise component of the flow is increased which has several disadvantages. For instance, the tip loading is increased which leads to a heavier wing structure. Also, the problem of tip stall is exacerbated and $C_{L_{max}}$ is reduced. However, since the new design features a lower flight speed the sweep angle can be reduced and these side effects are in favour of the design.

When calculating the new required sweep angle corresponding to the cruise speed dictated by the new engine, the assumption is made that the difference between the A320 cruise Mach number and critical Mach number stays the same for the new design. This means that the relation between the cruise Mach number and critical Mach number is constant. With this assumption it is now very easy to calculate a sweep angle belonging to a new cruise speed with the cosine method.

$$M_{eff} = M_{\infty} cos(Sweep) \tag{4.1}$$

With Equation 4.1 the perpendicular component of the flow on the airfoil is calculated. This number is the critical Mach number of the airfoil. When a new flight speed is inserted in the equation, the corresponding minimum required sweep angle can be determined. For the redesigned A320 with UDF engines, the cruise speed is Mach 0.72. Then, the sweep angle should be at least 17 degrees to prevent negative transonic effects on the wing.

4.2.4 Tail sweep

The sweep angles for the tail surfaces are less critical and easier to determine than that for the wing. It is desired to have a higher critical Mach number on the tail than on the wing, in order to make the tail stall after the wing and to prevent a loss in elevator effectiveness at high speeds. From page 76 of Raymer [33] it can be seen that the sweep of the horizontal tail surface is usually set to five degrees more than on the wing.

The sweep angle for the vertical tail surface is also used to increase the critical Mach number. Again from Raymer [33] it can be seen that this sweep angle varies approximately from 35 to 55 degrees. The vertical tail sweep of the A320 is twelve degrees more than the wing sweep angle. For both the horizontal and vertical tail it is decided to keep the difference in sweep with the wing constant. Therefore, on the new design the horizontal and vertical tail sweep angles will be five and twelve degrees more than the wing sweep, respectively.

4.2.5 Taper

The developed computer program can be configured to find the fuel consumption (in [g/pax/km]) of a scaled aircraft. According to the scaling laws a very low taper of 0.05 (or even lower, but 0.05 is set as a limitation) is beneficial for a lower fuel consumption. However in the derivation of these scaling laws topics as controllability and control surface placement were not taken into account. The objective of this subsection is to account for these topics.

In order to have safety when wing stall occurs, it should first occur at the wing root and not at the tips. Stall first occurs at the location with the highest c_l. For straight untwisted wings, the location with the highest c_l is defined by Equation 4.2, from Torenbeek [34]. This equation indicates that a lower taper ratio causes the tip to stall first.

$$y/b/2 = 1 - \lambda \tag{4.2}$$

Furthermore, a low taper ratio leads to a small chord length at the tip, leading to a lower Reynolds number at the tip. Which lowers the stall lift coefficient at the tip. In Subsection 4.2.1 the effect of spanwise wing twist was also introduced as a precaution to prevent premature tip stall. However, the role of taper ratio in preventing tip stall is dominating.

Besides, in order to have sufficient roll controll. The ailerons need to have a minimum size. Both in chordwise and spanwise direction.

To prevent stall starting at the tip, and to have a minimum chord length for the ailerons. There was decided to use a minimum taper ratio constraint. To determine this minimum taper ratio constraint, use was made of Figure 4.3 from Torenbeek [34].

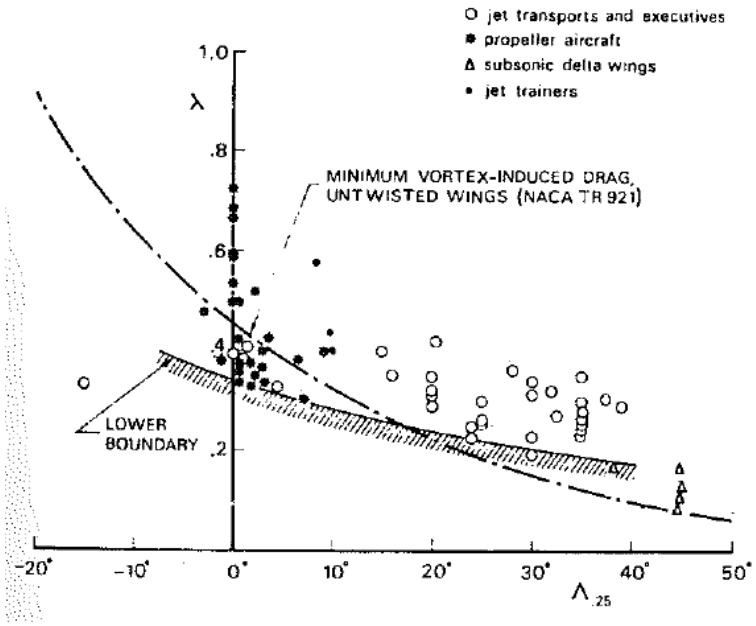

Figure 4.3: Taper ratio as a function of sweep angles, based on historical data.

From the lower boundary, indicated in the figure, it is concluded that the minimum required taper ratio for the new design with a quarter chord sweep of 15 degrees should equal 0.25.

4.2.6 Lift

The computations of the lift produced by the wing are quite straight forward, as AVL computes the lift coefficient for the given wing geometry. With the lift coefficient and the wing characteristics the lift is computed. However, this is not the lift produced by the aircraft as the horizontal tail plane will produce a down force to assure a stable aircraft. The lift produced by the horizontal tail plane is not computed by AVL, instead the following method is used.

$$L_{tail} = -\frac{1}{2}\rho V_{tail}^2 \frac{S_h}{S} S C_{L_{tail}} \tag{4.3}$$

Where the flow velocity experienced by the tail is derived from Equation 4.4 and the tail to wing area ratio equals 0.17 and corresponds to the reference aircraft. This methods is was taken from [35].

$$V_{tail} = V_{upstream} 0.85^2 \tag{4.4}$$

The total produced lift equals the lift produced by the wing minus the down force produced by the horizontal tail. As there is little to no information available on fuselage pitch and the angles under which the wing is mounted to the fuselage, the aerodynamic program is executed for multiple angles of attack. From this it was derived that the angle of attack of the wing at the root, kink and tip should equal three, one and minus four degrees respectively. This value applies to the cruise condition in which the aircraft weight will equal the empty operational weight, the design payload weight and half the design fuel weight. For the aircraft AOA during cruise the program provided an angle of one degree. This value was obtained in the following way. The normal minimum operating weight of the aircraft during cruise is derived. It is assumed that this weight equals the empty operating weight and the design payload. The lower bound constraint of the pitch equals zero, as a negative pitch would lower the aerodynamic performance and it is furthermore preferred to have a pitch angle close to zero at the end of cruise. With these design requirement the minimum and

maximum aircraft AOA during cruise equals 0.11 and 1.88 degrees respectively. A representation of these values and the corresponding lift coefficients can be found in Figure 4.17.

4.2.7 Drag

The drag of the complete aircraft consists of the following components: wing induced drag, induced drag by the horizontal tail, parasite drag of the wing and parasite drag of the rest of the aircraft. Besides the spanwise lift distribution, also the spanwise drag is of importance for the computation of the structural weight. The induced and parasite drag components will be discussed briefly.

4.2.7.1 Induced Drag

As AVL provided an output file containing the induced drag coefficient per spanwise location, the corresponding induced drag can be computed in combination with the spanwise chord length distribution. When the spanwise parasite drag and induced drag are combined the total drag distribution is obtained. These computations are performed with equation 4.5.

$$D_{\frac{x}{s}} = \frac{1}{2}\rho V^2 c(C_{D_I} + C_{D_{0_{wing}}}) \tag{4.5}$$

The induced drag produced by the horizontal tail plane is not computed by AVL, instead an analytical method of equation 4.6 is used. The down side of the implementation of the analytical method is that it is static and will not take the effects of topology change into account.

$$C_{D_{I_{tail}}} = \frac{{C_{L_{tail}}}^2}{AR_{tail}etail\pi} \tag{4.6}$$

Where the following parameters are assumed to be constant: $C_{L_{tail}}$ equals 0.177, aspect ratio of 5 and the span efficiency factor equals 0.8.

The induced drag of the tail is computed as follows:

$$Drag_{tail} = \frac{1}{2}\rho V_{tail}^2 \frac{S_h}{S} S C_{D_{Tail}} \tag{4.7}$$

Where the flow velocity experienced by the tail is derived from Equation 4.4 and the wing to tail area ratio corresponds to the reference aircraft.

4.2.7.2 Parasite Drag

As mentioned before, the parasite drag of the aircraft is divided over two components. The parasite drag coefficient of the wing is equal to 0.006 and the parasite drag coefficient of the aircraft excluding the wing equals 0.0145. These values are based on a drag analysis from Torenbeek [34]. When combining the parasite drag coefficients the total parasite drag coefficient equals 0.0205 which complies with the A320 [36]. Changes in wing geometry or engine relocation will in reality effect the parasite drag, however, these effect are not taken into account.

4.3 Aerodynamic loading

The following graphs indicate the effects of the variation of geometrical parameters on spanwise lift and drag distribution. These graphs also contain typical reference data of an unwswept wing without twist. These result are of interest as the aerodynamic and structural scaling laws can be derived and explained from the distributions of the wing loading. The drag loading consists of the induced and parasite drag corresponding to the wing. On the y axis the dimension equals the local lift coefficient time the local chord length devided by the total lift coefficient times the average chord lenght. This is an indication of the relative lift distribution.

4.3.1 Angle of Attack

Figure 4.4 indicates that for increasing AOA relative more lift is generated towards the tip of the wing. The location where the different lift distributions cross each other, around 0.4 y/(1/2)/b, seems to correspond with the location of the spanwise kink. The same can be concluded for the drag distribution from Figure 4.5. Relatively more drag is produced toward the tip of the wing with increasing AOA. It is further noted that the lift reduces to zero at the tip of the wing, complying with finite wing theory.

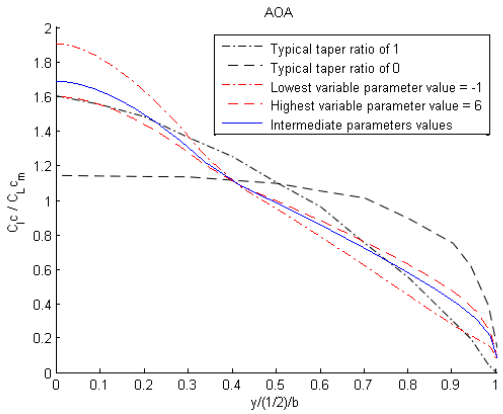

Figure 4.4: Relative lift distribution for the A320 configuration for varying angle of attack

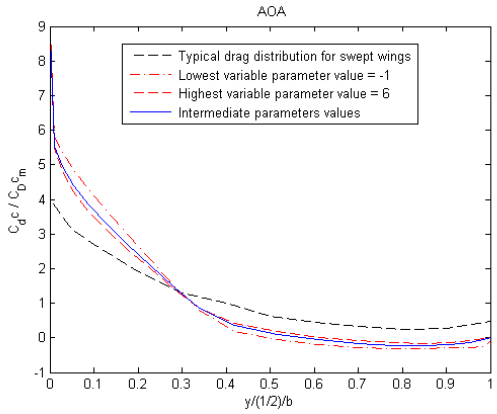

Figure 4.5: Relative drag distribution for the A320 configuration for varying angle of attack

These figures do not comply with typical trends for untwisted, untapered swept wings, it could have been expected that the lift towards the tip would be higher than at the root. This effect is discussed in the next section.

4.3.2 Sweep

The main change in lift distribution due to increasing sweep is the relative increase in lift at the root and the tip a relative decrease from the kink location towards the tip with increasing sweep angles. This effect will especially affect the bending moment of the wing as well as the span efficiency factor. The change in spanwise drag is also prominent. With increasing sweep the drag towards the tip approaches zero as a result of induced thrust. However, this decrease in drag towards the tip is compensated by the relative drag increase from the root to kink.

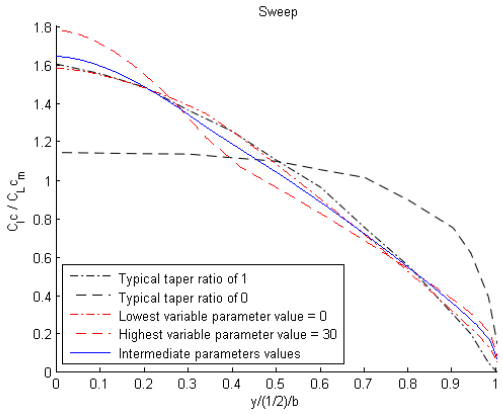

Figure 4.6: Relative lift distribution for the A320 configuration for varying sweep

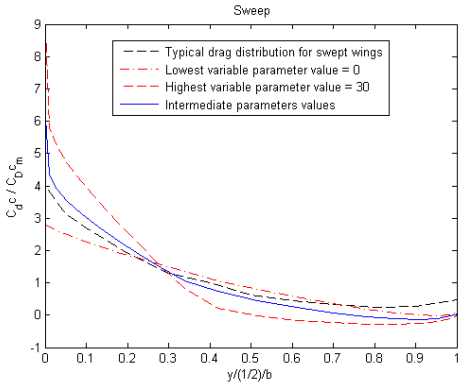

Figure 4.7: Relative drag distribution for theA320 configuration for varying sweep

Has the lift distribution does not comply with typical swept wings, the aerodynamic program is executed to find the reason for this deviation. Figure 4.8 illustrates the effect for an untwisted wing with a taper ratio of 1. It can be concluded that in this case the lift toward the tip is large than the lift at the root location.

How does this effect change if the taper ratio of the A320 is added. This effect is illustrated in Figure 4.9. If the effect of wing twist is added to the standard wing the trends of Figure 4.10 are obtained. From both graphs it can be concluded that the effect of taper is the main contributor to an increase in lift towards the root and a decrease toward the tip. The effect of spanwise wing twist has the same contribution to the lift distribution as the taper but less dominant. These effects could have been expected as they where introduced in section 4.2.5. The reason that this lift distribution does not comply with typical swept wing distribution can be connect to the prevention of premature tip stall and savings on structural weight as will be discussed in Chapter 5. This behaviour of the spanwise lift distribution will return in most of the upcoming lift distributions for different varying geometric parameters.

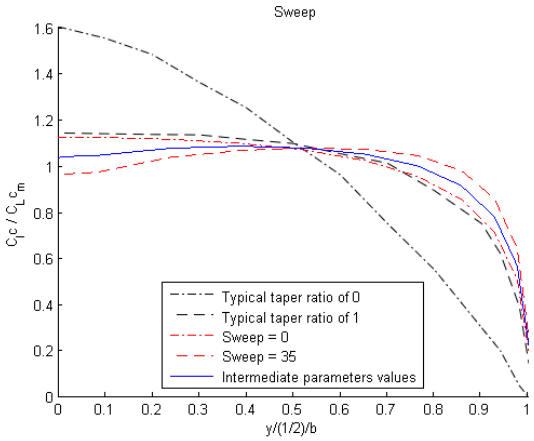

Figure 4.8: Relative lift distribution for untwisted wing with taper ratio of 1

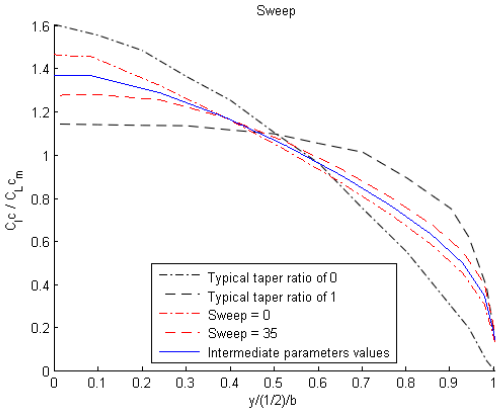

Figure 4.9: Relative lift distribution for untwisted wing wing taper ratio of 0.24

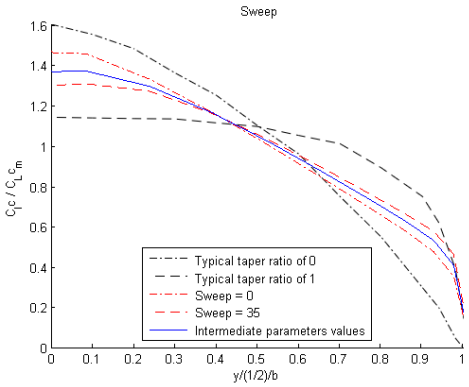

Figure 4.10: Relative lift distribution for twisted wing with taper ratio of 1

4.3.3 Taper ratio

With an increase in taper ratio the relative lift distribution at the root increases and decreases toward the tip, this can be seen in Figure 4.11 From Figure 4.12 it is noted that for high taper ratios the loading towards the centre becomes a negative instead of a drag. This is a result of the combination of sweep and wing twist. However, the drag over the remaining length of the wing increases. When validating the effect of taper on the spanwise lift distribution it is noted that the behaviour of the two reference data lines roughly corresponds to the effect of the computationally obtained data. The reason that the distribution of the obtained data does not accurately describes the reference data is due to the effect of twist in the wing.

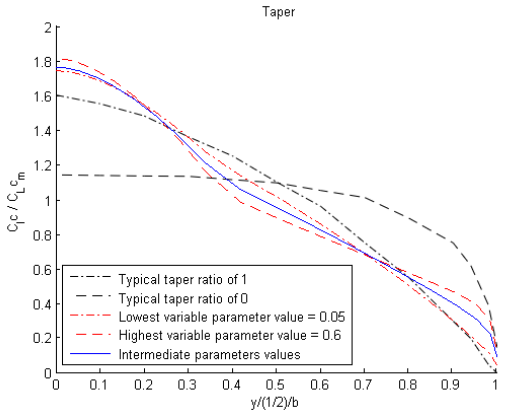

Figure 4.11: Relative lift distribution for the A320 configuration for varying taper

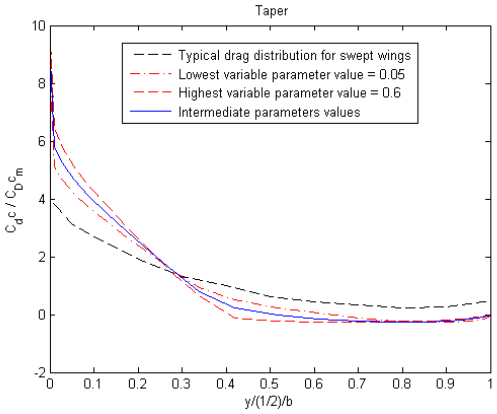

Figure 4.12: Relative drag distribution for the A320 configuration for varying taper

4.3.4 Aspect ratio

From Figure 4.13 it is clear that the lift distribution at the root increases with increasing aspect ratio. This is mainly a result of the large chord lenght from root till tip due to the 28 degree sweep. The drag distribution depicted in Figure 4.14 indicate that for small aspect ratios the loading towards the centre becomes a thrust instead of a drag. As the only varying parameter is the aspect ratio, the wing area is to remain constant, this means that both the chord and spanwise length change accordingly. It is further noted that the length from root till kink is a ratio of the the total span length and is equal to the A320.

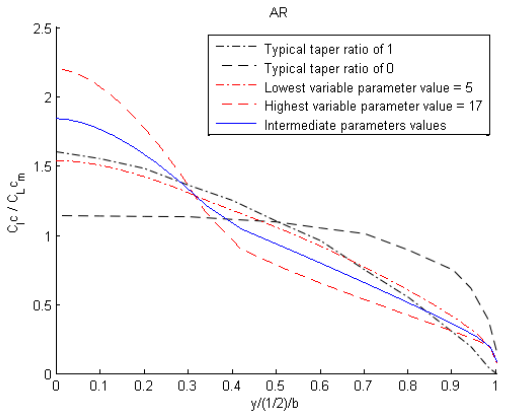

Figure 4.13: Spanwise lift distribution for the A320 configuration for varying aspect ratio

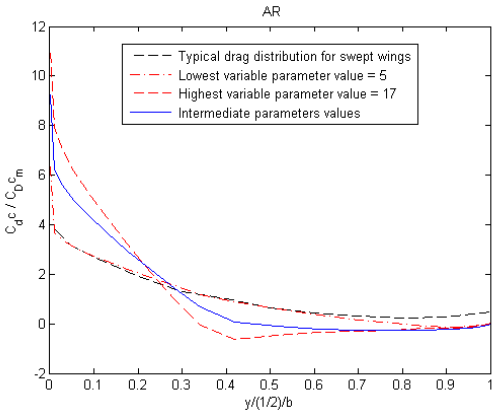

Figure 4.14: Relative drag distribution for the A320 configuration for varying aspect ratio

4.3.5 Wing Twist

The wing twist at the kink location plays a dominant roll in the change of load distribution in the spanwise direction as can be seen from Figure 4.15 and 4.16. As a result a significant change in the span efficiency factor will occur.

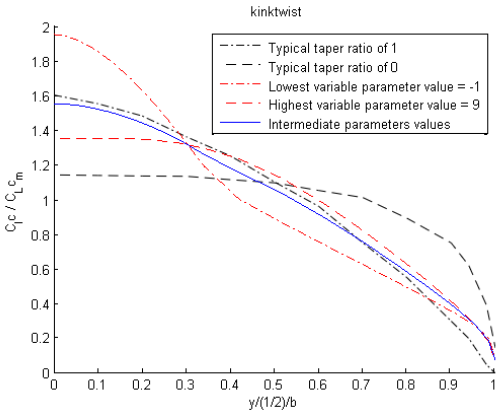

Figure 4.15: Relative lift distribution for the A320 configuration for varying kink twist. Twist at $root = 3°$, at $tip = -4°$

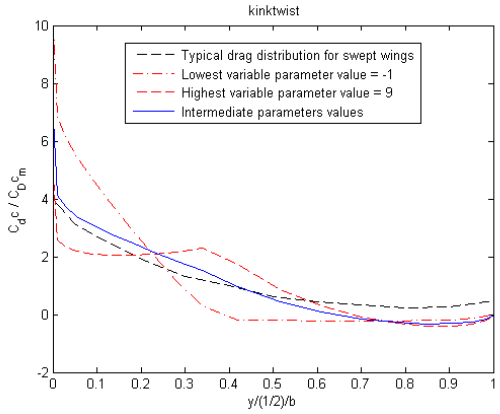

Figure 4.16: Relative drag distribution for the A320 configuration for varying kink twist. Twist at $root = 3°$, at $tip = -4°$

4.4 Performance Scaling Laws

The following scaling laws indicate the effect of varying one geometrical parameter on various aerodynamic parameters. The constant geometric parameters which are used as input are defined in Table 4.1. In most of the graphs four data points are inserted. The estimated cruise condition for the A320, the conditions corresponding to the maximum take-off weight and the weight at the end of flight. These two conditions specify the domain in which the A320 can operate during cruise and were specified in Subsection 4.2.6. The third point represents the condition at top of climb, this condition is of interest as it can be compared with the only reference data of the lift over drag of the A320 [22]. Furthermore, a trend line is submitted through the obtained data point. These data points are also plotted in the graphs and serve as verification of the derived trend line. At last, other available reference data is incorporated in the graphs and are used to validate the corresponding parameter values.

4.4.1 Varying Angle of Attack

From Figure 4.17 the first scaling law is obtained. This scaling law describes the effect of changes in the angle of attack on the lift coefficient of the aircraft. This trendline deviates from the theoretical trend for unswept infinite wings as would be expected. It does however shows very similar behavior to a typical lift curve of unswept wings. This makes the result valid. The next scaling law is the drag curve, which can be seen in Figure 4.18. Here the effect on the drag coefficient as a function of angle of attack is displayed. In the range of AOAs which are displayed the curve is almost linear, since the first term of the equation is very small. The non-linear parts outside this range are not of importance and can not be calculated exactly by the used methods. The A320 points on the curve lie within the range of reference data, which is displayed in green on the vertical axis. This validates the result. The information regarding the reference data and values corresponding to the different A320 weights have been explained at the beginning of this chapter.

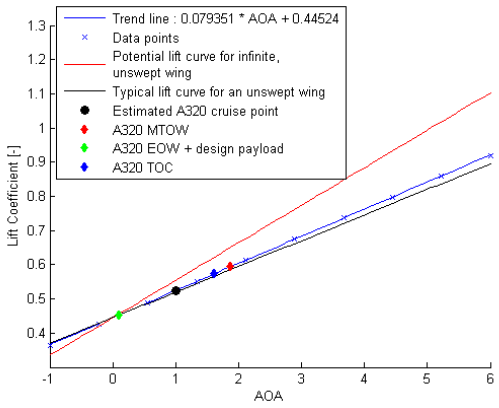

Figure 4.17: Lift coefficient for the A320 configuration with varying angle of attack

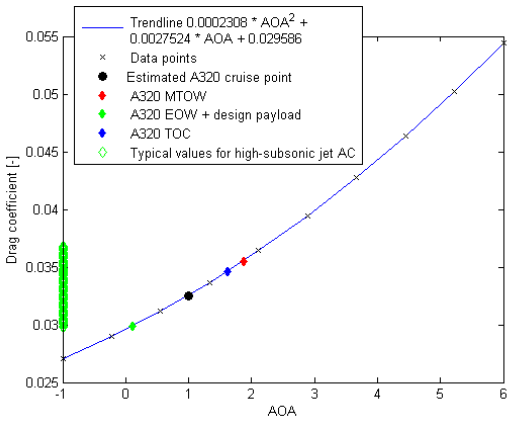

Figure 4.18: Drag coefficient for the A320 configuration with varying angle of attack

The scaling law for the Oswald factor as a function of angle of attack can be seen in Figure 4.19. The fact that this changes come from the changing lift distribution with angle of attack. On the vertical axis, the range of reference data is displayed again. The calculated values for the A320 lie within the range, which makes it acceptable to say that the result is valid. Figure 4.20 displays the variation of lift over drag ratio with angle of attack. Obviously, when the angle of attack becomes too large the drag rises significantly and efficiency reduces. The actual value of the A320 [22] is displayed in the figure, which deviates approximately 3% from the obtained curve.

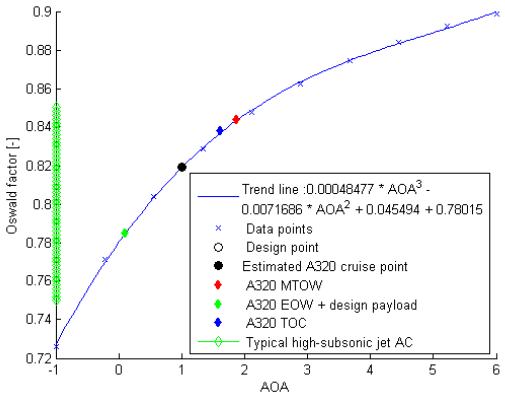

Figure 4.19: Span efficiency factor for the A320 configuration with varying angle of attack

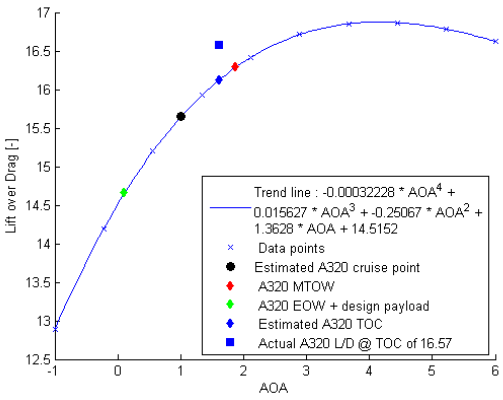

Figure 4.20: Lift to drag ratio for the A320 configuration with varying angle of attack

4.4.2 Varying Sweep Angle

Figure 4.21 shows the variation of the lift coefficient with changing sweep angle. The trend which can be seen from the curve is very obvious, increasing sweep angle beyond 10 degrees leads to a lower lift coefficient. As it was only possible to scale one geometrical parameter, it is not possible to change the lift distribution by altering the spanwise twist angles. The vertical scale is rather small, so the effects are not that significant. In Figure 4.22 the variation of drag with sweep is shown. The drag remains almost constant, since the decrease in lift is countered by a decrease in Oswald factor. This logically follows from equations 4.8

$$D_{D_i} = \frac{C_L^2}{\pi e A} \tag{4.8}$$

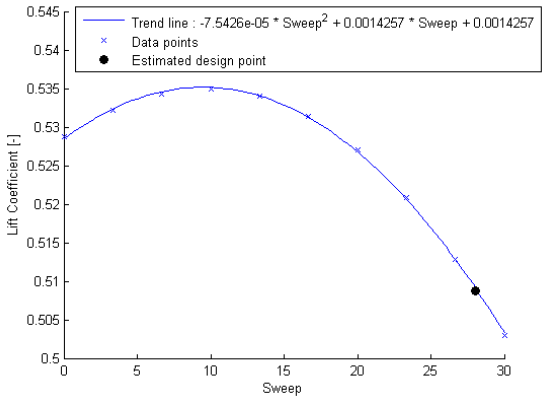

Figure 4.21: Lift coefficient for the A320 configuration with varying sweep angles

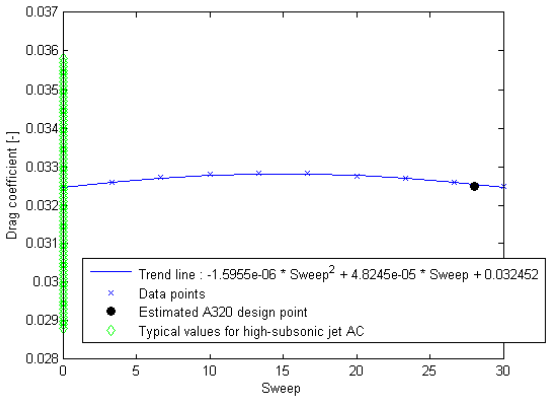

Figure 4.22: Drag coefficient for the A320 configuration with varying sweep angles

In Figure 4.23 the scaling law for the Oswald factor as a function of sweep angle can be seen. It can be noted that the efficiency is decreasing when the sweep angle is increased far beyond 20 degrees. For this particular aspect, the A320 design is not optimal. Note that this aspect may be compromised to improve the final design.

Figure 4.24, shows the variation of lift over drag ratio with sweep angle. This figure shows quite some similarities with Figure 4.23 w.r.t. the trend, however, the scale is different. The blue points in the figure indicate the estimated and actual values of the A320 at top of climb. The difference between these two is approximately 3%, which is accurate enough to validate the results.

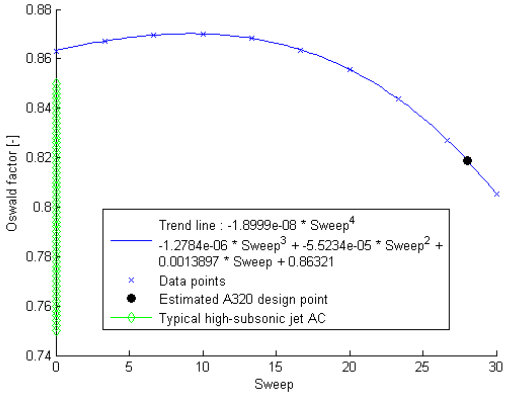

Figure 4.23: Span efficiency factor for the A320 configuration with varying sweep angles

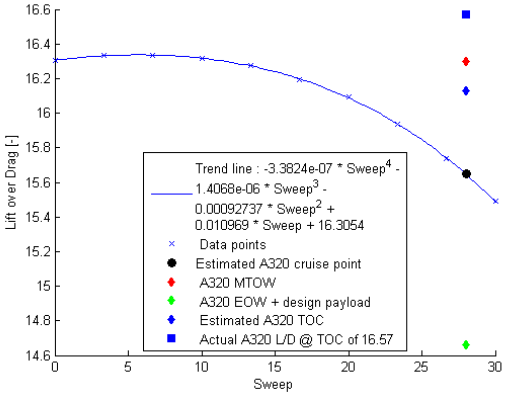

Figure 4.24: Lift to drag ratio for the A320 configuration with varying sweep angles

4.4.3 Varying Taper Ratios

In figure 4.25 the variation of the lift coefficient with taper ratio is displayed. As clearly can be seen, the relation is linear. Figure 4.26 shows a scaling law for the drag coefficient as a function of taper ratio. This graph shows the same trend as Figure 4.25, a linear decrease. However, the slope is less steep. This will result in a decreasing lift over drag ratio, as can be seen in Figure 4.28. In this figure also the actual and estimated values are shown. These, once again, differ by only 3% which validates this result.

Figure 4.27 displays the variation of the Oswald factor with the taper ratio. The taper ratio has a strong influence on the lift distribution, as can be seen in Figure 4.11, which in turn is a driving

parameter for the Oswald efficiency. The estimated cruise design point for the A320 is located at the top of the graph, which indicates that the taper ratio was optimised for the Oswald factor.

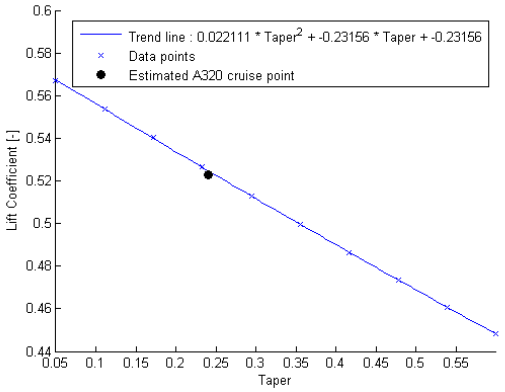

Figure 4.25: Lift coefficient for the A320 configuration with varying taper ratios

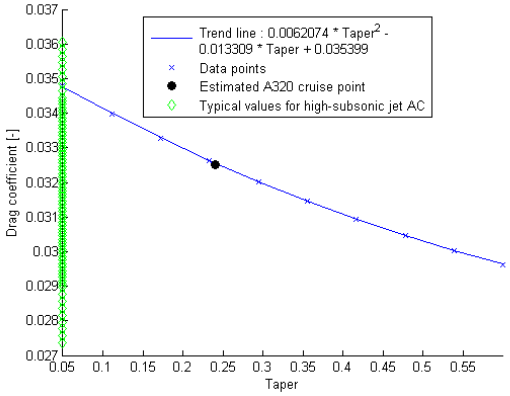

Figure 4.26: Drag coefficient for the A320 configuration with varying taper ratios

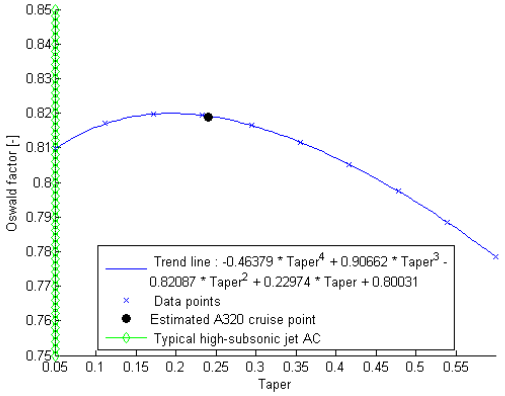

Figure 4.27: Span efficiency factor for the A320 configuration with varying taper ratios

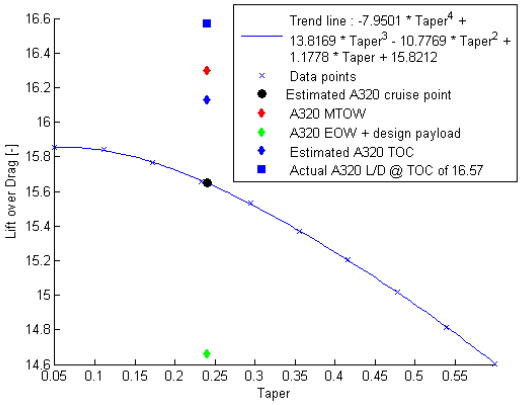

Figure 4.28: Lift to drag ratio for the A320 configuration with varying taper ratios

4.4.4 Varying Aspect Ratios

Figure 4.29 shows the scaling law for aspect ratio w.r.t. lift coefficient. The lift coefficient shows a clear increase with increasing aspect ratio, which can be attributed to the fact that lift is produced more efficiently, i.e. less lift at the tip which leads to less pressure loss. In Figure 4.13 it can be seen that the lift distribution changes, where less lift is located at the tip. However, the Oswald factor is influenced in a negative way, as follows from Figure 4.31.

When looking at Figure 4.30, it can be seen that the drag coefficient is decreasing with an increase in aspect ratio. This is obvious when looking at the formula for induced drag, where aspect ratio is in the denominator.

From the lift and drag coefficients it follows that the lift over drag ratio increases. This is made visible in Figure 4.32. The estimated and actual values of the A320 indicate again that there is a 3% difference, which was concluded to be acceptable before.

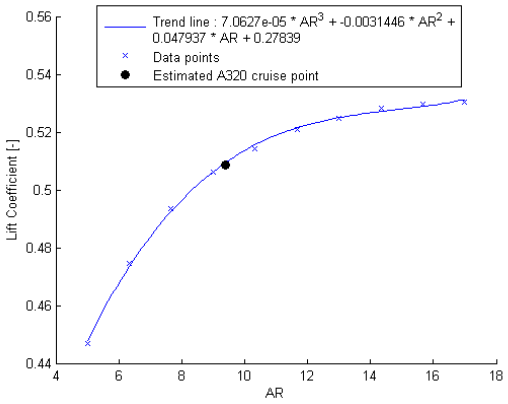

Figure 4.29: Lift coefficient for the A320 configuration with varying aspect ratios

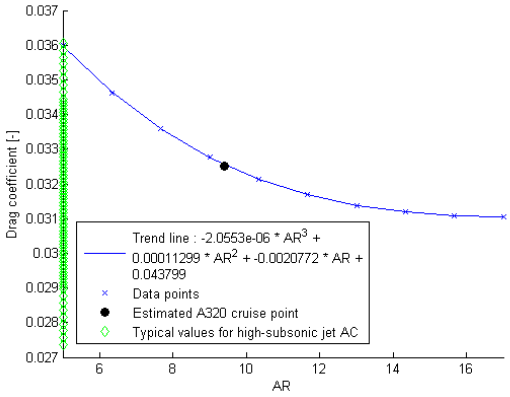

Figure 4.30: Drag coefficient for the A320 configuration with varying aspect ratios

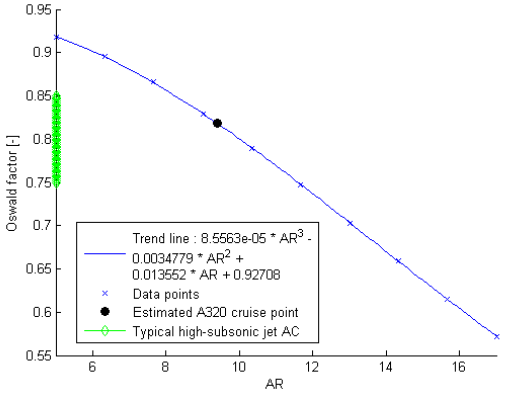

Figure 4.31: Span efficiency factor for the A320 configuration with varying aspect ratios

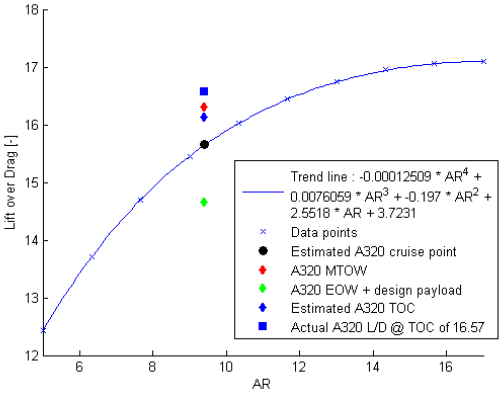

Figure 4.32: Lift to drag ratio for the A320 configuration with varying aspect ratios

4.4.5 Varying Wing Twist

Figure 4.33 shows how the lift coefficient varies with the twist at the kink location. Obviously, twist is directly linked to angle of attack and thus to lift coefficient. The relation is directly proportional. The same holds for the drag coefficient, displayed in Figure 4.34, except for the directly proportional relation. The figure shows that the relation is somewhat parabolic. It is also visible that the estimated values lie within the range of reference data, which is validating the results.

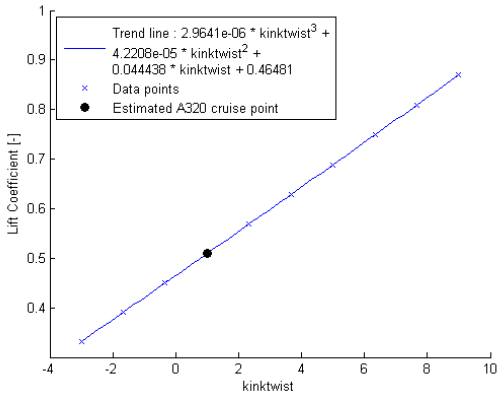

Figure 4.33: Lift coefficient for the A320 configuration with varying kink twist

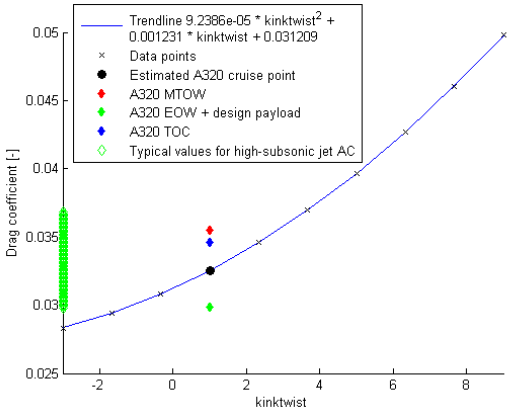

Figure 4.34: Drag coefficient for the A320 configuration with varying kink twist

The relation between Oswald factor and kink twist is displayed in Figure 4.35. The underlying reason for the increasing Oswald factor can be seen in Figure 4.15, which shows the lift distribution with changing kink twist. The shape of the lift distribution is changing in favour of the Oswald factor.

Figure 4.36 shows how the lift over drag ratio is changing with the kink twist. Up to a certain point, the lift is increasing faster than the drag. After this point, drag is increasing faster leading to an maximum lift to drag ratio at a kink twist of seven degrees.

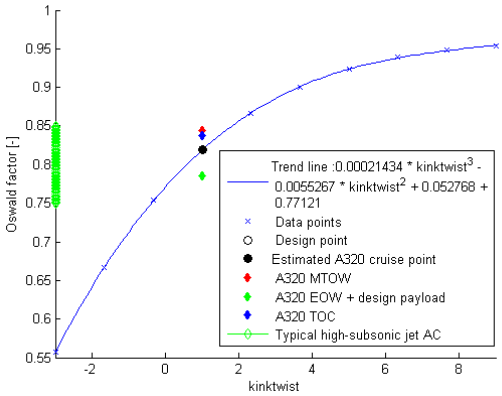

Figure 4.35: Span efficiency factor for the A320 configuration with varying kink twist

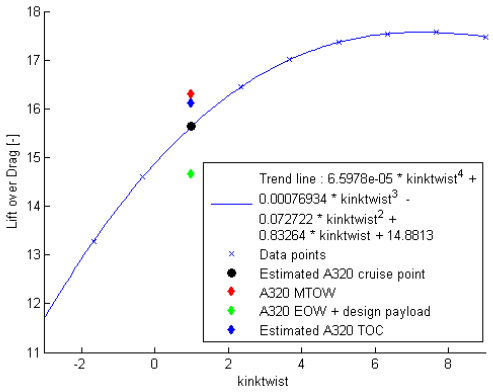

Figure 4.36: Lift to drag ratio for the A320 configuration with varying kink twist

4.5 Geometrical Scaling Laws

In the previous section the effects of changing one geometric parameter were presented. In this section the effects on the lift to drag ratio by varying two geometrical parameters are presented. Besides the effect that these geometric parameters have on the lift to drag ratio, also the trend for optimum lift to drag ratio for the two geometric parameters is presented. These trends will be the scaling laws. To give an indication of the absolute values the estimated cruise condition of the A320 is inserted, this point is visualised in the graphs by means of a yellow diamond. The graphs on the left side represent the reference aircraft with the following constant parameters: Mach 0.78 and a leading edge sweep of 28 degrees. The graphs on the right side represent the new design: Mach 0.72 and a leading edge sweep of 17 degrees. By illustrating the two scaling laws it can be

concluded whether or not a scaling law can be applied over a range of varying Mach and sweep numbers. The legend which applies to the graphs in this chapter is indicated in Figure 4.37. Beside this information, all graphs contain a legend with their corresponding scaling law.

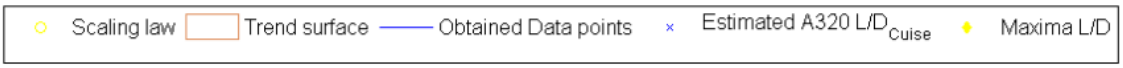

Figure 4.37: Scaling law legend

4.5.1 Angle of Attack as a Function of Sweep

Figure 4.38 presents the trend between AOA and sweep angle and the lift to drag ratio. As wave drag is not computed by AVL the results from both graphs would indicate the same trend. Therefore one graph is presented which is assumed to be valid for both Mach numbers. It also contains the scaling law for the optimum angle of attack for different sweep angles. The scaling law indicates that the optimum angle of attack is depending on the sweep angle. Also, from the trend surface it can be concluded that the lift to drag ratio decreases for higher sweep angles. At this point, however, it is noted that the graph might deviate from reality. As in reality the drag would significantly increase due to a decrease in critical Mach number as the angle of attack increases. This is a result of the compressibility effect and is not sufficiently taken into account. Hence, this trend surface and scaling law do only apply for aircraft which are not approaching the critical Mach number. This constraint also applies to the figures in the next subsection, Subsection 4.5.2.

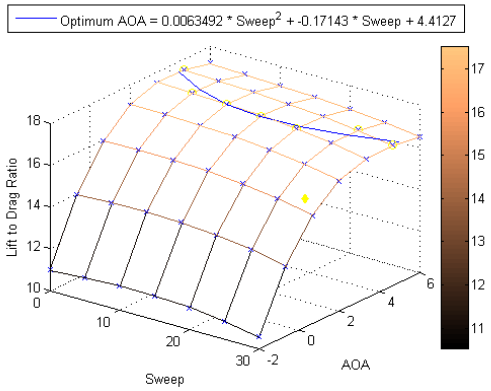

Figure 4.38: Lift to drag ratio for the A320 configuration with varying AOA and sweep

4.5.2 Angle of Attack as a Function of Aspect Ratio

In contrary to the previous trend surface, the trend surface of Figure 4.39 and 4.40 do not show exactly the same correlation in the lift to drag ratio. It does indicate that, regardless of the angle of attack, the lift to drag ratio increases with increasing aspect ratio. At the same time it is concluded that the increase in lift to drag ratio stagnates for high aspect ratios and high angles of attack. The scaling laws for the angle of attack as a function of the aspect ratio differ from each other. With increasing aspect ratio it is preferred to also increase the angle of attack to obtaind the most vavarable lift to drag rato. Increasing the AOA will result in a higher lift coefficient which might be unwanted. However, as this graph only allows two geometrical parameters to be varied, the effect of decreasing the wing area or flying at a higher altitude are not taken into account.

This effect is expected as it corresponds with the obtained data from the Sections 4.3 and 4.4. An increasing in aspect ratio elongates the lift distribution and therefore decreases the the span efficiency factor. While an increase in angle of attack increases the strength of the lift distribution towards the root and hence increases the span efficiency factor. It is once more noted that this trend surface and scaling law do only apply for aircraft which are not approaching their critical Mach number.

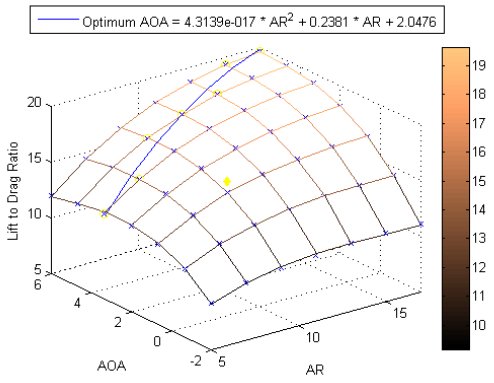

Figure 4.39: Lift to drag ratio for the A320 configuration with varying AOA and aspect ratio

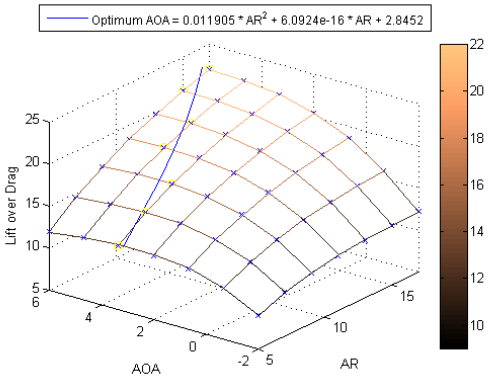

Figure 4.40: Lift to drag ratio for the new design with varying AOA and aspect ratio

4.5.3 Angle of Attack as a Function of Taper Ratio

Figure 4.41 and 4.42 give the indication of the lift to drag ratio for varying taper ratios and angles of attack. At first sight these trends seem to be equal. However, small changes are noted in the gradient of the lift to drag ratio with taper ratio, this is a result of the change in sweep angle of the two designs. The most interesting finding is that at low angles of attack it is most beneficial to have a low taper ratio while at higher angles of attack the most beneficial lift to drag ratio is reached for larger taper ratios. This opposite behaviour is a result of the spanwise wing twist in combination with the chord length, of which the spanwise chord length is depending on the taper ratio. When analysing the scaling laws it is evident that the effect of sweep affects the optimum AOA with taper ratio. The trend between the two scaling laws indicate that with decreasing sweep angles the optimum AOA becomes independent of the taper ratio.

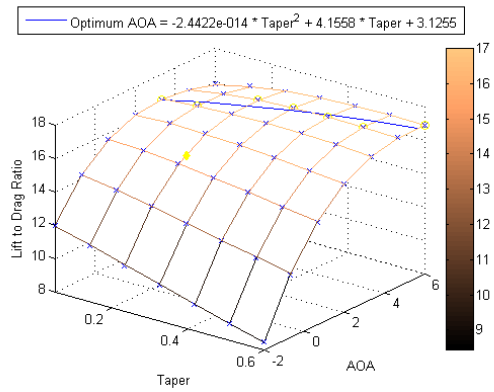

Figure 4.41: Lift to drag ratio for the A320 configuration with varying AOA and taper ratio

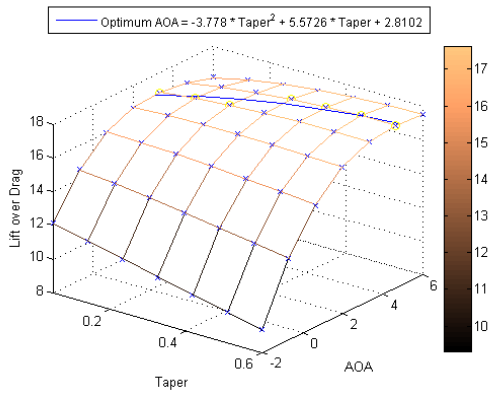

Figure 4.42: Lift to drag ratio for the new design with varying AOA and taper ratio

4.5.4 Aspect Ratio as a Function of Sweep Angle

Figure 4.43 describes the correlation between the sweep angle, the aspect ratio and the lift to drag ratio. An interesting finding is that the lift to drag ratio converges to a maximum for high sweep angles and increasing aspect ratio while for small sweep angles the lift to drag ratio increases more or less linear with aspect ratio.

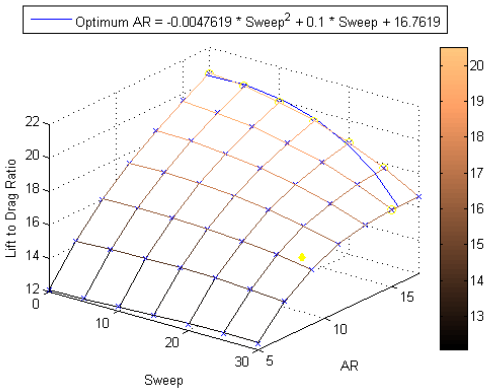

Figure 4.43: Lift to drag ratio for the A320 configuration with varying aspect ratio and sweep angle

4.5.5 Aspect Ratio as a Function of Taper Ratio

The Figures 4.44 and 4.45 can be considered one of the more interesting scaling parameters, as the induced drag is primarily depending on the span efficiency factor and the aspect ratio of which the taper ratio is of great influence. This is seen in Figure 4.27. It is concluded that the trend surface of the two designs differs in shape as well as in absolute values. The lift to drag ratio for the A320 has two local minima for high taper ratio while the new design only indicates one minimum. For the A320 configuration with a sweep of 28 degrees a maximum lift to drag ratio at high taper ratios is found within the domain of the aspect ratio. The opposite is true for the new design which has a sweep angle of 17 degrees, this configuration indicates that the maximum value occurs at the maximum aspect ratio available in the domain. From these finding it is concluded that for decreasing sweep angles the maximum achievable lift to drag ratio increases.

It is clear that it is impossible to apply one scaling law on aspect ratio and taper ratio for different sweep angles. This is one of the constraints of a three dimensional scaling law.

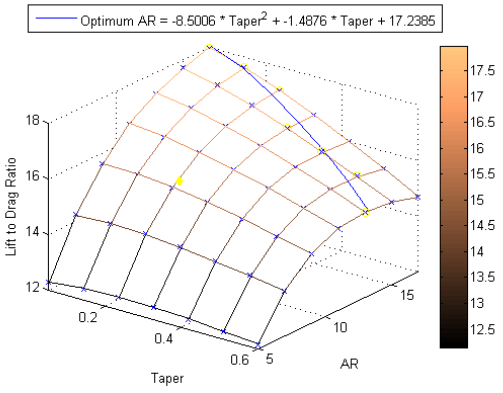

Figure 4.44: Lift to drag ratio for the A320 configuration with varying aspect ratio and taper ratio

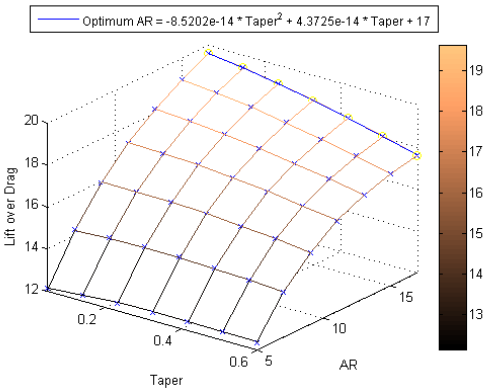

Figure 4.45: Lift to drag ratio for the new design with varying aspect ratio and taper ratio

4.5.6 Taper Ratio as a Function of Sweep Angle

Figures 4.46 and 4.47 indicate the effect on lift to drag ratio of taper ratio and sweep angle for the two different flight speeds. It can be directly concluded that the effect of flight speed does not influence the trend surface nor the scaling law. The lift to drag ratio decreases strong for high sweep angles in combination with high taper ratios. This is a result of the decrease in span efficiency and

has already been discussed in Section 4.4. The trend described by the scaling law complies with the trend observed of current aircraft.

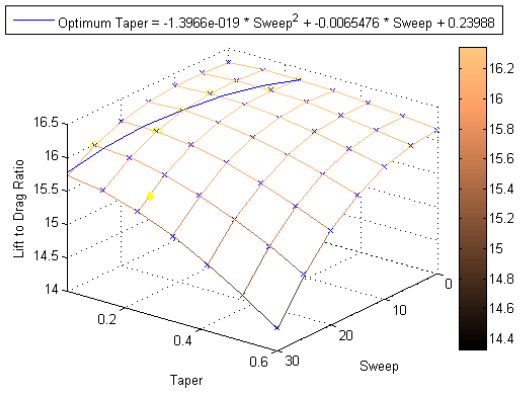

Figure 4.46: Lift to drag ratio for the A320 configuration with varying taper ratio and sweep angle

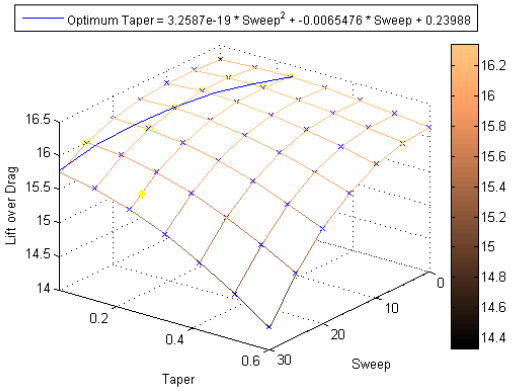

Figure 4.47: Lift to drag ratio for the new design with varying taper ratio and sweep angle

4.5.7 Taper ratio as a Function of Kink Twist

It is emphasised that the reader is conscious of the following: This section contains scaling laws based on variable kink twist which, at this point, is not taken into account by the structural weight analysis nor in the multi-disciplinary scaling laws. However, from an aerodynamic point of view this is an interesting parameter as it is able to increase the lift to drag ratio quite easily compared to the previous discussed parameters.

In Subsection 4.4.3 and 4.4.5 the effect of taper and the spanwise wing twist at the kink location were discussed, from this it followed that a decrease in taper ratio and an increase in kink twist is beneficial for the span efficiency factor. However, this effect does not completely comply with the findings in Figure 4.46 and 4.47. From these figures it is concluded that the decrease and increase in taper ratio and kink twist, respectively, only have a positive contribution to the lift to drag ratio up to a certain boundary. This boundary is specified by the scaling laws. Further, it is noted that the scaling laws corresponding to the two designs differ from each other. Hence, the scaling of taper and kink twist for different sweep angles requires multiple scaling laws. The following twist angles correspond to the two designs: at $root = 3°$, at $tip = -4\circ$ and are defined w.r.t the fuselage.

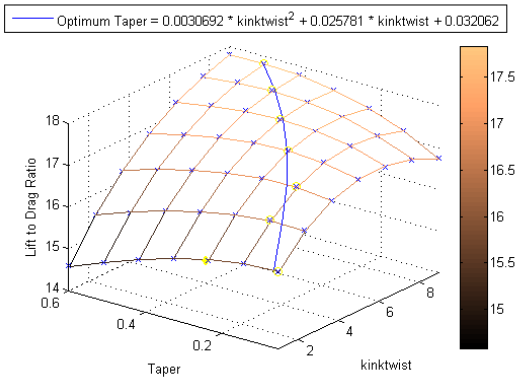

Figure 4.48: Lift to drag ratio for the A320 configuration with varying taper ratio and kink twist

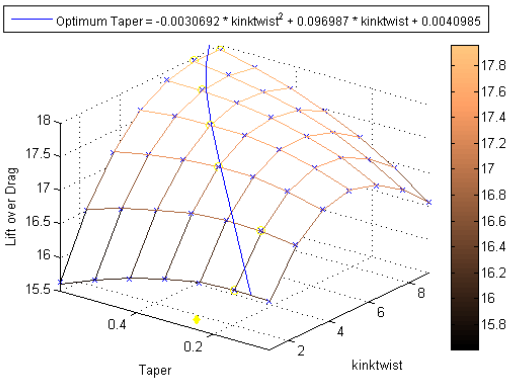

Figure 4.49: Lift to drag ratio for the new design with varying taper ratio and kink twist

4.5.8 Kink Twist as a Function of Aspect Ratio

Figure 4.50 and 4.51 describe the effect of the wing twist in the spanwise direction at the kink location and the aspect ratio on the lift to drag ratio. From these figures it is concluded that the surfaces of the two graphs show the same trend with changing twist and aspect ratio. The effect of the twist for low aspect ratio of the two designs show little to no difference on the effect of lift to drag ratio. However, for high aspect ratios the lift to drag ratio of the new design, with a lower sweep angle, increases. This is valid for the total domain of the twist at the kink location.

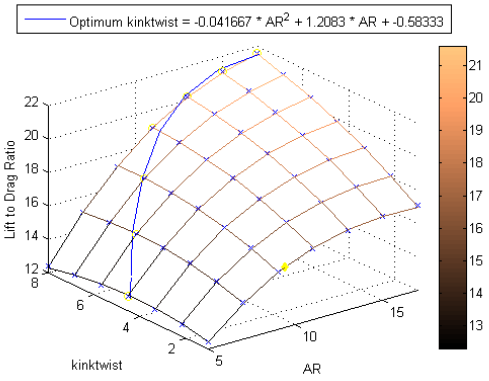

Figure 4.50: Lift to drag ratio for the A320 configuration with varying kink twist and aspect ratio

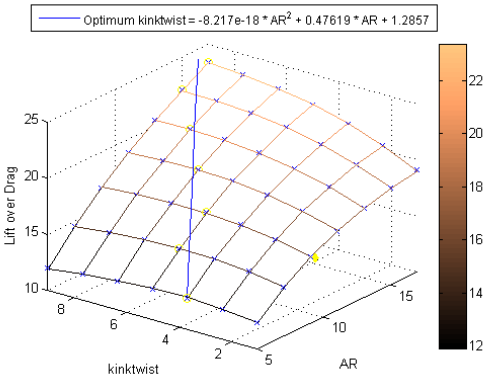

Figure 4.51: Lift to drag ratio for the new design with varying kink twist and aspect ratio

4.5.9 Kink Twist as a Function of Sweep

From Section 4.4 it was concluded that an increasing kink twist and a decrease in sweep angle led to an increase in the lift over drag ratio. However, from Figure 4.52 and 4.53 it is concluded that these effects do not hold for the combination of the two parameters. As can be seen from both figures, the lift to drag ratio actually decreases for the combination of low sweep and high twist angles. Furthermore, the scaling law indicates that it is preferable to have an increase in twist with increasing sweep angles, this complies with the observations from 4.52 and 4.53. Finally, it is also noted that the effect of flight speed does not influence the scaling law nor the trend surface.

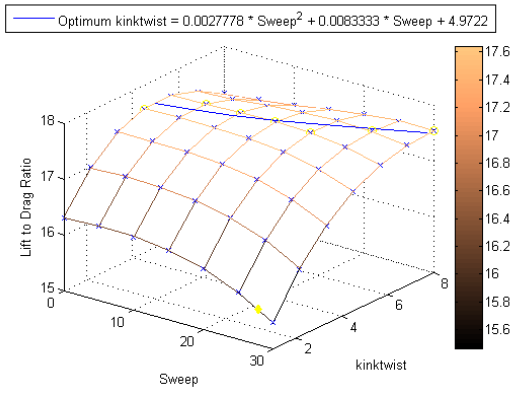

Figure 4.52: Lift to drag ratio for the A320 configuration with varying kink twist and sweep angle

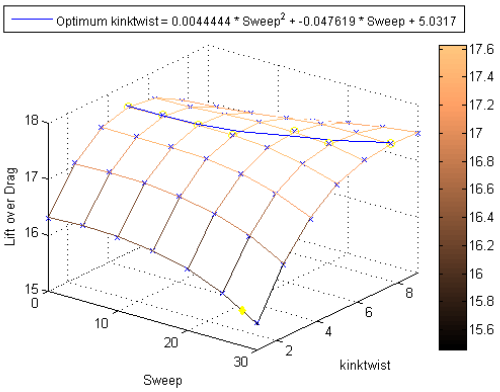

Figure 4.53: Lift to drag ratio for the new design with varying kink twist and sweep angle

4.6 Verification of the Aerodynamics program

As AVL is a commonly used program and it is therefore assumed verified. To verify the complete aerodynamic module, the program is executed for three different cases. The results which will be obtaind will be compared to three cases which have been manually computed by AVL alone. The wing geometry used for this verification is the standard A320 geometry as described in section 4.2.1. To obtain three different result the aspect ratio will be 5, 9, 13 and 17. The lift created by the horizontal tail is not taken into account as AVL does not derive these aerodynamic aspects. The results of the aerodynamic program are depicted in Figure 4.54, the result directly obtained from AVL and the data point from Figure 4.54 are summerized in Table 4.2. From this it can be concluded that the aerodynamic program is verified.

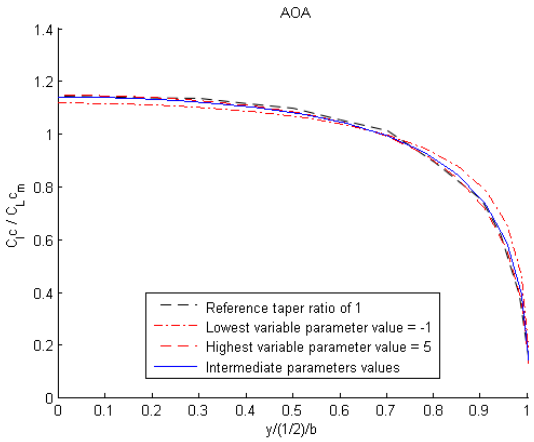

Figure 4.54: Lift coefficient as a punction of aspect ratio

Table 4.2: Verification aerodynamic program list

Aspect ratio	AVL value	Program value
5	0.463	0.463
9	0.5222	0.5222
13	0.5408	0.5408
17	0.5464	0.5464

Figure 4.54 does not only indicate the obtained result for the lift coefficient but also the polynomial trend line, since the trend line approaches the data points it is concluded that the derivations made for the trend line are verified. Beside this trend line, also all other graphs in this chapter contain data points and polynomial trend lines and polynomial scaling laws. As all these figures indicate that the polynomial trend approaches the obtained data points accurately.

4.7 Validation

To validate the mathematical part of the model, the program is executed once for the most basic wing geometry: Zero sweep, aspect ratio of 10 and zero change in spanwise twist. The angle of attack is varied from minus one degree to 3 degrees, an air density of $0.38 kg/m^3$ corresponding to a flight altitude of 3500 feet and a Mach number of 0.78. Figure 4.55 indicate the spanwise relative lift distribution. The figure clearly indicate that the reference lift [34] distribution corresponds with the obtained results.

As decreasing the taper ratio can significantly affect the shape of the vortex panels towards the tip in a negative way, it should be verified that this does not lead to invalid results. Improper vortex panel shapes will lead to strong local fluctuations in the lift and drag distributions. When these distributions are examined in Figure 4.11 it can be concluded that no fluctuations are present. Hence, the domain over which the taper ratio is examined leads to proper results.

A second validation method is performed by executing the program with the A320 characteristics and comparing the obtained aerodynamic performance data with the available A320 and typical high speed passenger jet aircraft. Table 4.3 summarises this validation results. It is noted that the obtained data lies within the reference range or shows a marginal deviation from the A320. With this observation, together with the validation performed in the previous mentioned chapters, it is concluded that the model solves the correct aerodynamic aspect. However, also a analyses is performed on the Boeing 747-100. This indicates quite large deviations with the reference data [34]. These result might show a larger deviation as a result of incorrect assumption on the wing and total aircraft geometrical lay-out. From this it can be concluded that the aerodynamic analysis is only applicable to the A320.

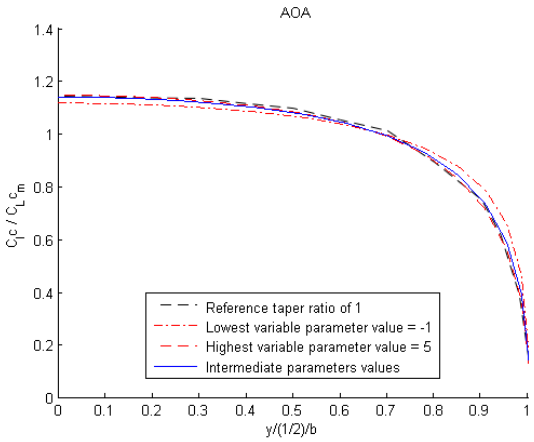

Figure 4.55: Spanwise lift distribution

Table 4.3: Model validation list

Parameter	A320 program value	A320 Reference value	Figure	B747 program value	B747 Reference value
L/D	16.1 (TOC)	16.7 (TOC) [22]	4.20	13 (max)	17.6 (max) [22]
Oswald factor	0.82	0.75 - 0.85	4.19	0.83	
Drag coefficient	0.033	0.029 - 0.037	4.18	0.043	

4.8 Discussion

The main conclusion is that it is impossible to apply one scaling law to multiple change geometrical parameters, this is one of the constraints of a three dimensional scaling law. Therefore the main computational program should incorporate multidimensional scaling laws.

It is further concluded that the cruise point of the A320 does not comply with the optimum lift to drag ratio and the corresponding geometrical parameters. Hence, significant improvement on the lift to drag ratio can be obtained, from an aerodynamic point of view, by scaling the geometric parameters. What the result of the scaling laws are in combination with the other design requirements and components will be presented and discussed in Chapter 11.

It is also concluded that the optimisation of the lift to drag ratio based on most of the trend surfaces indicate that both geometrical parameters should be scaled to the boundaries of the scaling law. This might indicate that there is space for further improvement if the scaling laws would have been designed based on a large geometrical parameter domain.

With the three dimensional scaling laws a preferable design for the new aircraft, purely based on aerodynamic performance and the constraint of varying only two parameters, can be designed. The parameters and values for such a design are listed in Table 4.4.

Table 4.4: Aerodynamic Design Options for Sweep of 17 and Mach cruise nr. of 0.72

Parameters	**Parameter 1**	**Parameter 2**	**Optimum $\frac{L}{D}$**	**Figure**
AOA : Taper	4	0.6	18	4.42
AOA : AR	6	17	23	4.40
Taper : AR	0.05	17	20	4.45
Wing Twist : Taper	8	0.6	18	4.49
Wing Twist : AR	8	17	23	4.51
Sweep : Taper	17	0.14	16	4.47
Sweep : AR	17	17	19	4.43
Sweep : AOA	17	4	17.5	4.38
Sweep : Wing twist	17	6	17.5	4.53

The minimum and maximum possible geometrical parameter values are of course constrained by the domain and range of the scaling laws. If these constraints would not be applied one can expect that the aspect ratio would go to infinity for an optimum lift over drag ratio. A user of the scaling laws should not insert parameter values which exceed the domain for which the laws where designed, as this can lead to inaccurate or even invalid results.

Chapter 5

Structural Design

One of the most important aspects that has to be considered when scaling an aircraft is the structural design. The structure of the aircraft is very important as it determines whether the aircraft is able to sustain the loads it has to endure throughout its life. Furthermore, it is important to optimise the structure as it has a very large influence on the total weight of the aircraft. As such, this chapter focuses on two main aspects of the aircraft. The structural design is considered and the different weight estimations of the aircraft are discussed.

First, a general method is described which is used by the model to scale the different weights of the aircraft. Next, the structural design methodology is described for the wing, the horizontal and vertical stabiliser and the fuselage. After that, initial scaling laws are described which give an indication how the weight of the different wing types should change based on multiple parameters. Followed by finding more detailed scaling laws by running the individual modules a large number of times. However, all of these data are of no relevance if they are not verified and validated to represent reality. As such, this chapter shall also describe the verification and validation of the structure. Finally, the structural result will also be analysed and recommendations will be given based solely on structures.

5.1 Weight Scaling Methods

The aircraft weight will be scaled based on three aspects. Certain weights change with the structural weight of each element. Scaling based on structures will be discussed in more detail later in this chapter. However, besides the structure, certain elements will also scale with the Maximum Take-off Weight (MTOW). Furthermore, there are elements that scale with the engine and the fuel load. These are calculated separately. These weights are discussed in Chapter 6.

The weight of the aircraft that is calculated is based on scaling. Instead of estimating the exact weight of each element, an estimate is made for how much the weight changes due to a certain effect. For example, suppose the fuselage structure module estimates a weight of ten per cent. Now suppose that the actual fuselage structural mass of the A320 is 9000 [kg]. This means that a fuselage structural weight of 9900 [kg] (ten per cent higher than the actual A320) can be incorporated for the new design.

5.1.1 Weight of the elements

The aircraft can be broken down into five main elements. These parts are the fuselage, wing, engine, horizontal and vertical stabiliser. The sum of the weights of these elements results in the operating empty weight (OEW). Including the payload and fuel will then lead to the MTOW. The weight of each element has to be incorporated for scaling purposes. Since the elements will scale, the weights will be divided into two categories;

- The fixed weight which stays constant and is irrespective to change even when scaled.
- The variable weight: the weight which changes due to scaling.
  - Structural: weight varying due to changes in structures.

– MTOW: weight varying due to changes in MTOW.

As can be seen, the variable weight will be further subdivided into a weight varying with structures and a weight varying with MTOW. These weights have been estimated using the subsystems of the aircraft. A weight breakdown for the A320-200 [37] is used for further estimations. The locations of these sub systems are estimated using for example maintenance photos. Most of the sub systems can be attributed to just one of the elements of the aircraft. Examples of such elements are the APU [38] and payload. However, others like the hydraulics are laid out through multiple elements of the aircraft [39]. These weights have to be accounted for. Therefore, the weight is split up over the elements according to their contribution. Also, whether these systems will scale or stay relatively constant is determined.

The A320 data [37] is taken from a different source as the usual Airbus datasheets [40]. Since the OEW differs slightly between both datasets, it has to be accounted for. The difference in weight is distributed proportional over the subsystems. The ratio is obtained from the relation between the two OEW's. This ratio is multiplied with every subsystem except for the payload and fuel, thus resulting in the same OEW. Every element weight has been determined. The percentage of the structural weight that is fixed is estimated. Hence, the fixed and variable weights of the elements can be determined. The results are shown in Appendix B.

5.2 Material properties

At the Mid Term Review presentation the allowable design stress in the pressure cabin under cruise conditions was set to 286 [MPa]. This limit was set after a study and calculations on allowable fatigue stress. The allowable stress for the rest of the aircraft structure at maximum load factor then was equal to: VMSy/1.5 = 300 [MPa], this limit was not set by a fatigue limit. The feedback from the tutors and coaches on these allowable stresses was that 286 [MPa] for the pressure cabin under cruise conditions was way too high. From their experience they said that this value should be closer to 100 [MPa] instead. Furthermore they recommended the Aerospace Materials department of the TU Delft (ASM TU Delft) for further advice. This was done and the acquired knowledge and understanding about materials resulted in a change of the calculated allowable stresses, which is explained in the rest of this chapter.

The allowable stresses due to fatigue are based upon $VMSN_L$ curves, which in turn are based on tests with coupons. Coupons are test pieces with an uniform stress distribution. The use of a lower limit curve in an S-N diagram is valid to design for the entire lifetime of a coupon. However, fatigue on a coupon is different than in an aircraft. This is caused by at least: stress concentrations, corrosion and scratches on the surface. Due to these and more effects in an aircraft a crack might appear much earlier than in a coupon. Therefore the use of the lower limit in a $VMSN_L$ diagram becomes invalid. Crack growth calculations can predict life expressed in number of cycles after a crack initiation. For the sake of brevity these calculations are not considered in this project.

Instead of performing the more complex crack propagation calculations, design experience from the ASM TU Delft has been used. Their theory states that calculations on the actual fatigue life with crack propagation, can be replaced by a calculation with only $VMSN_L$ diagrams. This theory is allowed to be applied in initial design stages, which require less accuracy on the fatigue life. However to do that one needs to multiply the total amount of loading cycles during the lifetime with a factor between 4 and 8. For the SCALAIR project a factor of 6 was chosen, this results in 240000 cycles to be taken into account. Furthermore, twice the pressure cabin stress during cruise should be taken into account during the calculation.

When taking into account those recommendations, the calculation of allowable cruise operating stress for the pressure cabin also arrives at around 100 [MPa]. This is when aluminium alloys $2024-T3$ or $2024-T351$ are used in the pressure cabin. The fatigue expert from the ASM TU Delft confirmed that 100 [MPa] is a common value used by aircraft designing companies. However in this initial design phase, there is insufficient (test) data about the material. This makes it hard to calculate the exact allowable stress values. The 100 [MPa] will be used to design the material thickness in the pressure cabin. This allowable stress value is considered to be sufficiently verified,

since multiple experts in this field recommended this value for the project. Additionally the fatigue expert from the ASM TU Delft looked at the fatigue calculation approach and confirmed that this is correct.

The calculation of the fatigue stress in all parts of the aircraft except the pressure cabin was also performed again, since the new calculation approach has different fatigue criteria. This generally results in a lower allowable stress. The material used in the fatigue calculation for the aircraft structure, excluding the pressure cabin, is also aluminium alloy $2024 - T3$ or $2024 - T351$. The resulting allowable stress at maximum load factor of $n = 2.5$, due to fatigue criteria, is 308 [MPa]. However for these aircraft components fatigue is not the dominating allowable stress. Since at no load factor it is allowed to exceed the yield stress of VMSy=270 [MPa].

Summarising, the fatigue calculation methodology and results presented in the MTR were correct for the first part of fatigue lifetime, where no cracks have initiated yet. However to calculate fatigue lifetime, crack initiation and propagation should be taken into account as well. This has been done and the obtained allowable stresses have been verified and validated with the help of experts from the ASM TU Delft.

5.3 Structural Design Methodology

In order to find the structural weights of each component, it is important to model the structural elements in some manner. How this is done will be explained in the following section.

5.3.1 Wing Structure

The wing structure is the most dominant structure of the entire aircraft. As such, it is important to model the wing structure accurately. As a general rule, the wingbox weight consists of around 70% of the entire wing structural weight [41]. As such, modelling the wing box can be used to scale the entire wing structural weight. First, a program will be generated that describes the entire wing box structure. Next, this program can be used to generate detailed scaling laws for the wing structure. The wing planform and structural lay-out which are considered are illustrated in Figure 5.1, where the root is located in the center of the fuselage.

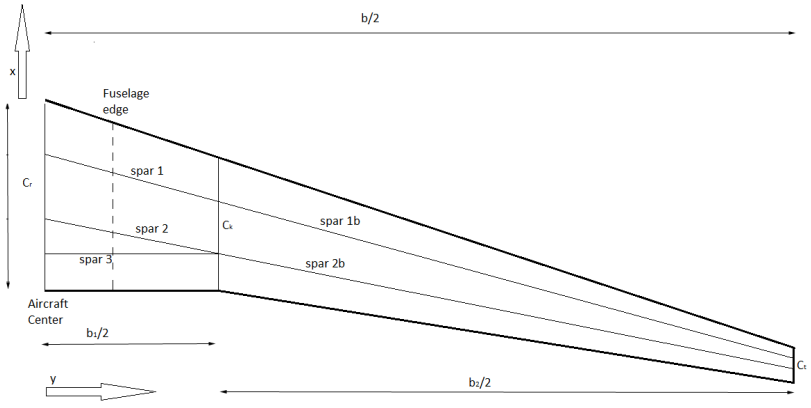

Figure 5.1: Wing planform and spar lay-out

First of all, it is important to calculate the planform and all different dimensions of the wing box. The lay-out of the wingbox is derived from the Airbus A320 [42]. This lay-out includes the rib pitch and count, stringer pitch and count and spar locations. Next, the different loading cases have to be calculated. A loading factor as calculated in Chapter 6 is incorporated. The loading cases that are considered are as follows:

1. Upward bending moments due to lift and weight.

2. Bending due to thrust and drag.
3. Upward shear force due to lift and weight.
4. Shear force due to thrust and drag.
5. Torsion.

Once the loading cases have been calculated, it becomes possible to design the geometry based on the failure cases. The failure cases which are considered are as follows:

1. Von Mises Stress
   (a) Normal stress due to bending about the longitudinal axis.
   (b) Normal stress due to bending about the vertical axis.
   (c) Shear stress in vertical direction.
   (d) Shear stress in longitudinal direction.
   (e) Shear stress due to torsion.
2. Skin buckling due to compression.
3. Stringer Euler buckling due to compression (incorporating both the stringer and skin).
4. Stringer flange buckling due to compression.

These failure cases are then used to determine the wing box geometry. The wing is optimised such that all elements of the wing fail simultaneously at failure load. This is done in order to keep the weight as low as possible. How the module calculates the wing structure is as follows:

1. Loading diagrams are calculated based on the lift and drag distribution gotten from aerodynamics.
2. Section parameters are calculated (loading, enclosed area, stringer count...).
3. All thicknesses are estimated at three cm thickness.
4. VMS at all critical locations are calculated.
5. The model calculates the ratio of the VMS/VMS_{fail} at the critical locations, where VMS_{fail} is the allowable stress.
6. The local thickness is multiplied by VMS/VMS_{fail}.
7. The new stringer geometry is calculated based on stringer colum buckling (including skin) and stringer flange buckling.
8. The model iterates from step four untill it receives sufficient accuracy.
9. The cross-sectional area is calculated.
10. The model moves to the next wing section and repeats steps two to nine. This step is iterated untill all sections have been calculated.
11. The wing calculates the material volume.
12. The volume is multiplied with the density to calculate the wing box mass.
13. The wing structural mass is found by dividing the wing box mass by 0.7 [42].

Once the wing module is complete, it can be used to generate scaling laws. This is done by running the wing module a large number of times for a large number of combinations, depending on the scaling law that is to be found. Once these values have been found, the MATLAB function *polyfitn* is used to generate a polynomial scaling law through all of the points that have been calculated by the analytical module. In case of scaling laws that only depend on one parameter, the MATLAB function *polyfit* is used.

For a more extensive theoretical description, the Mid Term Review can be read [17].

5.3.2 Horizontal and Vertical Stabiliser

For the horizontal and vertical stabiliser a simpler approach is used with respect to the wing structure. This is because the empennage has a much smaller effect on the total weight of the aircraft. Furthermore, the changes with respect to geometry (excluding area) are much smaller than those for the wing. As such, it is assumed that the shape of the lift, drag and torque distributions stay the same. Furthermore, it is assumed that the maximum loads on these stabilisers vary with lift which boils down to the following parameters: $C_{L_{max}}, \rho, V$ and S.

The weight of the horizontal and vertical stabiliser can then be found using scaling laws. First of all, the scaling law presented in Figure 4.21 shows the effects of sweep on $C_{L_{max}}$ and therefore on the total load. If the scaling laws presented in Subsection 5.4.1 are then incorporated, the new structural weights of the horizontal and vertical stabiliser are found.

5.3.3 Fuselage

For the fuselage, there are only a few changes that are taken into consideration. First of all, moving the engine (and therefore the wing) changes the load distribution across the fuselage. Furthermore, possible changes in drag and thrust also have an impact on the fuselage. The general fuselage geometry is considered to be constant.

The fuselage structure is modelled based on a single cross-section which sustains the average internal loads (cabin pressure, bending, normal force). First, these average loads are calculated. Next, the skin thickness is sized based on the pressure cabin. Once this is done, buckling is taken into consideration. Three types of buckling are considered, namely compressive skin buckling, compressive stringer column buckling and compressive stringer flange buckling. The result is then a stringer geometry and total stringer count. These results can then be combined with the skin thickness to find the cross-sectional area. Finally, the fuselage external structual mass of the Airbus A320 is then scaled by the ratio of the cross-sectional area calculated for the scaled aircraft divided by the cross-sectional area calculated for the Airbus A320.

Once the fuselage module is complete, it can be used to generate scaling laws. This is done by running the fuselage module a large number of times for a large number of combinations, depending on the scaling law that is to be found. Once these values have been found, the MATLAB function *polyfit* is used to generate a polynomial scaling law through all of the points that have been calculated by the analytical module.

5.4 Structural Scaling Laws

The main goal of this project is to find scaling laws and then use these scaling laws to design a new aircraft which is based on the Airbus A320. For the structural design, these scaling laws will be discussed in this section.

5.4.1 Scaling Laws Wing

Once the MATLAB module of the wing is complete it becomes possible to run this module a large number of times in order to find the effects of certain parameters on the wing structural weight. The results that are found can then be represented in graphs. By fitting a polynomial function through such a graph, it becomes possible to find scaling laws. These scaling laws can then be incorporated in the model in order to run it quickly. These graphs and scaling laws are described in this section.

Besides running the structural part of the wing module, all aerodynamic aspects that change parameters such as the shape of the lift distribution and the lift over drag are also incorporated in the following scaling laws. Also note that each scaling law is run twice: once for the Airbus A320 and another time for the expected new aircraft design, where a clean wing with a sweep angle of 17 degrees is considered as is described in Section 4.2.3.

Furthermore, the scaling laws presented in this section only incorporate scaling laws based on one or two changing parameters. The rest is considered constant. As such, these scaling laws should

be used cautiously when ceteris paribus is no longer valid. Also note that for each different graph, the respective scaling law is presented in the graph itself. The graphs relating to the Airbus A320 also present the actual A320 reference data inside the graph [37].

Finally, the two-dimensional graphs that are presented in the following section also include graphs based on initial scaling laws. These initial scaling laws are derived from bending relations that consider material failure. They assume that the shape of the lift distribution is constant at all times. Furthermore, they also assume that the lift over drag is constant and that the total loads on the wing scale linearly with the MTOM or loading factor. These scaling laws include scaling laws such as the square cubed law and similarly derived scaling laws. The comparison between these initial scaling laws and the detailed scaling laws gives an indication of the accuracy of such simple scaling laws.

5.4.1.1 3D Effects of Taper and Aspect Ratio

In the end, there are only two main parameters of the wing that can be determined independent of the aircraft requirements, namely taper ratio and aspect ratio. Other parameters, such as sweep angle and surface area, are mainly the result from the given requirements on speed, wing loading and MTOW. However, it is possible to optimise the aircraft for a combination of taper and aspect ratio incorporating both the aerodynamics and the structural weight. As such, it is interesting to look at the three-dimensional effects arising from a change in aspect and taper ratio. These effects can be seen in Figures 5.2 and 5.3 for the Airbus A320 and the new aircraft respectively.

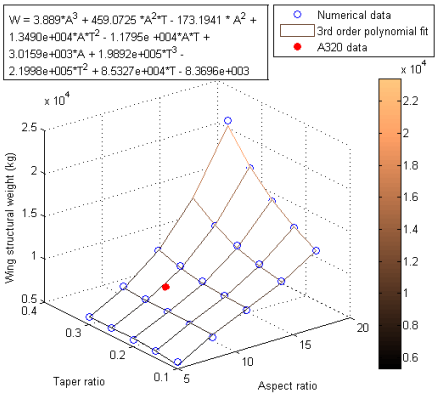

Figure 5.2: 3D scaling laws for the A320 wing structural weight based on aspect and taper ratio

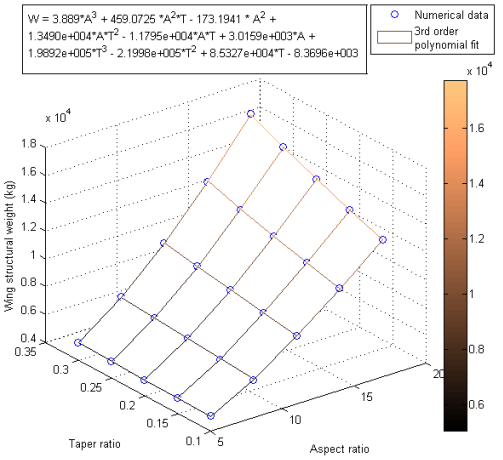

Figure 5.3: 3D scaling laws for the new wing structural weight based on aspect and taper ratio

As could be expected, the wing structural mass increased quickly with increasing aspect ratio. This is due to the fact that a higher aspect ratio leads to a decreasing chord length and thickness, which then llead to a much lower moment of inertia. A large thickness increase is required to compensate for this reduction in moment of inertia. Furthermore, an increasing aspect ratio also leads to an increase in moment arm, further increasing the thickness and wing structural mass.

A next matter which can be concluded is that an increase in taper ratio also leads to an increase in wing structural mass. This is also logic as an increase in taper ratio means that the root chord is reduced, therefore causing a lower moment of inertia at the root, which is a much more critical location for the structural mass than the tip. Furthermore, as Figure 4.11 shows, an increasing taper ratio also leads to a lift which is more concentrated towards the tip, thus leading to a larger moment and larger structural mass.

5.4.1.2 Effects of Aspect Ratio

Besides the multi-dimensional scaling laws for aspect ratio and taper ratio, it is also interesting to see what happens when only the aspect ratio changes. The graphs that are presented in this manner provide a better overview. It is also easier to compare them to the reference data and the initial scaling laws. As such, the effects and the scaling laws for a change in wing structural weight based on aspect ratio are presented in Figures 5.4 and 5.5.

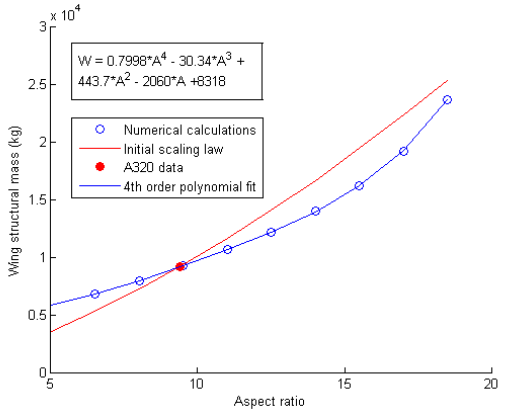

Figure 5.4: Scaling laws for the A320 wing structural weight based on aspect ratio

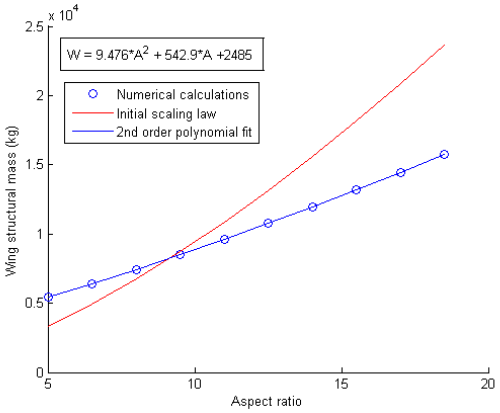

Figure 5.5: Scaling laws for the new wing structural weight based on aspect ratio

Something that is interesting to note is that the initial scaling for aspect ratio deviates from the detailed scaling laws. However, this can be explained. As Figure 4.31 shows, an increase in aspect ratio leads to a less elliptical lift distribution. This lift distribution has more lift distributed near the root and less towards the tip. As such, the moment increases more slowly than what would be expected if the shape of the lift distribution remains constant.

Furthermore, while an increase in aspect ratio leads to a larger moment arm and therefore directly to a larger moment, this is not the case for the shear force and torque. If the shapes of the lift and torque distributions do not change, the shear force and torque distributions do not change. The result is that the effect of a changing aspect ratio on the wing structural mass is smaller than what could be expected based solely on bending moments.

5.4.1.3 Effects of Taper Ratio

The second effect which is included in the scaling laws in Section 5.4.1.1 which is also interesting to consider alone is the taper ratio. The effect of taper ratio on the wing structural weight is presented in Figures 5.6 and 5.7.

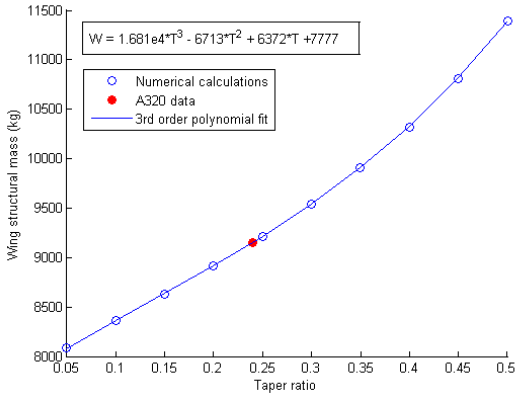

Figure 5.6: Scaling laws for the A320 wing structural weight based on taper ratio

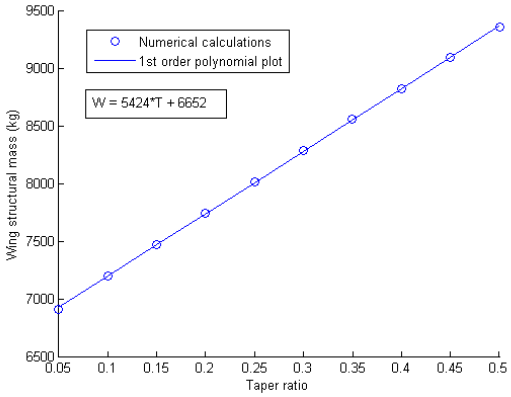

Figure 5.7: Scaling laws for the new wing structural weight based on taper ratio

As has already been explained in Section 5.4.1.1, an increasing taper ratio leads to an increase in weight, which could be expected. However, there is no initial analytical scaling law with which the detailed scaling law can be compared.

5.4.1.4 Effects of Change in Cruise Speed

Another parameter which is interesting to consider is the cruise speed as the angle of attack changes for changing cruise speed. The effect of changing speed on the wing structural mass is presented in Figures 5.8 and 5.9.

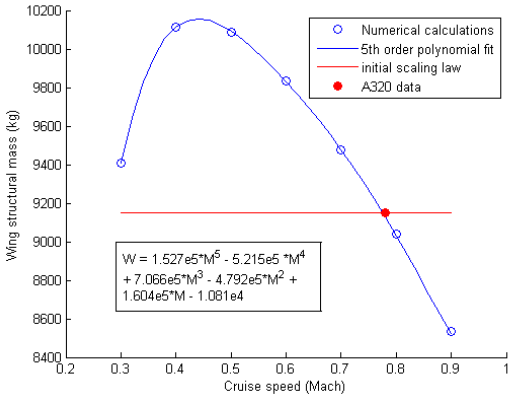

Figure 5.8: Scaling laws for the A320 wing structural weight based on cruise speed

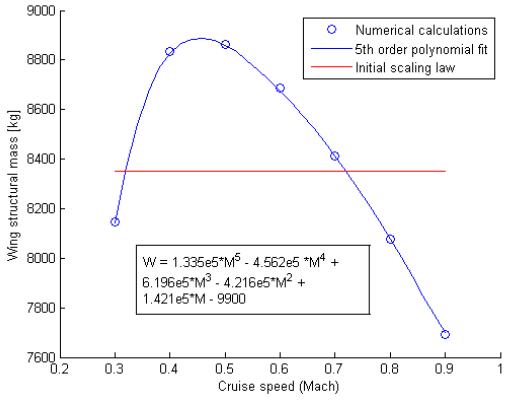

Figure 5.9: Scaling laws for the new wing structural weight based on cruise speed

The effect that can be seen in Figures 5.8 and 5.9 is interesting, as it deviates substantially from the assumed constant weight. However, a decreasing trend between Mach 0.45 and Mach 0.9 can be explained. It can be noted that flying at a higher speed means that it is possible to fly at a lower angle of attack. As Figure 4.17 shows, a lower angle of attack leads to a lift distribution which is located much towards the root of the aircraft. The result is a lower moment and a decrease in wing structural mass.

However, Figures 5.8 and 5.9 also show that the weight increases between a cruise speed of Mach 0.3 to Mach 0.45. This is more difficult to explain. As a check, the required lift coefficients are calculated at these flight speed, using the following equation: $C_L = L/(1/2\rho v^2 S)$. Applying this formula at a flight altitude of 35000 feet shows that a lift coefficients of over 1.65 is required for a flight speed of Mach 0.45 and even a lift coefficient of over 3.7 for a flight speed of Mach 0.3. It can be noted that is unrealistic to flight at such lift coefficients during cruise. As such, it can be concluded that Figures 5.8 and 5.9 provide unrealistic data for flight speeds below Mach 0.5.

5.4.1.5 Effects of Change in Surface Area and MTOM

When the aircraft is changed to a different design, something that changes considerably is the MTOW. Under the condition that the wing loading remains constant, this would also mean that the wing surface area increases. As such, it is also important to look at the effect of MTOW combined with surface area on the wing structural weight. The graphs and scaling laws that represent this are presented in Figures 5.10 and 5.11.

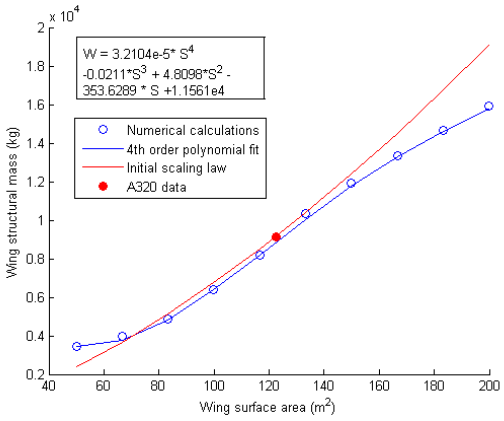

Figure 5.10: Scaling laws for the A320 wing structural weight based on surface area and MTOW

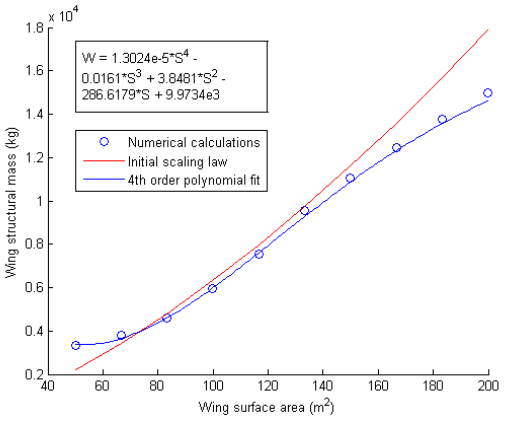

Figure 5.11: Scaling laws for the new wing structural weight based on surface area and MTOW

Figures 5.10 and 5.11 show that the square cubed law is very accurate if the wing area and MTOM do not decrease by more than 50 per cent or increase by more than 20 per cent. However, beyond those ranges, the deviation becomes larger. This can be explained. It can be noted that the square cubed law only take bending into consideration. However, if the surface area is reduced, the moment arm is also reduced. As such, the moments decrease faster than the torsion and the shear forces. As such, the total loads on the wing decrease more slowly than what would be the case based solely on bending. This effect can also be applied for increasing surface area, where the total loads increase more slowly than what would be the case if only bending is considered.

5.4.1.6 Effects of Change in Surface Area with Constant MTOM

Naturally, during the iteration process of the model, the surface area changes with the MTOW. However, suppose the wing loading of the aircraft changes. In this case, the surface area changes while the MTOW does not. As such, it is also interesting to find out how the wing structural weight changes with changing surface area under the condition that the total loads remain constant. The results are found in Figures 5.12 and 5.13 for the Airbus A320 and the new design respectively.

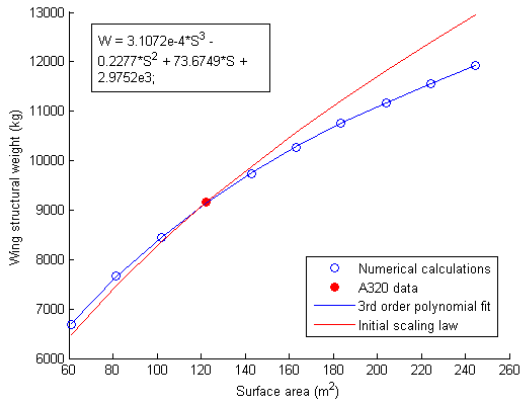

Figure 5.12: Scaling laws for the A320 wing structural weight based on surface area with constant MTOW

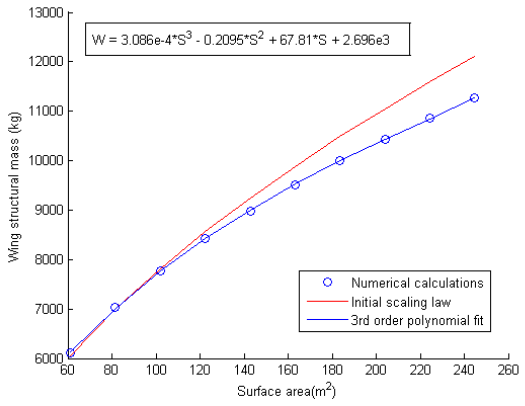

Figure 5.13: Scaling laws for the new wing structural weight based on surface area with constant MTOW

Figures 5.12 and 5.13 show an effect similar as is described in Section 5.4.1.5. The analytical

scaling law, based purely on bending increases more quickly than the detailed scaling law which incorporates multiple effect. However, this can be explained in the same manner as is done in Section 5.4.1.5. The shear forces and torsion increase more slowly than the bending moments, resulting in a slower increase in structural mass than what would be the case if only bending is considered.

5.4.1.7 Effects of Change in Sweep Angle

The next interesting parameter on the wing structural weight is the sweep angle. This effect is represented in the graphs and scaling laws presented in Figures 5.14 and 5.15 for the Airbus A320 and the new design respectively.

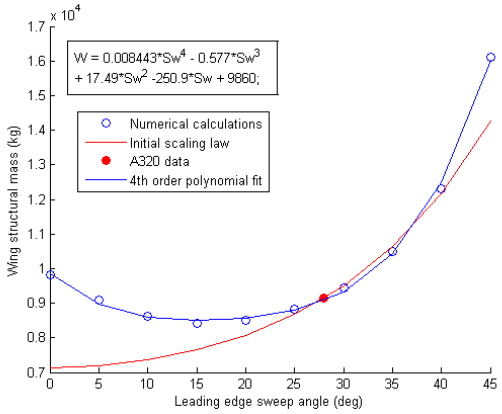

Figure 5.14: Scaling laws for the A320 wing structural weight based on sweep angle

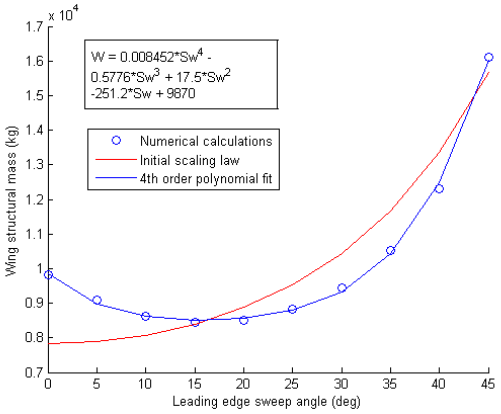

Figure 5.15: Scaling laws for the new wing structural weight based onsweep angle

From Figures 5.14 and 5.15 the effect of sweep angle on the structural mass can be seen. It can be seen that the initial scaling law deviates by as much as 30% from the detailed scaling law for low sweep angles. However, this can also be explained. As is seen in Figure 4.21 the lift coefficient for a sweep angle of ten degrees is lower than the lift coefficient for a wing without sweep. As such, a higher angle of attack would be required for a lower sweep angle, should the total lift remain constant. Figure 4.19 then shows that the Oswald factor increases for a higher angle of attack. This in turn means that the lift distribution would become more elliptical which in turn means that the lift is moved more towards the tip. As such, the moment becomes larger which causes the weight to increase. If however the angle of attack remains constant, this effect does not occur. Furthermore, for very low sweep angles, the effect of sweep is very small on the length of the moment arm and the length of the spars. As such, the initial scaling law for sweep with constant angle of attack can still be used.

5.4.2 Detailed Scaling Laws Fuselage

The next major structural component of the aircraft consists of the fuselage. As the fuselage shape and payload remain constant, it is not interesting to look at the internal structure. However, with the changing engine location, there are changes in the external structure. As there is an extremely high amount of interdependency for the fuselage, the scaling laws that can be obtained by running only the fuselage module are less interesting than those of the wing. After all, the design of the fuselage structure is based on the rest of the aircraft design.

5.4.2.1 Fuselage Scaling Laws Wing Location

Naturally, what is still interesting to see is how the external structural weight of the fuselage changes for wing and fuselage mounted engines. As such, the resulting scaling laws and trend lines are

presented in Figures 5.16 and 5.17 respectively. Note that the graph for the fuselage only incorporates the change in engine location. It does not incorporate changes in tail area and MTOW. In order to incorporate these effects, it is necessary to run the entire aircraft module. Furthermore, the actual Airbus A320 data is incorporated in the graph for the wing mounted engines. The method that is used to derive these scaling laws is described in Subsection 5.3.3.

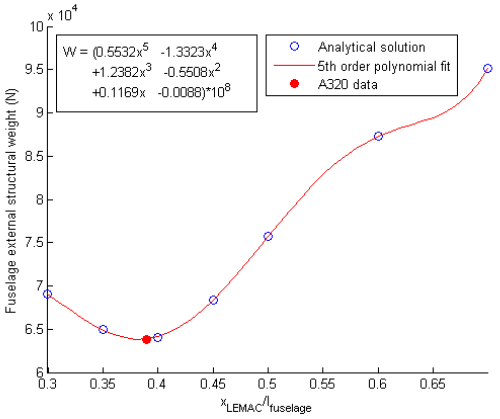

Figure 5.16: Scaling laws for the fuselage external structural weight based on wing location for the wing mounted engine aircraft

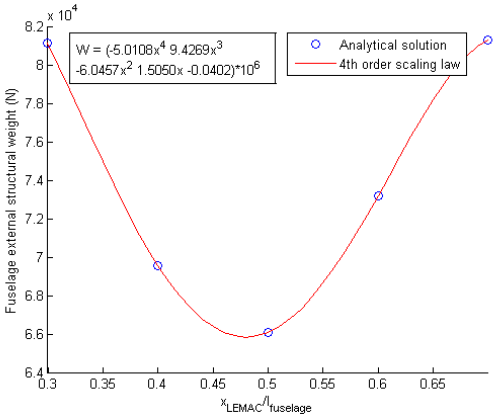

Figure 5.17: Scaling laws for the fuselage external structural weight based on wing location for the fuselage mounted engines aircraft

It can be noted that the minimum values which can be found in Figures 5.16 and 5.17 correspond to the point where static equilibirum holds. It is therefore not interesting to look at different wing locations as an aircraft with a different wing location would not be stable.

A next matter which can be noted is that the wing location is located more aft for the fuselage mounted engine aircraft. This was to be expected as the center of gravity if moved aft. Hence, the wing should also be moved aft.

Furthermore, a next matter which can be seen is that the minimum value of the external fuselage structural mass is slightly higher for the fuselage mounted engine than for the Airbus A320. This makes sense as the propulsive forces of the engine generate a compressive force across the entire fuselage. If the engine is located on the wing, the tail is not compressed due to the engine. As such, buckling is more critical for the fuselage mounted engine aircraft and the fuselage structural mass is higher.

5.4.3 Detailed Scaling Laws Empennage

Finally, there are also interesting scaling laws for the horizontal and vertical stabiliser. However, all of these scaling laws are based on the scaling laws presented in Section 5.4.1, where the tail wing areas are found based on Stability and Control, which is described in Chapter 8.

Furthermore, the scaling law for sweep also incorporates the effect of the scaling law presented in Figure 4.21. As such, the individual scaling laws are not listed in this section. However, the results will be shown, both in two and three dimensions. The three dimensional scaling laws for the horizontal tail will be shown first, followed by two-dimensional graphs for both the horizontal and vertical tail weight. The shown weights represent the entire weight of the respective wings. Furthermore, reference data of the A320 is also presented.

It can be noted that the accuracy of the structural empennage module is lower than that of the structural wing module due to the fact that the scaling laws which are used have been derived for the wing instead of the tail wings. Furthermore, superposition inaccuracies can also occur due to the fact that multiple scaling laws are combined.

However, the changes that occur for the tail wings are also smaller than those for the wing. For example, the aspect ratio and taper ratio of the different tail wings is kept constant. There are no

effects due to changing aspect and taper ratio.

5.4.3.1 3D Scaling Laws Tail

There are four parameters of the stabilisers which are chosen to change with respect to the Airbus A320, namely MTOW, stabiliser surface area, sweep angle and speed. However, it is not possible to view the combined effect of all these parameters in a single graph. For this reason, two three-dimensional graphs are made and presented in Figures 5.18 and 5.19. These graphs show the effect of these four parameters on the total weight of the horizontal stabiliser. Similar graphs can be made for the vertical stabiliser. However, including these effects would be at the expense of the overview.

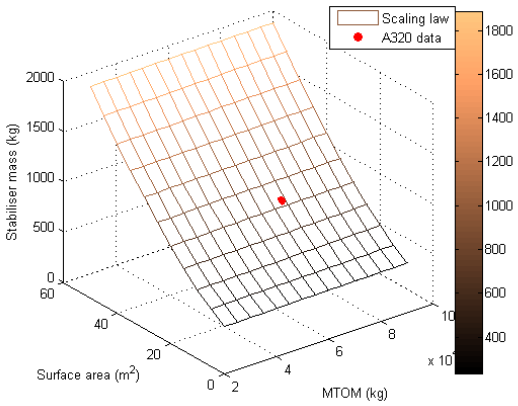

Figure 5.18: Scaling laws for the horizontal stabiliser weight based on MTOW and surface area

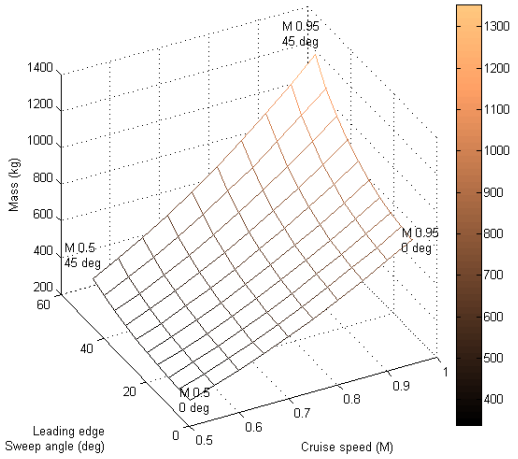

Figure 5.19: Scaling laws for the horizontal stabiliser weight based on MTOW and surface area

5.4.3.2 2D Scaling Laws Tail

In order to present a better overview of the individual effects of the scaling laws presented in Figures 5.18 and 5.19, two dimensional plots can also be made. The effects of the different individual scaling laws are presented in this section. Besides the effect on the horizontal stabiliser, the graphs presented in this section will also provide the effects of the different scaling laws on the vertical stabiliser. The resulting trend lines for area, MTOW, cruise speed and stabiliser sweep angle can be seen in Figures 5.20, 5.21, 5.22 and 5.23 respectively.

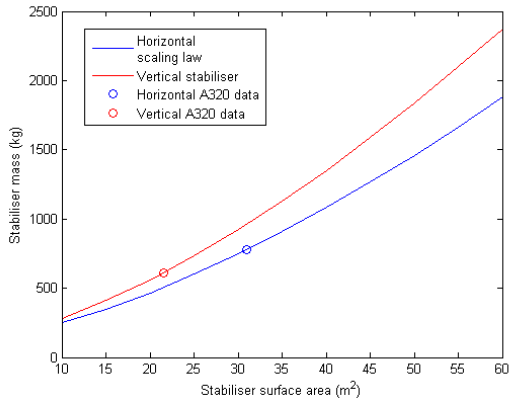

Figure 5.20: Scaling laws for the empennage weight based on stabiliser surface area

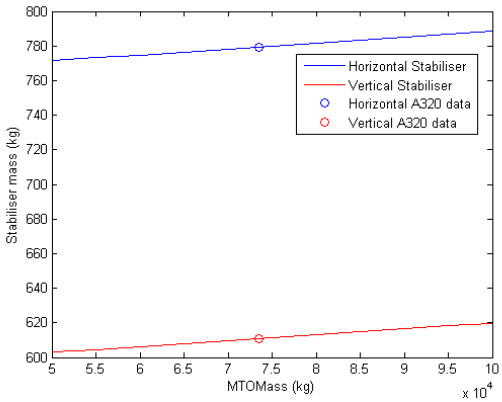

Figure 5.21: Scaling laws for the empennage weight based on MTOM

Figure 5.20 shows that the empennage weight increases with increasing tail wing area. This

makes sense. Both the squared cubed law and the scaling law derived in Figure 5.11 illustrate this effect.

Figure 5.21 shows that the MTOM has little direct effect on the empennage mass. This is expected as the total loads and the planform of the tail are not affected. However, some deviation is can still be seen in Figure 5.21. This is due to the fact that it is assumed that the hydraulics of the entire aircraft are scaled with the MTOM. However, this effect is still very small.

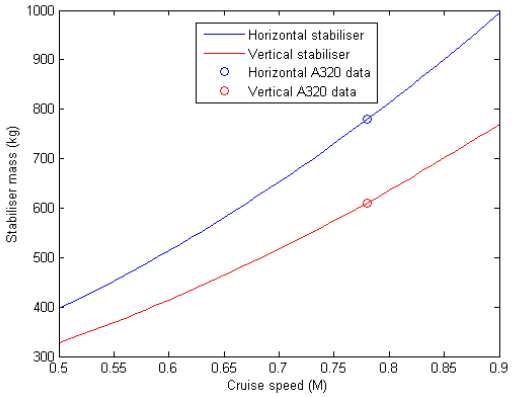

Figure 5.22: Scaling laws for the empennage weight based on cruise speed

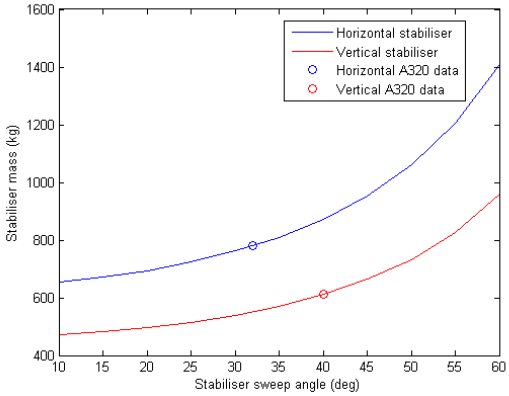

Figure 5.23: Scaling laws for the empennage weight based on stabiliser leading edge sweep angle

Figures 5.22 and 5.23 show that the empennage weight increases with increasing increasing speed and sweep. This is to be expected as an increase in speed leads to an increase in lift and therefore in all the loads. Furthermore, an increase in sweep angle leads to an increase in moment arm and spar length, which also results in an increase in wing weight.

5.5 Structural Verification

With the results known, a next important phase starts, namely the verification. The verification has to be performed in order to find out whether the model represents the devised analytical methods. If this is not the case, the data is unreliable. Again, the verification will be split into multiple sections, namely the verification for the wing, fuselage and empennage respectively. Furthermore, verification will be done based both on the actual modules as well as on the found scaling laws.

5.5.1 Verification Wing Structure

The wing module consists of very eleborate calculations. If these calculations are not checked throughout the design process, bugs are bound to arise in the program. The following section will describe how the wing module was verified throughout the design process. First, the verification process of the detailed wing module will be discussed, followed by the found scaling laws.

5.5.1.1 Verification Wing Module

In order to verify the wing module, all calculations have been performed analytically incorporating a number of simplifications. As the verification process has been performed throughout the entire design process, the individual calculated results are not interesting. Verification already started when it was known that the model still had bugs in it. Furthermore, as certain inputs changed, the expected results also changed.

The first thing that had to be verified consists of the loads on the wing. In this case, the different loading distributions (moment, shear force, torsion) were calculated by the model. Also, these same loads were calculated analytically, using certain simplifications. For example, for the moment, a loading factor of 2.5 was considered. As such, under MTOW conditions, the lift of half a wing should be 1.25 times larger than the MTOW. The same was done for the engine weight. It was then assumed that the lift was a point force at a third of the half span of the root. By multiplying the arms with the lift and engine weight, an approximation of the moment is found. This calculation can be illustrated using Figure 5.24. A similar approximation is used for the other loading cases.

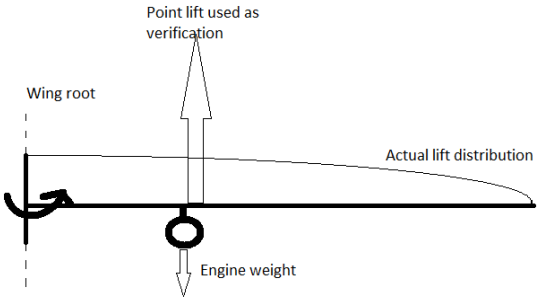

Figure 5.24: Actual and assumed load distribution for moment verification

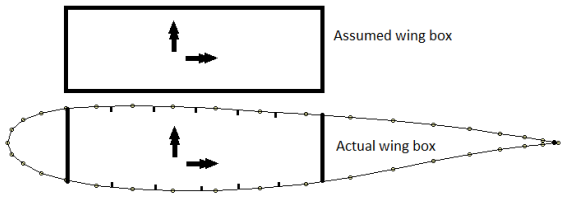

Figure 5.25: General actual and assumed wing box shape.

Next, the model was run. Using simple logic, it could be concluded that the bending stress would have to have the largest contribution to the VMS and that the thickness of all skins should not be larger than a few centimeters. Also, the bending stress is calculated analytically by approximating the wing box as a rectangle with constant thickness everywhere. This is represented in Figure 5.25. The same approximation is used to calculate the torsional stress and the stress due to pure shear. The stresses and thicknesses are calculated by the model and these values are also calculated for a simplified wingbox. If these do not correspond, then there is an error in the program which should be found.

A similar approach can be used with respect to the different buckling types. If the maxmimum compressive normal stress is known - which should be close to the yield stress as bending is the dominant failure criterion - the thickness to height ratio of the stringers can be calculated analytically based on stringer flange buckling. This should correspond to the value calculated by the model. Similar calculations can be performed for the other buckling types, which can then be compared to those values calculated by the model.

Once the failure and thickness calculations of the model have been verified, the weight still has to be verified. This can be done by calculating the cross-section of the wingbox analytically at certain locations. If these cross-sections correspond to the cross-sections calculated by the model, it can be checked whether the model integrates the weight correctly by manually calculating this integration.

When all of these verification calculations have been performed, it can be found that the model corresponds to the analytical calculations.

5.5.1.2 Verification Detailed Scaling Laws

A next matter which has to be considered is the verification of the detailed scaling laws. These scaling laws are verified based on the graphs presented in Section 5.4.1. It should be checked whether the scaling laws correspond to the values calculated by the wing module. This means that the scaling laws should stay very close to the scatter points (blue circles Section 5.4.1), which are calculated by the wing module. Furthermore, the scaling laws are not allowed to oscillate in between these points as that would render the scaling laws useless.

As can be seen in the graphs in Figures 5.2 to 5.15, the detailed scaling laws are fit very close compared to the scatter graphs calculated by the wing modules. Furthermore, none of these graphs oscillate between different scatter points. As such, it is safe to conclude that the detailed scaling

laws are verified with respect to the model.

5.5.2 Verification Fuselage Structure

The next module which has to be verified is the fuselage. Again, this verification consists of two parts, namely verification of the numerical fuselage module and verification of the scaling laws.

5.5.2.1 Verification Fuselage Module

In order to verify the fuselage module, the skin thickness can be calculated analytically first based on the pressure cabin. As a result, both the numerical and analytical solution present a result of 1.2 mm for the skin thickness for the given pressure difference. As such, the skin thickness calculation is verified.

Next, the calculations with respect to buckling have to be verified. First, the different load distributions have to be calculated. It can be noted that during steady flight the normal force (in longitudinal direction), vertical shear force (in vertical direction) and moment distributions should all begin and end at zero. These three different distributions can be seen in Figures 5.26, 5.27 and 5.28 respectively. It can be noted that part of the fuselage drag acts as a point force on the front of the fuselage. As such, the normal force distribution jumps away from zero already at the front of the fuselage. The shape of Figures 5.26, 5.27 and 5.28 are as was predicted and are therefore verified.

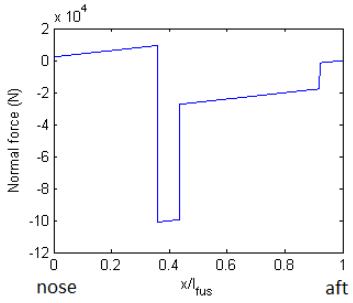

Figure 5.26: Normal force distribution

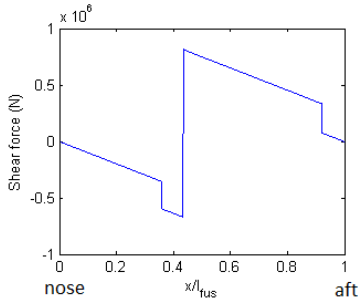

Figure 5.27: Shear force distribution

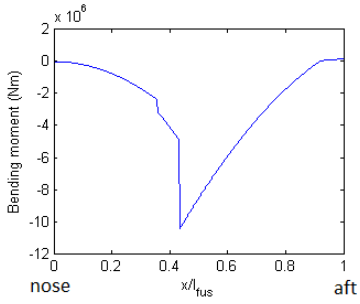

Figure 5.28: Moment distribution

Next, the buckling results have to be verified. This can be done by considering the final characteristics of the fuselage module, namely the stringer count, stringer geometry, skin thickness, average moment and average compressive force. All of these parameters can then be used to calculate the maximum compressive normal stress at the cross-section. It can then be calculated whether the skin or stringers buckle at this stress. They should be exactly at the point where they start to buckle.

5.5.2.2 Verification Fuselage Scaling Laws

The next matter which is to be verified consists of the scaling laws for the fuselage structure, which can be found in Figures 5.16 and 5.17. First of all, it has to be checked whether the scaling laws correspond to the values calculated by the fuselage module. Figures 5.16 and 5.17 confirm this. Furthermore, the scaling laws do not oscillate. As such, the scaling laws for the fuselage are verified.

5.5.3 Verification Empennage Structure

The scaling laws for the empennage are based on the scaling laws which are illustrated in Subsection 5.4.1. As such, verifying the stabiliser structure consists of showing that the empennage module represents the scaling laws. Due to the fact that the scaling laws are simple consequential polynomial functions, they can be calculated manually. Performing these manual calculations shows leads exactly to the same results as those that are calculated by the model. As such, the empennage structural module is verified.

5.6 Structural Validation

Besides knowing that the modules represent the analytical solution, it should also be shown that they represent reality. As such, a validation procedure is important which is described in this section.

5.6.1 Validation Wing Structure

With such an extensive wing module as has been described in Section 5.3.1, it is necessary to validate it before it is used to generate scaling laws. As the wing module is a general module, it should be applicable for a wide range of aircraft. As such, the wing structure is validated by comparing the calculated wing structural weight with the actual wing structural weight. For this, one file is used as main reference to find the structural wing weights [37]. This is chosen because it accurately lists the wing structural weight and other weights of multiple aircraft. However, the weight calculated by the model only includes the wing box, not the entire structure. In general, it appears that the wingbox weight is 70% of the total wing structure weight [41]. As such, the estimated wingbox mass is divided by a factor of 0.7 to find the structural wing mass of each aircraft.

For this validation, it was chosen to run the model for a number of different aircraft. The module was run using both the aerodynamics and structures part of the module as this provides a more accurate structural weight than running the wing structure seperately. The parameters that were changed for modelling these aircraft are as follows:

1. Leading edge sweep angle
2. Taper ratio
3. Surface area
4. Aspect ratio
5. Wing span (through surface area and wing span)
6. Engine location
7. Engine weight
8. Engine count
9. Engine thrust
10. Maximum loading factor
11. Aerodynamics calculated by AVL
12. Cruise speed

It can be noticed that the change in airfoil is not taken into consideration. This means that only aircraft with airfoils similar to the Airbus A320 can be considered. From the list presented in the main reference file [37], there are only two aircraft of which it can be determined that the airfoil is similar, namely the Fokker 100 and the Boeing 747-100. Other aircraft, such as the ATR-42 have a much thicker airfoil. Also, aircrafts such as the Boeing 727-200 have airfoils of which the shape is unknown. As the thickness to chord ratio has a large impact on the second moment of area, these aircraft can not be considered.

If the wing module is run for these three different aircraft, the results presented in Table 5.1 shows the accuracy of the wing structural module. As Table 5.1 shows, the model is very accurate for the Airbus A320 and the Fokker 100. For the Boeing 747 it shows a deviation of 16% which is still reasonable. However, the Boeing 747 actually has a thickness to chord ratio of fourteen per cent [43] which is higher than that of the Airbus A320 (11.8 per cent). As such, the moment of inertia is higher which means that the weight can be reduced. Implementing the actual airfoil of the Boeing 747 would therefore lead to a lower weight estimation and lower deviation.

However, even though the weight esimation is off by sixteen per cent, this is actually very accurate considering the fact that the MTOW of the 747 is six times higher than that of the A320. This means that the wing module offers a very accurate approximation for a vast amount of configurations. The Airbus A320 is a mid-size aircraft with wing mounted engines. The Fokker 100 is a much smaller aircraft with fuselage mounted engines. Finally, the Boeing 747 is a very large aircraft with four wing

mounted engines. Even though these aircraft are so different, the wing module can approximate all of them accurately. This means that any weights generated by the wing module can be considered validated.

Table 5.1: Validation Results Wing Module

		Airbus A320-200	**Fokker 100**	**Boeing 747-100**
Estimated structural wing mass	[kg]	8843	4540	45937
Actual structural wing mass [37]	[kg]	8801	4669	39841
Deviation	[%]	+0.46	-2.77	+16.3

5.6.2 Validation Fuselage Structure

In a manner similar to the wing, the fuselage also has to be validated. There are two main methods in which the fuselage is validated: one depending on logic and the scaling laws and another depending on detailed empirical data.

First of all, it is important to look at the scaling laws presented in Figures 5.16 and 5.17. It can be noted that the minimum average moment occurs when the aircraft static equilibrium applies. This corresponds to level flight. When the Airbus A320 is modelled, this corresponds to the case where the wing location is the same as the A320 wing location. Figure 5.16 shows that this is the case. Furthermore, it can also be noted that the wing should be located further aft for a fuselage mounted engine aircraft. This again can be seen by comparing Figures 5.16 and 5.17. The minimum weight of the fuselage - for a fuselage mounted engine aircraft - is clearly found for a more aft location of the wing when compared to the wing location.

However, the scaling laws alone only take into effect the change in wing location. It is still necessary to compare the fuselage to actual data. As such, once the model was finished, the entire model was run for both a wing mounted and fuselage mounted configuration, where the range, aspect ratio and taper ratio remain constant. These values can then be compared with actual data which is presented in Table 5.2.

Table 5.2: External fuselage structural weight characteristics [44]

Aircraft type	**Fuselage or wing mounted engines**	**Fuselage external structural mass [kg]**	**MTOM [kg]**	**Weight fraction [%]**
DC-8	F	11288	140614	8.03
MD-83	F	7453	72600	10.27
Boeing 727	F	7977	72570	10.99
Boeing 720	W	8792	100800	8.72
Boeing 747	W	32958	377842	8.72
Boeing 737	W	5366	62800	8.55
Airbus A320 [37]	W	6257	73500	8.51
Fuselage mounted average	F			9.76
Wing mounted average	W			8.63
Airbus A320 calculated	W	6257	73644	8.50
New aircraft calculated	F	5913	61990	9.54

What Table 5.2 clearly shows is that the Airbus A320 fuselage weight is perfectly represented by

the model. This can be seen as the fuselage external structural weights for both aircraft are identical and the size of this weight compared to the MTOM is nearly identical. Furthermore, what the table also shows is that the relative size of the fuselage structural mass compared to the MTOM that is calculated by the model is perfectly in line with actual reference data. As such, it is safe to say that the fuselage structure module is validated.

5.6.3 Validation Empennage Structure

The final structural elements which have to be validated are the horizontal and vertical stabilisers. These stabilisers are validated in two manners. First, for all the graphs which are shown in Figures 5.18 to 5.21, it should be checked whether these graphs can represent the actual Airbus A320 data. For all of these graphs, it can be seen that the actual A320 data corresponds perfectly to the graphs as the A320 data are always located on the empennage scaling trend lines.

Next, it is checked that these graphs represent reality. As these scaling laws are based on the scaling derived in Section 5.4.1 and these scaling themselves have been validated, this also means that the empannage structure is validated.

Chapter 6

Performance

6.1 Wing and Thrust loading

The mass of the engine is related to its thrust and can be found using the thrust loading. Therefore, to calculate the mass of the engine, the necessary thrust loading has to be obtained. The wing area is related to the wing loading, so in order to determine the area, the wing loading needs to be known. These two parameters are fixed for an airfoil, wing, high-lift-device-configuration. This parameter, known as the design point, can be found in the wing loading vs thrust loading diagram. A graphical representation of the wing loading versus the trust loading is shown in Figure 6.1.

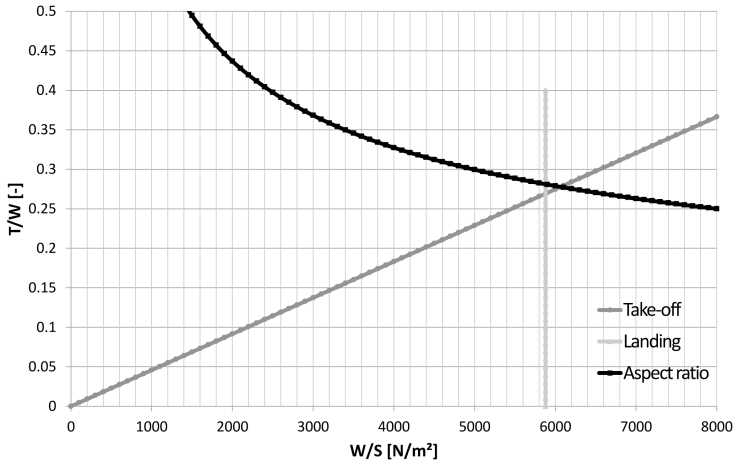

Figure 6.1: Thrust loading versus Wing loading

This diagram has three lines of data. These are related to; the take-off, landing and aspect ratio. A higher wing loading and lower trust loading are preferred. However, these are limited by other factors. The limiting lines are of the aspect ratio group and the corresponding lift coefficients of the take-off and landing. The necessary wing and trust loading is determined by obtaining the intersections between the 'landing' with the 'Aspect ratio' and 'Take-off' lines.

The wing loading during landing is obtained using the stall speed (6.1).

$$\frac{W}{S} = \frac{1}{2}\rho V_s^2 C_{L_{max}} \tag{6.1}$$

The wing loading is then implemented into the 'Take-off' and 'Aspect ratio' to calculate the corresponding thrust loadings (6.2)(6.3). The highest value of the trust loadings is decisive.

$$\frac{T}{W} = \frac{W}{S}\frac{1}{kC_{L_{max}}\sigma} \tag{6.2}$$

$$\frac{T}{W} = \frac{c}{\sqrt{\frac{W}{S}\frac{2}{\rho}\frac{1}{C_{L_{climb}}}}} + \frac{C_{D_{climb}}}{C_{L_{climb}}} \tag{6.3}$$

Using this approach a thrust loading can be derived. This thrust loading is used to determine the thrust which the engines have to generate. It also serves as an input for the scaled engine mass, which will be handled in Chapter 7.

All known and used performance parameters are summarised in the Table 6.1. The $C_{l_{max_{Flapp}}}$, $C_{l_{max_{TO}}}$, $C_{l_{max_{Clean}}}$ and k are kept constant with respect to the A320.

Table 6.1: Performace characteristics

Parameter	**Value**
$C_{L_{max_{Flapp}}}$	3.00 (Depends on Sweep angle)
$C_{L_{max_{TO}}}$	2.56 (Depends on Sweep angle)
$C_{L_{max_{Clean}}}$	1.63 (AVL: AOA=15°)
C_{D_0}	0.0205
k	7800Pa (Take off Parameter)
$V_{appraoch}$	68.9m/s (A320)
V_{stall}	57.4m/s (A320)
$n_{lim_{man}}$	2.5 (Defined by the CS25)
$n_{lim_{man}}$	-1.0 (Defined by the CS25)
C_{L_α}	4.38
$\frac{T}{W}$	0.3018 (Design Configuration)
$\frac{W}{S}$	6382 (Design Configuration)
$n_{max_{Design}}$	3.75 (Desing Configuration)
$n_{min_{Design}}$	-1.5 (Design Configuration)

6.2 Loading Diagram

The minimum and miximum loading factors are determined using the loading diagram. These load factors are then later on used to size the wingbox and other load carrying structures. Several steps are followed to create a loading diagram. First, the loading diagram consists of two different diagrams, one being the load factor during manoeuvres and the other in a gust situation. The largest of the two determines the limit load factor.

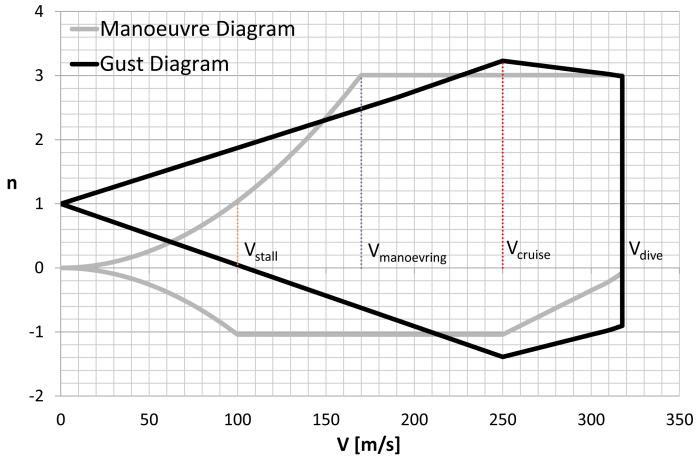

Figure 6.2: an example V-n diagram of the aircraft

6.2.1 Maneuver Loading

The manoeuvre loading diagram consists of several parts as can be seen in Figure 6.2. The first part represents the loading due to the maximum lift produced. That particular curve is produced by the following equation.

$$n = \frac{qC_{L_{max}}}{\frac{W}{S}} \tag{6.4}$$

This curve goes up till it reaches the maximum limit load factor which is specified by the CS-25 in this case. The CS-25 states that the maximum load factor cannot exceed 2.5 for transport aircraft with a MTOM over 50000lbs [45]. This given load factor actually represents the maximum positive load factor for the manoeuvre diagram. This load factor is kept constant up and till the dive speed. For this project it was assumed that the dive speed equals the dive speed of an A320, i.e. $M_d = 0.88$. The maximum negative load factor is also given by the CS25, which is -1 for transport aircraft [45]. However this load factor is only valid up to M_{cr}. So the maximum negative curve starts abeam the stall speed and ends at the cruise speed. The last part of the manoeuvre diagram is again parabolic as the first part was, it is in fact given by the negative of Equation 6.4.

6.2.2 Gust Loading

The second diagram gives the load factor during a gust. The gust diagram is normally evaluated at three different flight regimes; speed at which maximum angle of attack occurs, cruise speed and dive speed. In this case only the cruise speed will be evaluated as this normally gives the highest loading factor. The loading factor is given by the following equation.

$$n_{max} = 1 + \Delta n \tag{6.5}$$

Where Δn represents the incremental load factor. The incremental load factor depends on the incremental lift, produced by the temporary increased angle of attack due to the gust. This Δn is given by the following equation.

$$\Delta n = \frac{\rho V C_{L\alpha} u}{2\frac{W}{S}} \tag{6.6}$$

Equation 6.6 uses a parameter u, which represents the normal component of the gust velocity. This normal component is the product of the load allevation factor K and the statistical gust velocity. The gust velocity used in the model is 10.67m/s [46]. The load allevation factor can be determined as follows.

$$K = \frac{0.88\mu}{5.3 + \mu} \tag{6.7}$$

and μ is given by,

$$\mu = \frac{2\frac{W}{S}}{\rho g c C_{L_\alpha}} \tag{6.8}$$

Note that Equation 6.7 uses imperial units. If these steps are followed in a proper manner, a sloped curve should be the result, reaching a maximum at cruise speed. The curve itself starts at a positive load factor of one. The negative part is perfectly equal to the positive part but opposite in sign.

Normally the two diagrams are drawn above each other in order to determine or read the maximum value of the diagram. In this case the model determines the maximum positive and negative value of all load factors using a simple max() function. These maximum load factors are then multiplied by a safety factor of 1.5 to arrive at the design load factor. When all parameters of Table 6.1 are used, the load factor of the design configuration results to be dominated by the manoeuvre diagram. The load factors are +2.5 and -1.0, these are given by the CS25 regulation [47]. Which is a reasonable figure seen that the A320 maximum load factors equal +2.5 and -1.0 [48].

6.3 Fuel Estimations

The model should be able to scale for fuel mass. For this reason, the model simulates the flight in order to generate a fuel weight.

6.3.1 Design Methodology

The method that has been used to estimate the fuel weight is based on fuel fractions [49]. These fuel fractions are based on the flight profile presented in Figure 6.3. The fuel fractions for cruise and loiter condition are based on the Breguet equation [50].

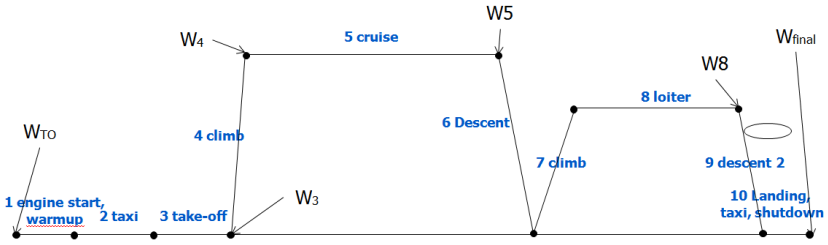

Figure 6.3: Flight profile

This method of estimating the fuel weight is then used to find the fuel weight of the Airbus A320. However, solving this method leads to a fuel estimation of over 20 000 kg instead of the actual 17 940 kg [40]. As such, the fuel weight is scaled in order to reproduce the actual A320 fuel weight. The fuel fractions and Breguet range equation are then used together with the scaled fuel weight to estimate the necessary fuel for the design range, or another given mission range. These are then used to calculate the fuel use per passenger per kilometre. By changing the input, the same method can be applied to different aircraft with different ranges.

6.3.2 Fuel Scaling Laws

If the fuel module is run a number of times, it becomes possible to find scaling laws. These were set up by calculating severall points using the fuel module and then apply a certain polynomial function to those points. The most interesting parameters regarding scaling laws are L/D, Range, MTOM and speed. As it is not possible to represent all of these parameters in a single graph, the scaling laws are split in two three-dimensional plots. The graphs and scaling laws that represent the fuel weight as function of the Range and MTOM are represented in Figures 6.4 and 6.5 for the original and new aircraft, respectively. The same graphs, based on the cruise L/D and the cruise speed, can be found in Figures 6.6 and 6.7.

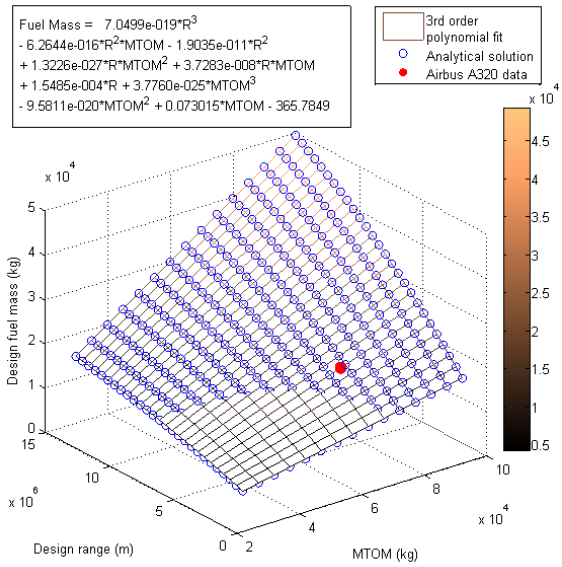

Figure 6.4: Scaling laws for the fuel weight based on MTOM and range for the Airbus A320

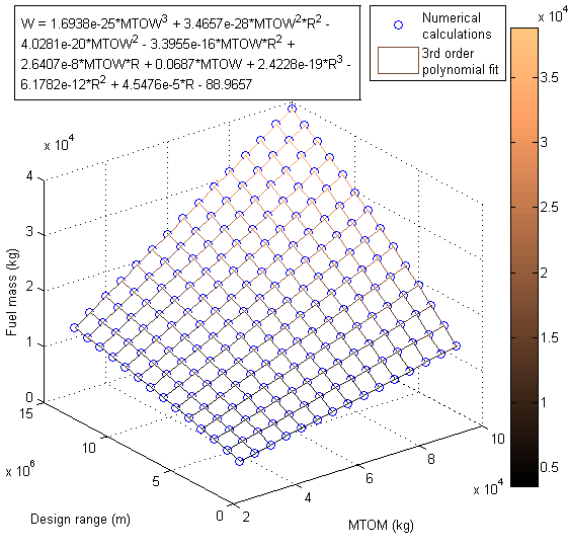

Figure 6.5: Scaling laws for the fuel weight based on MTOM and range for the new aircraft

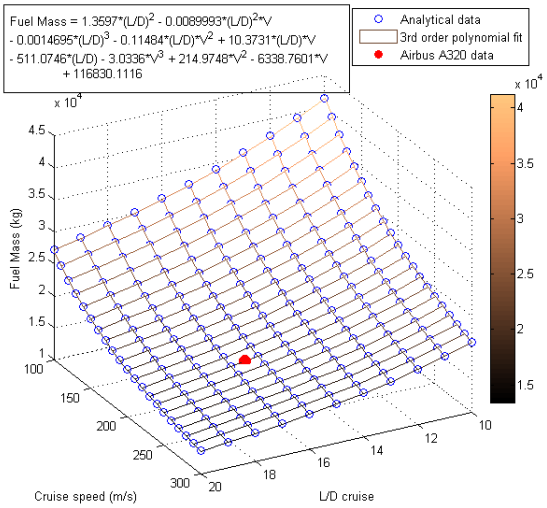

Figure 6.6: Scaling laws for the fuel weight based on L/D and speed for the Airbus A320

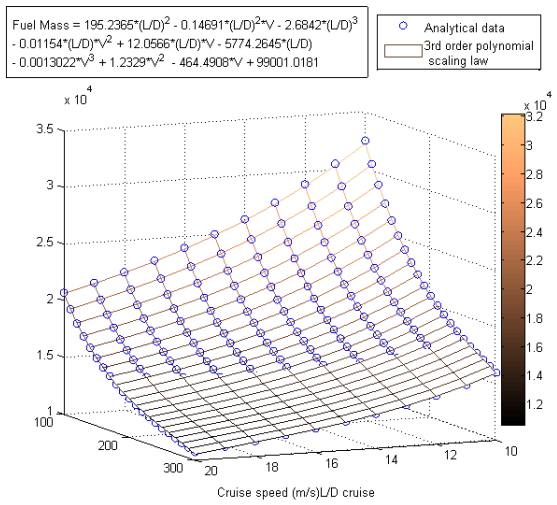

Figure 6.7: Scaling laws for the fuel weight based on L/D and speed for the new aircraft

6.3.3 Verification Fuel Module

Naturally, it is also important to verify the fuel module. As no complex mathematical constructions are used, this can be done analytically. Calculating the values analytically and numerically shows that both methods lead to the same values.

6.3.4 Validation Fuel Module

Calculating a fuel weight itself is interesting but the question always remains whether the data which are delivered by the model are correct. As such, the model has to be validated. This is done by comparing the calculated fuel weights to the actual fuel weights of the A320 for different ranges [51]. Furthermore, as the data about the A320 is relatively limited and the A320 has a limited flight

range, the fuel estimation is also validated based on the aircraft which are most similar to the A320, namely the Boeing 737-700ER and the Boeing 737-800 [52], where the range and take-off weight are the changing input variables. The validation data is presented in Table 6.2.

Table 6.2: Validation data fuel estimation

Aircraft type	**Range[km]**	**Take-off mass [kg]**	**Actual fuel mass [kg]**	**Calculated fuel mass [kg]**	**Deviation [kg]**	**Deviation [%]**
Airbus A320-200	5,000	73,500	17,940	0	0.00	
Airbus A320-200	2,900	73,500	12,914	12,873	-41	-0.32
Boeing 737-700ER	10,186	77,600	32,539	30,071	-2,468	-7.58
Boeing 737-700ER	5,000	72,600	18,100	17,720	-380	-2.10
Boeing 737-700ER	2,000	65,800	9,050	9,437	387	4.28
Boeing 737-700ER	0	60,500	3,365	4,106	741	22.02
Boeing 737-800	9,445	79,000	31,734	29,160	-2,574	-8.11
Boeing 737-800	5,000	72,600	18,600	17,720	-880	-4.73
Boeing 737-800	2,000	72,600	9,868	10,412	544	5.51
Boeing 737-800	0	66,100	33,68	4,486	1,118	33.19

As Table 6.2 shows, the fuel estimation is very accurate. Compared to the known A320 data, the fuel estimation is always within a 0.32% margin. Even when compared to a different aircraft, the deviation is no more than 8.11% for ranges between 2,000 and 10,186 km. As such, the fuel estimation can be considered validated.

However, what can be noted is that the fuel estimation does not take the change in specific fuel consumption into consideration for different speeds. Figures 6.6 and 6.7 therefore show that increasing the speed leads to a decrease in fuel consumption. This does not represent reality. As such, the model should only be used for the engine design speeds.

Chapter 7

Engine Characteristics

During the MTR, initial engine sizing was performed. This sizing was based on weight data of comparable aircraft to find the required thrust. With the required thrust in mind a market analysis was performed to come up with three engine options. Based on a trade-off between the engines combined with their respective layouts, it was chosen to use the General Electric UDF, see Figure 7.1.

The UDF is a propfan engine which was developed in the late 80's by GE as a technology demonstrator. It was used on MD81 which served as flight test platform. The purpose of the test platform was to demonstrate a approximate fuel reduction of 30% with respect to a turbofan engine, and that at a reasonable altitude and Mach number, i.e. in the range of 0.7 to 0.85. The UDF makes use of an GE F404 as core engine and a counter-rotating propeller. The counter-rotating propeller consists of two fans, each with eight highly swept blades which have a high loading.

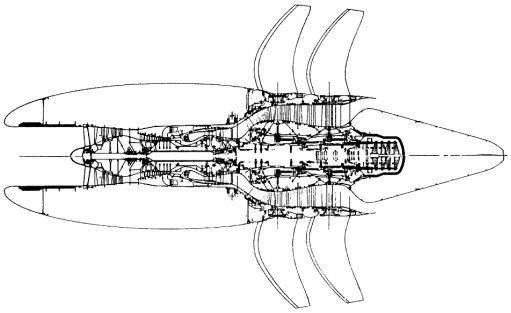

Figure 7.1: GE UDF cross section [53]

This section will start of with a brief summary of all engine dimensions and specifications, and an estimation of the engine power and efficiencies. Then the engine will be analysed. Followed by a discussion on engine noise and noise certification. The last section will handle the engine scaling laws used in this project, these scaling laws mainly serve as a relation between the engine thrust and the engine mass.

7.1 Dimensions and Specifications

In order to determine most of the relevant engine characteristics of the UDF it is logical to start of with the dimensions that can be found in the technical reports of NASA's Advanced Turboprop Project [18]. These are however not complete and up to date, therefore more recent data will be used from NASA's research model of an UDF that was used to simulate performance of a geared vs direct drive propfan. For this section the model data will be used.

Table 7.1: GE UDF Engine Characteristics [18, 22]

General Dimensions		
Quantity	**Imperial**	**metric**
D_{fan} (front/rear)	10.9/9.9 ft	3.32/3.02 m
$D_{nac_{max}}$	5.5 ft	1.68 m
l	15.6 ft	4.75 m
m_{engine}	6250 lb	2490 kg
$m_{installed}$	8040 lb	3647 kg
$m_{pyl,nac}$		1157 kg
T_{static} (Sea Level)	22,120 lb	98 kN
TSFC	0.169 lb/lb-h	4.78 g/kNs
T_{TO}	17,500 lb	78 kN
TSFC	0.252 lb/lb-h	7.13 g/kNs
T_{Cruise}	4,600	20 kN
TSFC	0.394 lb/lb-h	11.15 g/kNs

Performance	
Quantity	**Value**
BPR	32
PR	27
PR_{fan}	1.17
T/W (SL/Cruise)	2.75/0.57
M_{cruise}	0.72
M_{ne}	0.88
M range	0.60 - 0.84
Alt_{cruise}	35000 ft
Alt_{max}	39000 ft
$\eta_{j_{cruise}}$	0.9
$\eta_{j_{Ground/TO}}$	0.65 -0.7

Propeller		
Quantity	**Value**	
Counterotating	8 x 8 or 10 x 8 config	
c_{r_1}	17.51 in	0.445 m
c_{r_2}	17.47 in	0.443 m
$(t/c_1)_max$	11.1	
$(t/c_{r_2})_max$	11.2	
Radius Ratio 1	0.42	
Radius Ratio 2	0.41	
$\Lambda_{tip1,0.5c}$	33	
$\Lambda_{tip2,0.5c}$	29	
AR_1	2.39	
AR_2	2.35	

With the data of Table 7.1 the total efficiency of the engine can be determined as well as the power ratings in the three given flight regimes. The total efficiency, η_{tot}, can be determined using Equation 7.1. Note, this approach assumes that the thrust delivered by the engine comes purely from the propeller. Meaning that the jet thrust produced by the exhaust part of the engine is neglected. This can be seen as a reasonable assumption as this jet thrust normally accounts for 5 to 15% maximum for regular turboprop engines. Also the model data was used instead of the real data because that data is not available, i.e. this is rather an estimation of the engine characteristics. But the purpose of Table 7.1 and the rest of this section is the inform, give an overview and an indication of the propfan engine that is used.

$$\eta_{tot} = \frac{TV}{H^L m_f} = \frac{V_0}{H^L SFC} \tag{7.1}$$

The cruise speed at 35000ft can be determined as follows.

$$T = T_0 - 1.98\frac{Alt(ft)}{1000} \tag{7.2}$$

This gives that the temperature at 35000ft equals $-54.3°C$ or 218.85K. Now the local speed of sound at cruise altitude can be found, $a = 296.54m/s$, which leads to a cruise speed, V_{cr}, of 213.53 m/s. Using this cruise speed the total efficiency in cruise can be determined to be as much as 44.7%. Using the total efficiency and the propulsive efficiency, the thermodynamic efficiency in cruise can be found.

$$\eta_{th_{cr}} = \frac{\eta_{tot_{cr}}}{\eta_{j_{cr}}} = 49.7\% \tag{7.3}$$

The power of the engine can also be determined for cruise condition.

$$P_{a_{cr}} = T_{cr} V_{cr} = 4270kW \tag{7.4}$$

$$P_{s_{cr}} = \frac{P_a}{\eta_{j_{cr}}} = 4744kW \tag{7.5}$$

Following, the power available at take-off can be found to be 6633kW . Using $M_{TO} = 0.25$ or $V_{TO} = 85m/s$ at sea level. In order to determine the shaft power at take-off the propulsive efficiency is needed. This can be found assuming that the thermodynamic efficiency stays constant between cruise and take-off condition, which is reasonable as the thermodynamic efficiency is defined as follows.

$$\eta_{th} = \frac{engine\ output\ power}{energy\ input\ power} = \frac{P_s}{P_q} = \frac{P_s}{m_f H^L} \tag{7.6}$$

The difference between cruise and take-off for the engine is mainly speed and atmosphere condition. As altitude increasing the mass flow through the engine decreases, but the output power, P_s, decreases proportionally to that mass flow. Meaning the thermodynamic efficiency can be assumed constant. The propulsive efficiency in take-off condition can be found as follows.

$$\eta_{j_{to}} = \frac{\eta_{tot_{to}}}{\eta_{th_{to}}} = 56.1\% \tag{7.7}$$

As the $\eta_{tot_{to}}$ equals 0.279, which was found using Equation 7.1. With $\eta_{j_{to}}$ known the $P_{s_{to}}$ is found to be 11818kW. For this estimation the static shaft power, $P_{s_{st}}$ can be assumed to be equal to $P_{s_{to}}$. Because as the thrust increases from take-off to static conditions the propulsive efficiency decreases in a quasi similar fashion. The actual $P_{s_{to}}$ cannot be calculated, because even though the T_{static} is given the $\eta_{j_{st}}$ equals zero as V_0 is 0. All results can be found in Table 7.2.

Table 7.2: Engine Power and Efficiencies

Quantity	Imperial	metric
$P_{a_{cr}}$	5724 SHP	4270 kW
$P_{a_{to}}$	8891 SHP	6633 kW
$P_{s_{cr}}$	6359 SHP	4744 kW
$P_{s_{to}}$	15842 SHP	11818 kW
$P_{s_{st}}$	15842 SHP	11818 kW
$\eta_{tot_{cr}}$	44.7%	
$\eta_{j_{cr}}$	90.0%	
$\eta_{th_{cr}}$	49.7%	
$\eta_{tot_{to}}$	27.9%	
$\eta_{j_{to}}$	56.1%	
$\eta_{th_{to}}$	49.7%	

These are reasonable figures compared to other high power turboprops like the Progress/Ivchenko D27 ($T = 102kN, P = 14000SHP, m = 2300kg$) Europrop TP400 ($T = 83kN, P = 10500SHP, m = 2085kg$).

7.2 Noise

Noise is a very delicate topic in aircraft design nowadays, as the demand for aircraft keeps rising and the airfields get more and more embedded in populated area, thus demanding quiet aircraft. The MTR[17] clearly shows that the UDF is considerable good option when aiming an appropriate amount of fuel reduction due to the propulsion system. In order for the open rotor technology to stand a chance against the Ultra High Bypass(UHB) technology it should be competitive with respect to the produced noise levels.

According to the latest FAA noise regulations; "*every aircraft which applies for a type certificate on, or after January 1, 2006, should show that the noise levels are not exceeding the Stage 4 noise limit* [54]". The Stage 4 noise limit is given by the ICAO. These Stage 4 limit of an individual measurement is the same the as in Stage 3. Stage 4 aircraft are required to have a margin of at least 2 EPNdB for any two measurements combined, to stage 3. The cumulative margin of all 3 measurements should be less than 10 EPNdB compared to the Stage 3 limits[54][55].

The model data that was used to determine the engine TSFC, also provided model data on the noise production of the engine[22]. These levels are given in Table 7.3.

Table 7.3: Computed Rotor Noise levels and Certification Limits for a 70000kg Aircraft [22]

	Computed Value	Stage 3 & 4 Limit	Stage 3 Margin	Stage 4 Margin
Lateral (EPNdB)	92.8	96.5	3.7	(5.2)(10.3)
Flyover (EPNdb)	87.6	91.0	3.5	(5.2)(10.1)
Approach (EPNdB)	91.7	100.3	8.6	(10.3)(10.1)
Cumulative (EPNdB)	272.1	287.8	15.7	5.7

As can be seen from Table 7.3 the UDF lies within the Stage 4 certification limit. However it will not be the quietest aircraft around. But a lot of research was done, and is being done on

open rotor propulsion. Noise reduction is one of the main topics of these research projects. There is a general understanding of open rotor noise generation and how to reduce it. Conclusions of NASA's experimental research on the F-7/A-7 propeller performance and acoustics, i.e. the blade configuration used by the UDF, are given in the preceding text[56].

Increasing the number of blades has a positive effect on the noise production of the UDF. This is actually a twofold. On the one hand a there's a decrease in steady loading noise due to a reduction in blade loading and tip speed. On the other hand, there is a decrease in the rotor-to-rotor interaction noise. Which is created by the interaction of the aft blades with the wakes and tip vortices of the forward rotor blades. Because the tip speed decreases of both blades, the wakes and tip vortices of the forward blade decrease, and the interaction also decreases as the aft blades also have a lower tip speed

Increasing the spacing between the two blade rows results in a decrease of the produced noise. But this decrease is rather limited. However if the spacing is increased together with an aft-reduced-diameter blade configuration, the reduction becomes non neglegible.

The steady-loading as well as the total noise decreases with tip speed for a given thrust and blade number. This is however not linear, if the tip speed is further decreased through an optimum, the noise level starts increasing with decreasing tip speed of the blades. Because if an equal amount of thrust needs to be produced at lower tip speed, the AOA needs to be increased. This increase in AOA leads to stronger wakes. Also if the blades have a larger angle of attack, the spacing between the two rows decreases. These two effects combined result in an increase in rotor-to-rotor interaction noise for a decrease in tip speed beyond the optimum for noise.

Reducing the aft blade diameter results in dramatic reductions of the sound pressure levels compared to an equal diameter configuration. This reduction is mainly attributed to the absence of vortex/rotor interaction tones

The presence of a pylon does not have any effect on the rotor-to-rotor noise. It does however have an effect on the steady loading noise. If the engine loading increases the effects of the pylon interaction decrease and vice versa.

Besides the NASA, other organisations and manufacturer are researching this topic quiet intensive. An example of such an effort to reduce noise levels is the use of pylon blowing, which by isolating the contra-rotating open rotor inflow through flow acceleration effectively reduces the higher harmonic oscillations for front rotor tones [28]. As it is these tones that contribute most to the annoyance, it is an important result for passenger and community comfort. Another novel solution to achieve lower noise levels inside the cabin is the use of noise and vibration suppression systems by Bombardier for the Q400 [26], where cancelling signals are generated to diminish the residual noise. It is also possible to use passive noise and vibration reduction. In that case e.g. improved insulation is to be fitted.

All in all, the prognosis for turboprops is definitely promising when it comes to future noise reductions.

7.3 Scaling

The engine mass should be scalable with respect to the thrust within a certain range. Because the UDF was chosen based on the thrust and MTOW of the A320 reference aircraft. It is likely that an aircraft using the UDF has a considerable fuel reduction, that, together with other factors should result in a lower MTOW. Also by using high aspect ratio wing the wing loading and thrust loading of the aircraft change, which can be seen in Section 6.1. All this together results in a lower thrust need.

Scaling of the installed engine mass is divided in two parts. First, the engine mass is scaled according to the method proposed by Torenbeek [34].

$$Enginemass \propto Thrust^{n} \tag{7.8}$$

Where n is a constant defined between 1.07 and 1.14. This scaling, called "*rubberising*" by Torenbeek, is valid for turbo engines and assumes that the technology stays constant. That is the

thermodynamic specifications of the engine are kept constant. But this can only be done within a 15 to 20% margin of the original engine specification. If an average scaling factor of 1.1 is assumed the engine mass ranges from 1948kg to 3042kg, see equation 7.9. This corresponds to a thrust range between: 78.4-117.6kN.

$$m_{Scaled} = (\frac{T_{Scaled}}{T_{Original}})^n \cdot M_{Original} \tag{7.9}$$

Note, that this range is very important, because based on this simplistic method one can see that the engine weight decreases faster than the thrust. This could lead to a wrong conclusion that it is better to use a large number of small engines instead of a small number of large engines. Hence this scaling range should be used with care.

Except from the engine mass it was assumed that the nacelle and pylon are also part of the installed engine mass. For this particular case the pylon/nacelle mass is a very large bit.

In order to find how this mass changes with thrust, it is necessary to find a relation between the thrust and the pylon length. This length is split up into two parts a variable and fixed part. Once the engine position is known the fixed part can be determined, this is 1.92m. The variable part depends on the fan diameter and engine diameter. This diameter changes as thrust changes in the following manner.

$$Diameter^2 \propto Thrust \tag{7.10}$$

The thrust of an propeller can be determined with the actuator disk theory or momentum theory. According to this theory, thrust is delivered as the time rate of change of momentum of the fluid that goes through the disk [21].

$$T = A(p_2 - p_1) = \frac{\pi}{4} D^2 (p_2 - p_1) \tag{7.11}$$

As can be seen in Equation7.11, the thrust is proportional to the diameter. Note that when using a propfan, the actuator disk is actually an actuator annulus. So the annulus area is used to determine the effective disk diameter.

$$A_{effective} = A_{fan} - A_{nacelle} = \frac{\pi D_f^2}{4} - \frac{\pi D_n a c^2}{4} = 7.687 m^2 \tag{7.12}$$

This results in an effective disk diameter, $D_{eff} = 3.122m$. Using the maximum thrust range of the previous scaling relation the disk diameter range can be found.

$$D_{eff_{Scaled}} = \sqrt{\frac{T_{Scaled}}{T_{Original}}} \cdot D_{eff_{Original}} \tag{7.13}$$

The disk diameter should be between 2.792 and 3.420m. Of course in order to get the actual propfan diameter, the engine diameter is needed. It is safe to assume that the engine diameter depends on the shaft power that the engine delivers. This power depends on the mass flow that goes through the engine. So the engine power is proportional to the engine thrust. Meaning that Equation 7.10 may also be used to determine the engine diameter. Again using the thrust range from Equation 7.8, the diameter lies between 1.503 and 1.840m. For simplicity, the program uses the complete diameter instead of dividing it into two parts and rearrange it back at the end. This gives that the variable length, $l_{variable}$, ranges from 1.485 to 1.818m. A statistical relation between the pylon length and it is mass is given in Figure 7.2.

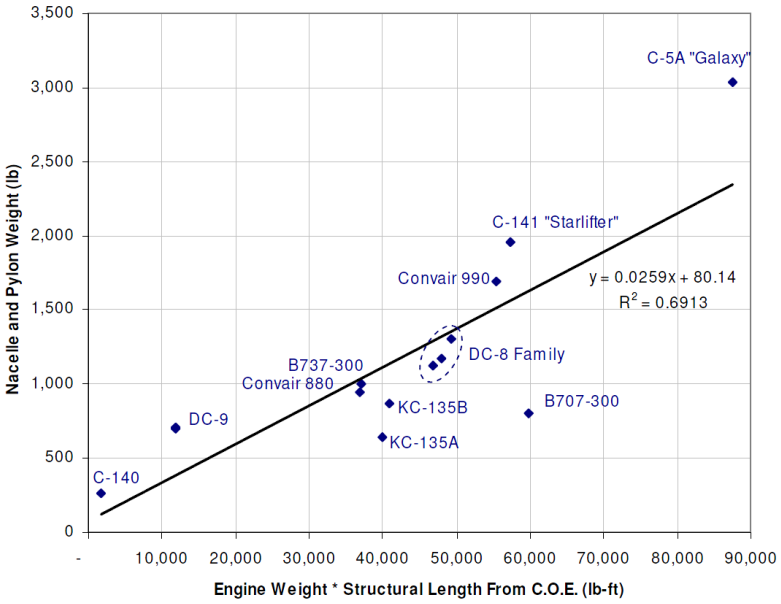

Figure 7.2: Pylon Weight Trendline (Note: Imperial Units)[57]

$$m_{PylNac_{Scaled}} = (0.0259(\frac{l_{fixed+variable}}{0.3048}\frac{m_{Scaled}}{0.4536}) + 80.14)0.4536 \tag{7.14}$$

According to Equation 7.14, $m_{PylNac_{Scaled}}$ boundaries are 600kg and 1003kg. Which is a bit low compared to the $m_{pyl,nac} = 1157kg$, and that Equation 7.14 gives a 32% lower result. This error is probably caused by the fact that all statistics that where use by Gisin are based on wing mounted engines [57]. Wing mounted pylons are generally lighter as they do not need to carry the bending moment belonging to the engine weight itself. Therefore it is assumed that the Torenbeek method can be used to scale the installed engine weight. All engine scaling limits can be found in the following Table7.4.

Table 7.4: Engine Scaling Range

Quantity	**Standard**	**Minimum**	**Maximum**
n	1.1	1.07	1.14
m_{engine}	2490kg	1948kg	3042kg
$m_{pyl,nac}$	1157kg	905kg	1415kg
$m_{installed}$	3647kg	2853kg	4457kg
T_{static}	98kN	78.4kN	117.6kg
D_{eff}	3.122m	2.792m	3.420m
D_{fan}	3.320m	2.970m	3.636m

Chapter 8

Stability and Control

In this chapter the stability and control of the model is addressed with, first, the methodology used for the sizing of the empennage in Section 8.1. Then, the scaling laws derived from the simulation results are described in Section 8.2. Sections 8.3 and 8.4 subsequently discuss the verification and validation of the model.

8.1 Methodology

The stability and control to be discussed mainly encompasses the empennage module. The methodology for this topic entails the sizing of the horizontal and the vertical stabiliser.

8.1.1 Horizontal stabiliser sizing

The horizontal tail sizing is performed by means of assessing the longitudinal stability with the longitudinal X-plot, as it is the tail's predominant function to provide longitudinal stability and control. The main assumptions made for the model are that the horizontal tail location is fixed with respect to the A320 location (i.e. low-tail configuration at 91 per cent of the fuselage length, measured from the nose) and that there is no interaction between the engines and the tail surface for the fuselage-mounted case nor any aeroelastic bending. Furthermore, the influence of control surfaces on the area are not taken into account and the effects of ice on the area needed are also not considered. In determining the Centre of Gravity (CG) it is assumed that the aircraft consists of seven groups (wing, engine, front fuselage, middle fuselage and back fuselage, horizontal tail, vertical tail) each with their weight acting at a 'group CG'.

The aerodynamic centre used in the model mainly depends on the wing contribution, but also the horizontal tail and thrust effects are taken into consideration. The latter accounts for the velocity stability induced by mounting the engines above the CG, for the fuselage-mounted case.

Note that all methods used are either depending on semi-empirical equations or data taken from *Torenbeek* [34]. The tail sizing method is implemented in the simulation, which requires most input values to be variable due to changes with each iteration in the simulation. Therefore, deviations from the actual values might occur when semi-empirical methods are applied.

8.1.1.1 Loading diagrams

The loading diagram is obtained by estimating all component weights of the A320 and determining a realistic weight distribution and CG location of each component based on the information in Chapter 42 of Obert [37]. Additionally, for the scaling a percentage of each component weight is assumed to be variable depending on the scaling factor. By adding all weights to the OEW, the total CG position can be computed. Next, all passengers, their luggage and the fuel are added and the maximum and minimum CG positions for different wing positions can be found.

8.1.1.2 Stability and controllability

In order to size the horizontal tail, its stability and controllability margins have to be defined as well, which are functions of the CG position (equation 8.2 and 8.2). All lift and moment coefficients of the wing and the aircraft are semi-empirically determined and have to change for each iteration. The aircraft is stable and controllable if the horizontal tail area corresponds to a normalised CG within both the stability and controllability regions, respectively to the left and to the right of the functions. Figure 8.1 (also called longitudinal X-plot) shows the two functions within a range of CG positions measured from the Leading Edge Mean Aerodynamic Chord (LEMAC), normalised with the Mean Aerodynamic Chord (MAC). Since the loading diagram consists of the same x-axis as the longitudinal X-plot, the two figures can be aligned and the optimal horizontal tail area and its corresponding wing position at the fuselage can be determined. This can be done by finding a horizontal line when connecting the intersection of the stability curve with the most aft CG positions and the intersection of the controllability curve with the most front CG positions. A graphical example is given in Figure 8.2. Note that the influence of the elevator control surface is not taken into account and that the attained area is assumed to be the minimum size possible for the selected configuration.

$$\frac{S_H}{S} = \frac{\bar{x}_{CG} - \bar{x}_{ac} + 0.05}{\frac{C_{L_{\alpha H}}}{C_{L_\alpha}}\left(1 - \frac{d\epsilon}{d\alpha}\right)\frac{l_H}{\bar{c}}\left(\frac{V_H}{V}\right)^2} \tag{8.1}$$

$$\frac{S_H}{S} = \frac{\bar{x}_{CG} - \bar{x}_{ac} + \frac{C_{m_{ac}}}{C_{L_{A-H}}}}{\frac{C_{L_H}}{C_{L_{A-H}}}\frac{l_H}{\bar{c}}\left(\frac{V_H}{V}\right)^2} \tag{8.2}$$

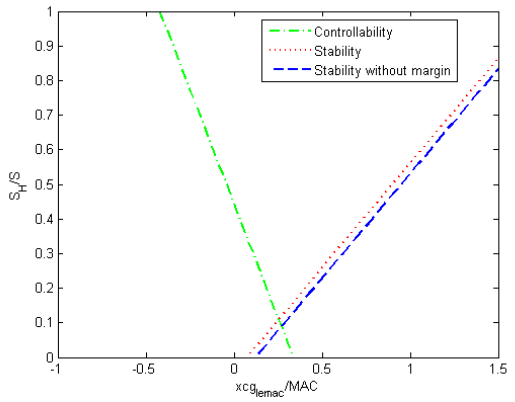

Figure 8.1: Longitudinal X-plot showing the stability and controllability curves using A320 parameters

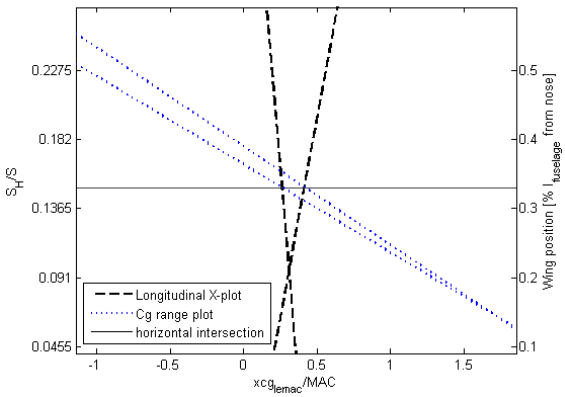

Figure 8.2: Combined scissor and CG range diagrams resulting in optimum tail size and wing position.

8.1.2 Vertical stabiliser sizing

The vertical stabiliser size is determined through a *fast vertical tail sizing for directional stability of fuselage-mounted engines aircraft* approach [35]. The main assumptions made for the model here are that the vertical tail location is fixed with respect to the A320 location and that there is no interaction between the engines and the tail surface for the fuselage-mounted case. Furthermore, the influence of control surfaces on the area are not taken into account and the effects of ice on the area needed are also not considered. The used method is only applicable for aircraft with fuselage-mounted engines. Therefore, in the wing-mounted case use is made of the A320 stabiliser size.

The used method to scale the vertical stabilizer depends on a linear relation between the vertical tail volume coefficient and the stability derivative C_{n_β} (see Figure 8.3). As the overall shape of the fuselage and the wing location (low configuration) do not change, C_{n_β} and the vertical tail volume coefficient are mainly depending on the CG position, which defines the moment arm length (using semi-empirical formulae form Torenbeek [34]).

8.2 Empennage Scaling Laws

Based on the trends observed from results of the program for varying sweep and aspect ratios the following scaling laws can be derived for the horizontal and vertical stabiliser.

8.2.1 Horizontal stabiliser size

Figure 8.7, 8.8, 8.5 and 8.6 show an example of the scaling laws created by the program for the tail section. The formulae are given in each figure, describing an estimated function in the given vicinity of the inputs, aspect ratio and wing sweep angle. The area ratio between horizontal stabiliser and wing ($\frac{S_H}{S}$) and the wing position are plotted against Λ and AR, respectively. It is important to mention, that both horizontal stabilizer size and wing position are coupled outputs and result in one scaling law because of the used method, which is optimising for stability and controllability. It is noteworthy, that for an increasing AR and Λ the structural weight of the wing is drastically increased as well, which can be seen in Section 5.4.1. The aerodynamic centre position is a function of AR and Λ, which generally moves aft for increasing AR and Λ according to Torenbeek [34].

Figure 8.4 shows an example case of the resulting change of AR. It can be seen that the CG and aerodynamic centre are relatively close to each other in case of a small AR, which results in a wing position farther from the nose and a bigger tail area due to the short moment arm. In case of a high AR the opposite effect occurs. A higher stability margin is obtained and the wing is positioned closer to the nose, resulting in a larger moment arm, hence a smaller tail area. The total trend of the scaling law is a decreasing tail area and the wing positioned closer to the nose with an increase in AR.

The same case as depicted in Figure 8.4 occurs for Λ. The stability margin changes proportionally to the previous case, namely increasing for increasing sweep and the same trend can be found as for the AR, decreasing the horizontal tail surface area.

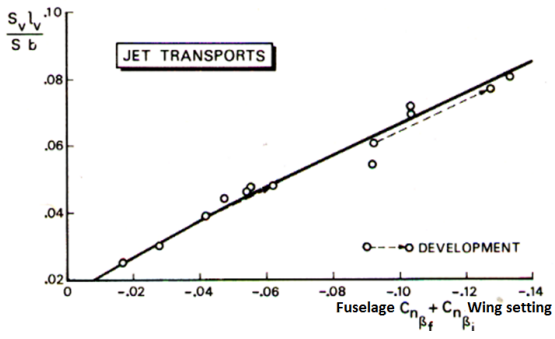

Figure 8.3: Relation between vertical tail volume coeffiecient and C_{n_β} [34]

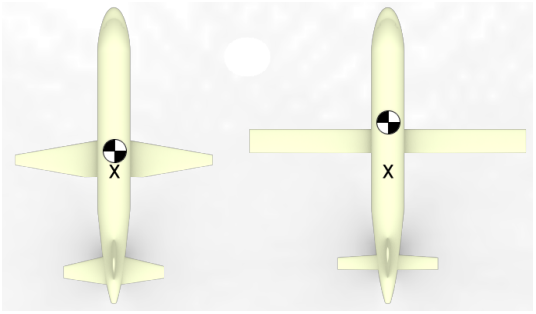

Figure 8.4: Influence of changing AR on wing position and horizontal tail area, not to scale. X indicates the aerodynamic centre location.

In both cases the area ratio is decreasing with increasing AR and Λ. The wing position shifts farther to the front of the aircraft for both increasing AR and Λ.

In case of a small Λ the wing is positioned farther to the back of the aircraft and the tail size is relatively big to counteract the short arm l_H. For a bigger Λ the CG shifts farther aft due to the wing structure and reduces the distance from the CG to the wings's aerodynamic centre. In order

to satisfy longitudinal stability and controllability of the aircraft the wing position is located closer to the nose and a decreased tail area is required due to a longer arm l_H.

For a small AR, the span of the wing is short compared to its chord length which results in a high MAC. Since the position of the aerodynamic centre influenced by the fuselage, nacelles, wing and engine position depends on $\frac{1}{c}$ [34], its location is close to the LEMAC for high MAC values. With the aerodynamic centre position closer to the LEMAC and thus closer to the aircraft's CG, the wing cannot not be positioned too far in the front and therefore a bigger tail area is required to satisfy stability and controllability. With increasing AR the aerodynamic centre shifts aft and the wing can be positioned farther to the front, reducing the required tail area.

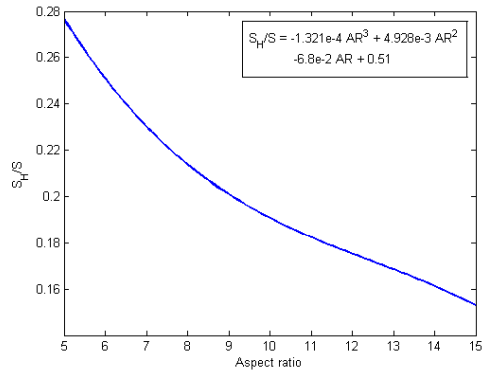

Figure 8.5: $\frac{S_H}{S}$ against wing AR with a Λ of 17° and fuselage mounted engines.

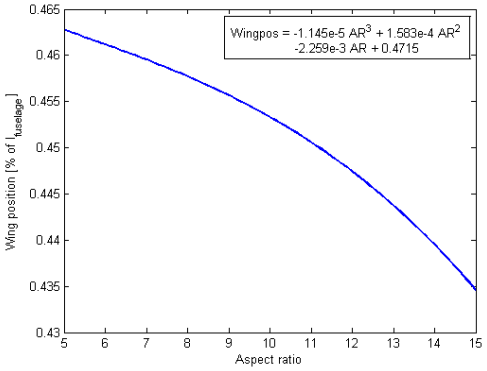

Figure 8.6: Wing position (% of $l_{fuselage}$) against wing AR with a fixed Λ of 17° and fuselage mounted engines.

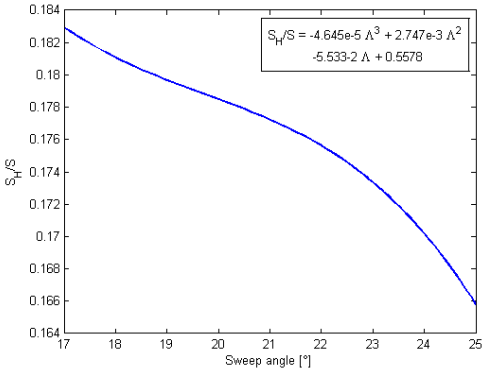

Figure 8.7: $\frac{S_H}{S}$ against Λ with fixed AR of 11 and fuselage mounted engines.

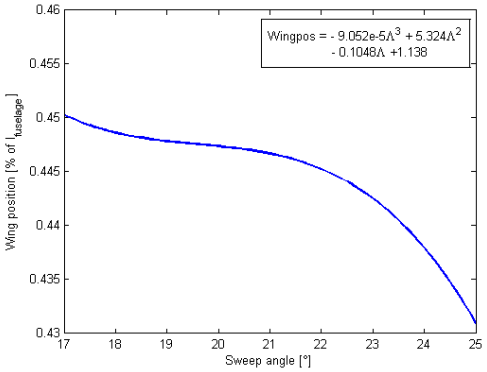

Figure 8.8: Wing position (% of $l_{fuselage}$) against Λ with fixed AR of 11 and fuselage mounted engines.

8.2.2 Vertical stabiliser size

Figures 8.9 and 8.10 show the vertical tail size depending on the aspect ratio and wing sweep angle. As explained in Section 8.2.1 the horizontal stabiliser size decreases with increasing AR and Λ due to an aft shift of the aircraft's CG. The same applies for the vertical stabiliser size, which depends on the distance between the aircraft's CG and the vertical stabiliser's aerodynamic centre (l_V) and the stability derivative C_{n_β}. Due to an increase in Λ, the CG shifts aft and the vertical stabiliser size decreases respectively. In case of the AR a peak can be found at AR=7.5, which originates

from the wing position initially positioned aft the fuselage CG. When the AR is increased, the total CG first moves aft until the wing's and fuselage's CG are aligned at AR=7.5 and reducing if AR is further increased.

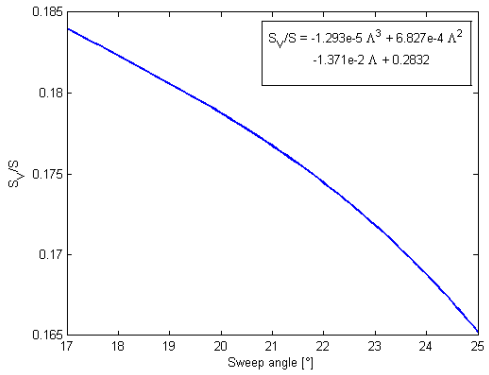

Figure 8.9: $\frac{S_V}{S}$ against Λ with fixed AR of 11 and fuselage mounted engines.

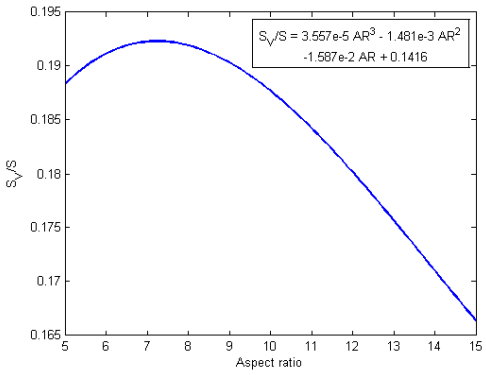

Figure 8.10: $\frac{S_V}{S}$ against wing AR with a fixed Λ of 17° and fuselage mounted engines.

8.2.3 Static Longitudinal Stability Margin

From the obtained horizontal tail area and its corresponding wing position, a static stability margin can be found which corresponds to the distance between the aircraft's CG and the *total* aerodynamic centre position (including the tail). The bigger the distance, the more stable the aircraft is but also tends to become harder to control. With the CG shifting during flight because of fuel being burnt and people move in the aircraft, it is important to provide sufficiently high margin. In Figure 8.11 and 8.12 the static stability margin is plotted against various AR and Λ values. The CG position is taken from mid-cruise flight which means that half the fuel is burnt.

Figure 8.11 shows linear behaviour of a decreasing stability margin with increasing Λ. As mentioned in section 8.2.1, the CG moves towards the LEMAC when increasing the sweep angle. The aerodynamic centre is also affected by the sweep and both changes combined result in a linear function. Consequently, a lower Λ provides a higher longitudinal stability margin.

Figure 8.12 displays rather different behaviour. In case of increasing AR, a higher stability margin can be obtained which peaks at an AR of approximately 13. The reason for that is the high influence of the AR on the aerodynamic centre position ($\bar{x}_{ac} = f(\frac{1}{c})$) [34]. For higher AR values the CG positioning starts to dominate and the stability margin decreases.

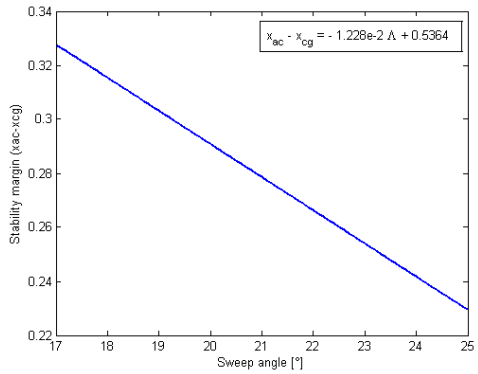

Figure 8.11: Static stability margin ($\bar{x}_{ac}$ - $\bar{x}_{CG}$) against Λ with fixed AR of 11 and fuselage mounted engines.

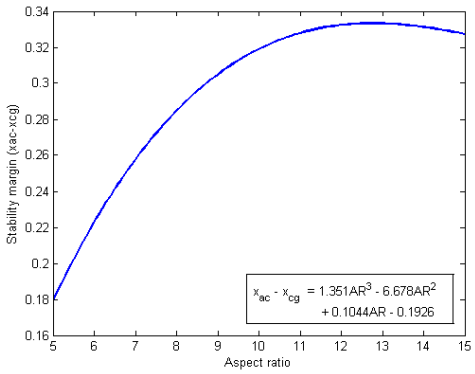

Figure 8.12: Static stability margin ($\bar{x}_{ac}$ - $\bar{x}_{CG}$) against AR with fixed Λ of 17° and fuselage mounted engines.

8.3 Verification

The following section addresses the verification of the implemented method, both for the horizontal and for the vertical tail.

8.3.1 Horizontal Tail

Figure 8.13 shows the loading diagram for a wing position of 34% of the fuselage measured from its nose. It can be seen that the CG shifts aft when the passengers are entering the aircraft which complies with wing-mounted narrow-body aircraft [35]. For the fuselage-mounted case the opposite effect is to be observed, as expected for this type of configuration [35].

For each wing position the minimum and maximum CG position including a 2% safety margin are plotted against the CG position in the CG range diagram, see Figure 8.14.

In case of the longitudinal X-plot the function's slopes for varying input can be compared (the denominator's inverse of equations 8.2 and 8.2, respectively) in order to verify its correctness. The difference between the slope of the A320 model and a changed configuration (AR=14, Λ=17, λ=0.05) are 0.068 for the stability and -0.192 for the controllability curve. Due to the change in slope it can be seen that the X-plot graph increases its range (like an opening scissor) where the tail can be sized, decreasing the required ratio $\frac{S_H}{S}$.

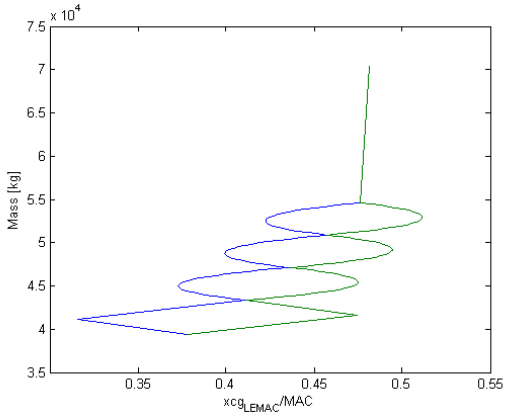

Figure 8.13: Loading diagram for wing position at 34% of the fuselage measured from the nose

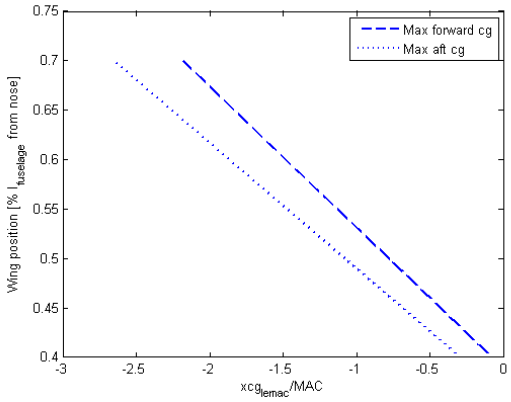

Figure 8.14: CG range diagram with A320 parameters

8.3.2 Vertical tail sizing

Similar to the horizontal tail size, the vertical tail area decreases for the new configuration, which reduces the area by 2.85 m^2 due to the change in wing position, located further aft. Thereby also displaying the expected behaviour.

8.4 Validation

The validation of the stability and control is conducted with respect to the A320 for the wing-mounted case and with respect to trends from existing aircraft for the fuselage-mounted case. The existing aircraft used for the latter case are the Boeing 727, McDonnell Douglas DC-9, Fokker 100, MD-80, MD-90 and Tupolev 134. The characteristics of these aircraft are compared with the computationally generated data on: wing positioning, the forward and aft CG, and the tail volume coefficient [37, 34, 33, 58]. The CG values are defined for the take-off and landing configurations, as this is the critical case (i.e. minimal CG range) within the operating limits regarding loading.

The comparison of the computational and the empirical values can be found in Table 8.1. Here the forward CG position is usually critical for trim [33]. From this table it can be concluded that apart from the CG at take-off (slightly aft of the take-off, aft-CG limit cite[59]), the computationally acquired CG is completely within the operating limits of the A320, regardless of the fuel loading. For the fuselage-mounted calculation, all CGs corresponding to all loading cases are well within the average operating limits known for existing aircraft. It is to be noted, however, that for the fuselage-mounted case the variance for the CG range is rather high and thus the boundary values do clearly not solely depend on the engine placement.

From Table 8.1 it can subsequently be concluded that the model is relatively accurate on account of the wing positioning with a deviation of 16 per cent from the actual A320 and a difference of less than ten per cent for the new aircraft with respect to the average for existing fuselage-mounted aircraft.

Furthermore, given the assumptions mentioned in section 8.1 the computed tail areas themselves will be smaller than their real world equivalent. For the validation the tail volume coefficients are used, as these are the primary indicators for the stability of the design. Since the horizontal tail volume coefficient e.g. highly influences c_{m_α}, which is the main predictor of static longitudinal stability. In the model the vertical tail volume coefficient, on the other hand, allows to evaluate the static directional stability (i.e. indirectly evaluating c_{n_β}). It is found that the horizontal tail volume coefficient of the new aircraft deviates only 1 per cent from the average coefficient for fuselage-mounted aircraft. Hence, the longitudinal stability behaviour is similar to that of existing aircraft. The vertical tail-volume coefficient is 24 per cent higher for the fuselage-mounted and even 36 per cent higher for the wing-mounted case. Ergo, the vertical tail sizing procedure is not accurate enough to represent the complex phenomena that are affecting the directional stability characteristics.

Table 8.1: Validation of stability and control characteristics [37, 34, 33, 58], F = fuselage-mounted, W = wing-mounted

Aircraft type	**Engine Position**	**Wing position** [$\%l_{fuse}$]	**Forward CG** [%**MAC**]	**Aft CG** [%**MAC**]	$\frac{S_h l_h}{S\,MAC}$	$\frac{S_v l_v}{Sb}$
Boeing 727	F	0.508	10.0	34.0	0.845	0.091
Douglas DC-9	F	0.482	16.3	39.0	1.150	0.080
Fokker 100	F	0.477	13.0	35.0	0.978	0.064
MD-80	F	0.482			1.030	
MD-90	F	0.524			1.228	
Tu-134	F	0.481			0.700	0.076
Airbus A320	W	0.391	16.0	41.0	0.799	0.086
Fuselage-mounted average	F	0.492	13.1	36.0	0.989	0.075
Fuselage-mounted variance	F	0.000	9.93	7.00	0.038	0.000
New aircraft calculated	F	0.452	CG_{OEW} $CG_{landing}$ $CG_{takeoff}$	= 22.7 = 26.9 = 29.4	0.980	0.093
Airbus A320 calculated	W	0.330	CG_{OEW} $CG_{landing}$ $CG_{takeoff}$	= 30.0 = 39.3 = 41.7	0.727	0.117

8.5 Discussion

From the validation it can be concluded that the preliminary design approach used for the empennage sizing is not accurate enough to account for all phenomena affecting the stability and control

characteristics. Especially the directional stability - as indicated by the vertical tail volume coefficient in table 8.1 - is not up to par, with a rather large deviation from the A320 itself and from the average value for fuselage-mounted aircraft. Therefore, given the assumptions of the sizing approach the current results are only valid for this simplified case. Extending the analysis with the consideration of control surfaces and for example aeroelastic bending in the longitudinal case, would give a more accurate representation of the tail sizes and wing position needed to guarantee stability and control.

Additionally the effect of the engine on the tail surfaces has not been taken into account. To be able to describe the stability and control of the aircraft in a more satisfactory manner it is therefore advised to make the configuration of the empennage variable to account for a change in stability behaviour due to interaction effects. An example of such a change would be a T-tail configuration, compared to the current low-tail configuration that is assumed constant. Further recommendations are discussed in chapter 14.

Chapter 9

Computational Model Description

The main goal of this project is to create a new design method in order to speed up the design process. This should be achieved by using scaling laws. These scaling laws can be found through analytical analysis, empirical data, or by modelling the aircraft. This chapter will elaborate on how the model is built up, its functionality, and how it is used to create scaling laws.

9.1 Design Space

The scalable model has several varying parameters. These parameters have a defined range for which they can be varied. To obtain the range for which they can be varied, a design space has to be defined.

The medium-size aircraft group is a class definition set upon by regulatory agencies. This group has characteristic definitions which apply on them. These parameter ranges are a source for the limits on the parameters. Another limiting factor is for example the accuracy of the program.

Speed - The design range for the speed is very limited. Although the model will give a design for varying speeds, its accuracy will be fairly low. This is due to the constant SFC of the engines. Accurate designs are scaled for the engine of the A320 at Mach 0.78 and for the UDF designs at Mach 0.72. These are the data points of the SFC for the respective engines on those speeds.

Aspect Ratio - The aspect ratio's range is confined by regulations set by FAA and ICAO [60, 61]. The aspect ratio is dependent on the wingspan and wing area only. The wing area of the aircraft is calculated using the stall speed of the A320. Hence, changing the aspect ratio results in a change in wingspan. Aviation regulations have a defined range for the wingspan which is based on categories. The A320 belongs according to FAA/ICAO classifications to the III / C category [62, 63]. If the target design is set on the same category as the A320, the wingspan will be rather limited. Therefore the range of the wingspan for the new design is set at the same and a higher class. This is tabulated in 9.1. The maximum span of 52 meters corresponds with an aspect ratio of 27.

Table 9.1: Constraints

	Min	**Max**
Airport	0	80
FAA/ICAO Class III/C	24 [m]	36 [m]
FAA/ICAO Class IV/D	36 [m]	52 [m]
Design Space	24 [m]	52 [m]

Taper Ratio - The taper ratio is allowed to vary between 0.25 and 0.5. This range has been estimated based on reference data. Furthermore, lower taper ratios can lead to inaccurate computations by AVL and can lead to designs which are difficult to produce. When using a low taper ratio, the aircraft should be checked for aileron size and tip stall.

Engine Options - A trade-off has been made on propeller engine possibilities for the new design. A fuselage mounted engine came out on top. In the model, the engine has two possibilities. When the model is run and the engine box is unchecked, the new model will use the engine settings of the A320. This is the default value of the model as it is the reference aircraft. When the box is checked, the turboprop engine option is used which is mounted on the fuselage. This is the engine that has been chosen through a trade-off.

Range - The range of the aircraft can be inserted as an input for the model. Values between 500 [km] and 12,000 km are defined as the limits. The design range for the aircraft is 5,000 km.

Sweep - The bounds of the sweep for the design are dependent on the cruise speed. At a cruise speed of Mach 0.72, which corresponds with the turboprop engine option, the minimum sweep angle becomes seventeen degrees. The engine of the A320 is designed for a cruise speed of Mach 0.78 which corresponds to a minimum sweep angle of 28 degrees. These minimum sweep angles are limited by the critical Mach number.

Table 9.2: Design Space

Parameter	UDF Engine	A320 Engine
Speed	Mach 0.72	Mach 0.78
Minimum Sweep	17 deg	28 deg
Maximum Aspect Ratio	27	27
Taper Ratio Range	0.05 - 0.5	0.05 - 0.5
Range	500 [km] - 12 000 [km]	500 [km] - 12 000 [km]

9.2 Data Flow

Because a model for a complete aircraft can become large rather quickly, a Data Handling Block Diagram can be a useful tool to understand the information flow. The data flow of this program can be found in Figure 9.1.

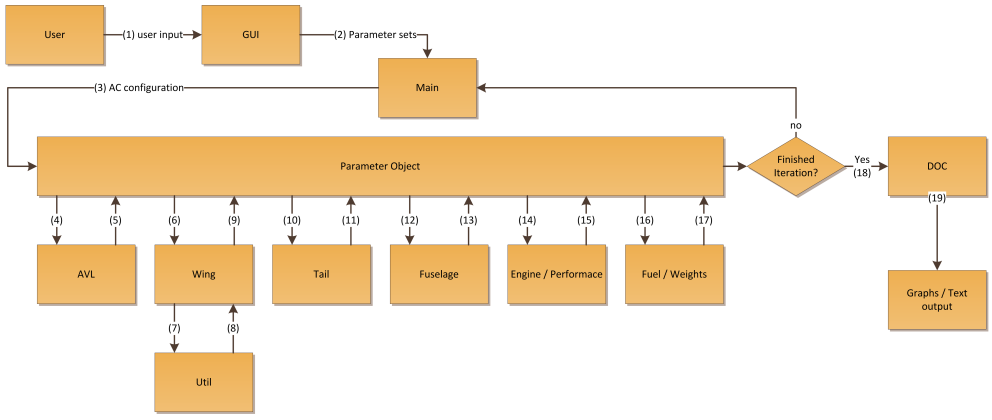

Figure 9.1: Data Handling Block Diagram

As can be seen in Figure 9.1, all modules of this program share the data stored in the Parameter object. This class contains the data that is applicable to more than one module. An example is for instance the wing area, which is important to both the wing module, AVL and the tail module. An overview of the data flow can be found below:

1. The user tells the program what the minimum and maximum parameter values are, and the number of steps by filling in the GUI.

2. The GUI sends the data to the main program, which is checked for validity.
3. the Main class uses the info from the GUI to create Parameter sets. Each set contains a combination of Speed, Aspect Ratio, Range, Sweep, Taper and engine location, plus an initial estimate for all other variables such as MTOM.
4. The first Module to be activated is AVL. AVL uses the initial estimate for the MTOM and the wingplan for its calculation.
5. The output of the AVL module is the spanwise loading distribution, together with the Oswald factor and total Lift over Drag.
6. After AVL has finished its calculations, the wing module is called. The input is the wing planform, the airfoil, wing loading, forces acting on it, and material properties.
7. Some of the functions used in the Wing module are defined in the Util module. This is a separate module that is not used on its own, but it contains functions which are useful in multiple locations in the program. One of those functions is Crosssection(). it calculates some cross-sectional properties of an airfoil, and uses the airfoil and spar locations as input.
8. The output of Crossection() is a list of cross-sectional areas, spar heights and skin lengths.
9. The Wing module output consists of spanwise cross-sectional properties and thicknesses, spar locations and the total wingbox mass.
10. After the wing is finished, the tail module can be called. The inputs are all the weights and their locations, the wing location and the engine location.
11. The Tail module returns the tail area, the estimated mass and wing location. This mass is calculated by using scaling laws that were found using the wing module.
12. The Fuselage module uses weight and lift distributions as input.
13. The Fuselage output consists of the stringer geometry, skin thickness, stringer count and the fuselage structural mass.
14. The Engine / Performance module uses information from other modules. The input includes: Lift over Drag, Maximum take-off mass, Sweep, Mach and MAC.
15. The Engine / Performance module gives back the engine properties and wing area.
16. Next, fuel mass and MTOM functions are called. The input includes: component weights, SFC and mission data (Range, Speed etc.).
17. The output of the Fuel and MTOM function is the Fuel mass and Total Mass. Furthermore, the output also includes the fuel use and efficiency.
18. Finally, the data is ready for displaying and exporting.

9.3 Components

The program is set up in a modular way, this means that components can be adjusted and expanded without causing problems in other modules. Also, this approach allows for many people to work on the same program without getting in each others way. Some of these components will be elaborated.

9.3.1 Wing Module

The wing module starts with converting the lift/drag/moment distribution and engine weight to shear, moment and torque distributions across the wing.

Next, the airfoil data used for the aircraft is loaded. This airfoil data consists of many coordinates, starting at the trailing edge, running over the top the the leading edge, back over the bottom and ending again at the trailing edge. With this data the spanwise spar heights, skin lengths and cross-sectional areas are found. The output of this function can be seen in Figure 9.2

In order to get the lowest possible wingbox weight, the wingbox is subdivided in slices. Of each slice, the lightest possible cross-section should be found. this means the lightest possible combination of thicknesses. The approach taken for this module is to equalise the Von Mises stresses in all critical locations to the maximum allowable stress.

At last, the mass of the wingbox is calculated by adding the volume of all slices together and multiplying it with the density of the used material.

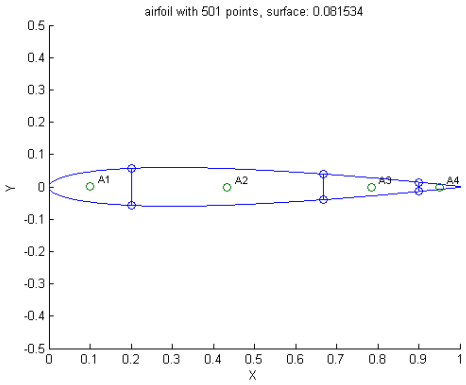

Figure 9.2: Cross-section function

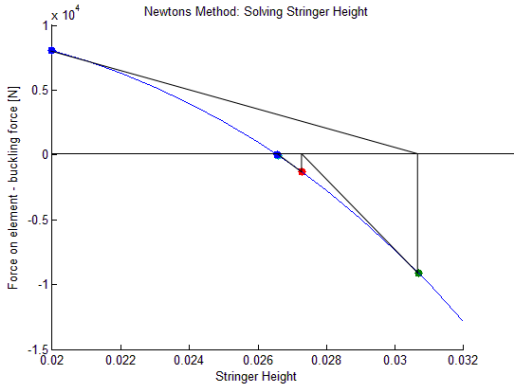

Figure 9.3: Newton method applied to required stringer height

9.3.2 Fuselage Module

The allowable forces in all elements in the fuselage can be calculated for different failure cases. By trying different configurations, the lightest combination that is strong enough can be found. However, since the stringer geometry depends on the skin thickness and vice versa, the method for solving this equation is not straightforward.

The formula defining the thicknesses and stringer geometry count turned out to be analytically unsolvable. Therefore the Newton method was used. Figure 9.3 shows how the solution was found in four iterations.

9.3.3 AVL interface

In order to make use of AVL, an interface is required. In this interface the input files are created, and AVL's output files are read. Also, this module can display information like the lift distribution, span efficiency etc. if the user requests those graphs.

9.4 Complete Model

Using the computational model, it is possible to find an optimal configuration for the new aircraft. However, since the aircraft is defined using many parameters, solving this problem is a complex task. Also, it should be noted that running the model for enough configurations is a time consuming process.

The project goal was to create a new high aspect ratio aircraft, capable of achieving a 30% fuel reduction. Therefore, it should be investigated what the effect of a higher aspect ratio is on fuel consumption.

To get a good view of the effect of the aspect ratio, several graphs were created by running the program for many different configurations.

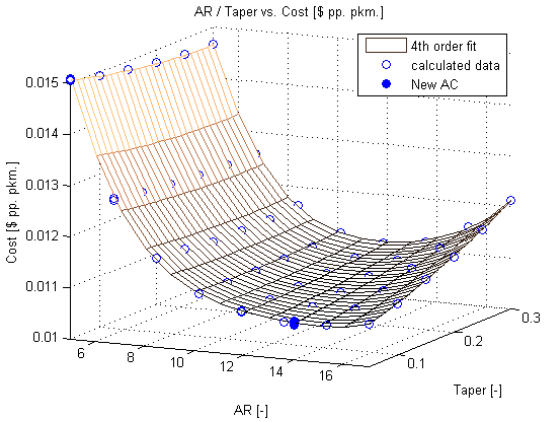

Figure 9.4: AR and Taper vs. DOC; range = 5,000 km, taper = 0.05)

From Figure 9.4, it is clear that the optimal aspect ratio at a range of 5,000 km is fourteen. Also, even though the effect is minimal, a small taper is preferred. However, the minimum taper is limited

due to the fact that the ailerons are located at the tip, and therefore the tip chord can not go to zero. Other consideration such as stall and the usability of AVL are also important for this.

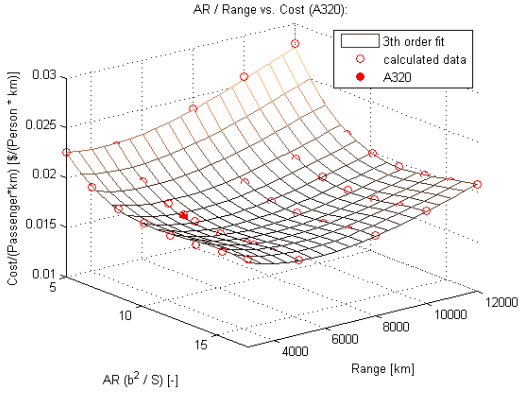

Figure 9.5: AR and Range vs. Cost / passenger kilometre (A320)

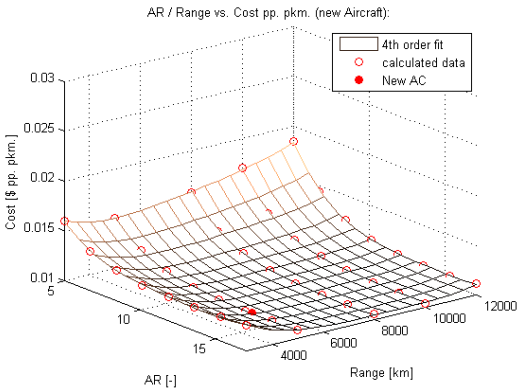

Figure 9.6: AR and Range vs. cost (New AC)

9.4.1 Effect of Range

Figure 9.5 and 9.6 show the cost per km per passenger for both the A320 and the new aircraft. Note that in both figures, the cost decreases from a range of 3,000 to 7,000 km. This is due to the fact that many different parts of the mission that produce cost do not occur during cruise flight and therefore, do not add to the distance travelled. Some of these aspects are taxiing, engine start-up, climb and descent.

It can also be seen that due to the large fuel savings, the new design is considerably more efficient than the A320 at larger ranges (12,000 km), since less fuel has to be taken along.

9.4.2 Effect of Sweep

From Figure 9.7, it can be seen that sweep has a negative influence on the fuel efficiency. However, it should be noted that since a vortex lattice method was used, no effects of local supersonic flow can be taken into consideration, and therefore, effects occurring because of a too low sweep for the Mach number are not shown. Further elaboration on the aerodynamic effects of the sweep angle can be found in Subsection 4.4.2.

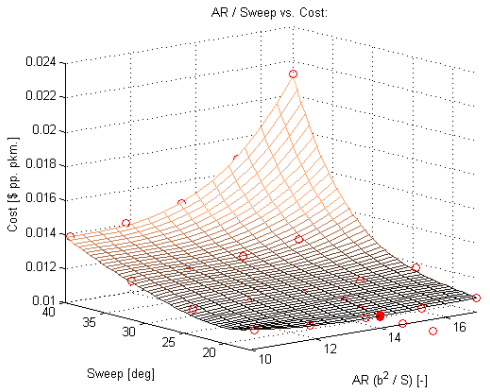

Figure 9.7: Sweep and AR vs. Cost / passenger kilometre

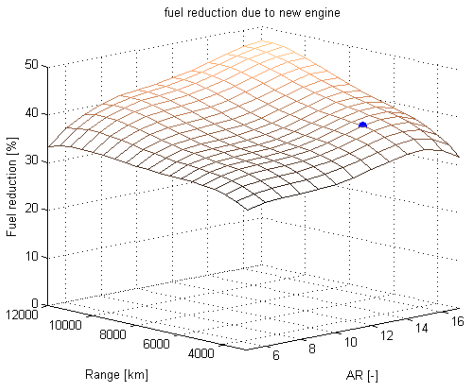

Figure 9.8: Range and AR vs. fuel saving / passenger kilometre

9.4.3 Effect of Cruise Mach Number

Since the new aircraft is using an engine which is currently still under development, exact numbers on the performance at different airspeeds are not available. Therefore no accurate predictions on the effect of Mach number can be found. Figure 9.9 shows the effect of a different speed on the lift over drag, but since many other effects are not taken into account this result is not very accurate.

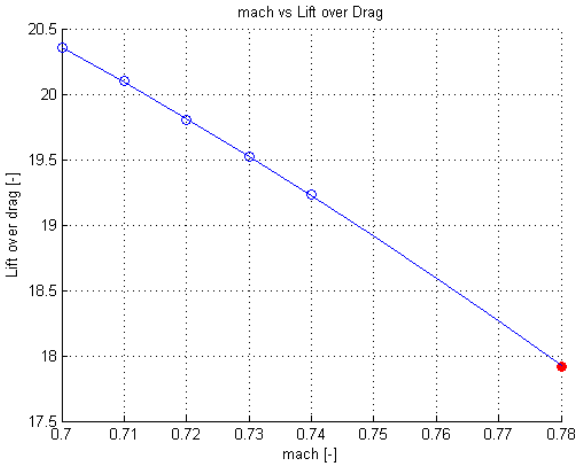

Figure 9.9: Mach vs. Lift over Drag

9.4.4 Effect of New Engine

By using a new engine, fuel consumption can be greatly reduced. Not only does the specific fuel consumption reduce with the new engine, it also has a snowball effect on aircraft weight. Due to having a lower MTOM, the wings and tail can be smaller and even the engine itself can be smaller. The fuel saving can be seen in Figure 9.8. The dot indicates where the new aircraft design is located. It can be seen that the fuel reduction due to the engine is around 38 per cent.

9.5 Sensitivity Analysis

In this section the sensitivity of the program is described for varying inputs, such as wing sweep or aspect ratio. The used method is *One-at-a-Time*, meaning only one input varies while the other stay unchanged. This is a simple and useful method to find how the simulation responds to changing input and whether the output diverges, converges or oscillates. Effects of varying several input at the same time cannot be taken into account and would require a rather complex analysis.

9.5.1 Sensitivity of Fuel Cost

Figure 9.10, 9.11, 9.12 and 9.13 show the effect on the fuel cost, which is the final and most important output (the fuel cost is the only varying part of the DOC in the program). For each figure, the other three inputs are kept constant (see Table 9.3. In all cases the output diverges with increasing or decreasing input values. A minimum can be found in each case which indicates the lowest fuel cost.

For Λ as input, its minimum is at 22° and diverges especially towards higher values. Note, that the lowest used Λ is 17° because of the drag divergence constraint.

The taper λ almost represents a linear line with fuel cost increasing drastically for high values of λ. In theory, the lowest achievable fuel cost would be at zero taper which is disregarded due to appearing problems with AVL.

In case of the AR, a parabola can be seen with a fuel cost minimum at 13. For both increasing and decreasing values of the AR it diverges with a steep slope.

The range shows a similar behaviour as the AR, with a minimum fuel cost at 9000 km and diverging values for lower and higher ranges.

In summary, the simulation is sensitive to especially high input values which cause the fuel cost to diverge with a steep increase. The interdependency between the inputs cannot be displayed with the *One-at-a-Time* method and it therefore disregarded.

Table 9.3: Magnitude of input values which stay constant while one changes, for engine located fuselage mounted.

Parameter	Magnitude
Λ [$\circ$]	17
λ	0.05
AR	14
Range [km]	5000

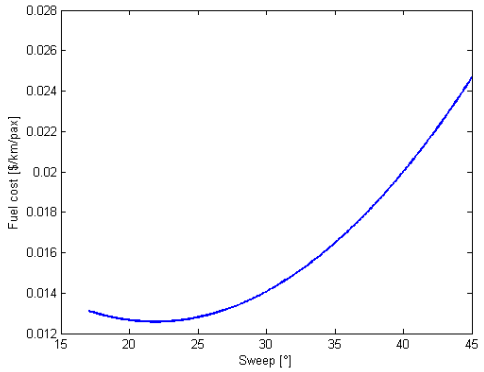

Figure 9.10: Fuel Cost [$/km/pax] plotted against varying wing sweep, Λ [$\circ$]

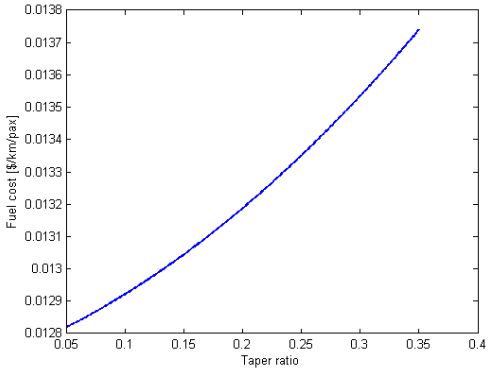

Figure 9.11: Fuel Cost [$/km/pax] plotted against varying taper ratio, λ

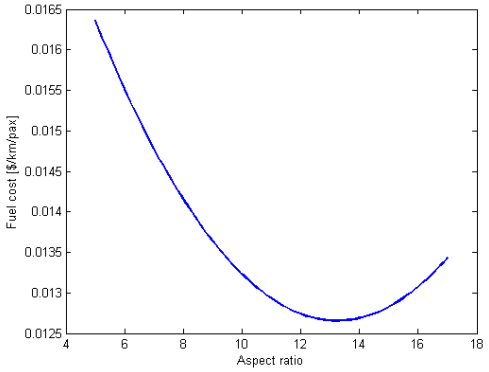

Figure 9.12: Fuel Cost [$/km/pax] plotted against varying aspect ratio

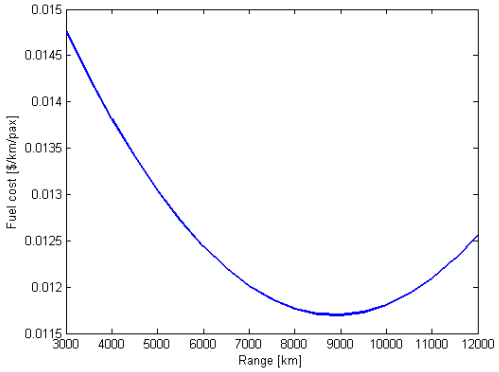

Figure 9.13: Fuel Cost [$/km/pax] plotted against varying Range [km]

9.6 Sensitivity Analysis for Initial Weight Changes

In this section the *snowball effect* of the simulation is analysed and described. The idea is to recognise how the program is reacting to small changes of the input mass, in this case the fixed fuselage mass. Several cases are compared, one with the actual A320 component mass and the other with an increment of 200 kg up to 800 kg added to the fuselage. Table 9.4 shows the changes and

impacts on the result - the MTOM, Fuel cost per year and CO_2 emission per year in kg. It can be seen that the MTOM increases by approximately 400 kg, thus an increase of a factor of 2 of the initially added mass. The difference in fuel cost per year adds up to an amount of 25,408 $/year and the CO_2 emission of 80,075 kg/year.

Figure 9.14 shows the MTOM plotted against initial mass changes of the fixed fuselage component. The mass change ranges from zero to 800 kg. The increase of mass is linear and can be explained with the functioning of the program which runs the mass calculation through a loop and stops after a fixed amount of iteration in order to save computational time. In case of the mass growth it shows a good overall picture of the *snowball effect* which causes a chain reaction in structural mass increment.

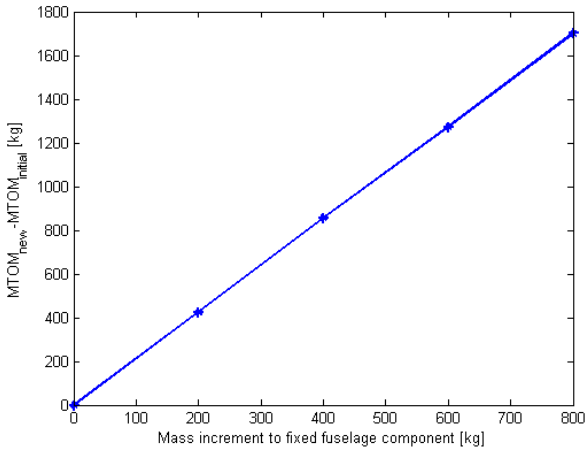

Figure 9.14: Change in MTOM due to change in initial fixed fuselage mass

Additionally, it shows the downside of the simulation, which highly depends on the initial mass values. In case of rough estimations of e.g. CG positions, component weights or component weight fractions which are fixed and scaled, a negative effect on the program's overall accuracy can be expected.

Table 9.4: Mass and cost changes due to 200 kg difference in initial Mass

Parameter	**Normal Mass - New Mass**	**Normal Mass/New Mass**
MTOM [kg]	410.28	1.0032
Fuel Cost [$/year]	25,408	1.0033
C02 emission [kg/year]	80,075	1.0033

9.6.1 Advantages and Disadvantages of Scaling Methods

The following bullet points state the advantages and disadvantages of the used scaling method, which were found during the project progress. The scaling method is compared with the *ab initio* design methodology of aircraft which has no topology constraints.

Advantages

- Generality of model, also applicable for other aircraft types within the topology constraints
- Increased cost and time efficiency due to skipping the initial design phase
- Use of existing knowledge, avoids cumbersome research
- Multidisciplinary approach includes realistic inter dependencies within the model

Disadvantages

- Short term solution for aircraft manufacturer, not innovative enough since no new technology is introduced
- Error/uncertainty propagation and possible amplification within model, small errors decrease accuracy of final outcome with each iteration
- Low accuracy when assumptions are included and initial values are incorrect (see Sensitivity Analysis)

Chapter 10

Risk Management

To enhance the development of the SCALAIR project, risk management has been continuously performed. This risk management consists of the subsequent four phases: risk identification, risk assessment, risk analysis and risk handling. Throughout the progress of the project new risks were discovered. For each risk the probability and severity of its consequences has been analysed. Section 10.2 on risk handling describes how risk cases are prevented.

10.1 Risk Identification and Analysis

The risks that were identified for the project are placed in the categories displayed in Table 10.1.

Table 10.1: Airport & FAA/ICAO Constraints

Abbreviation	Category
A	General design process risks
B	The scaling law risks
C	Computer program risks
D	Verification and validation risks
E	Feasibility of the computer program
F	Feasibility of a typical scaled aircraft from the SCALAIR project
G	Approval of a typical scaled aircraft from the SCALAIR project by the EASA

All the risks that were discovered during the project were analysed qualitatively, an overview of all the risks together with an explanation on them is given in Table 10.2.

Table 10.2: Risk overview

General design process risks		
#	Risk	Description
A.1	Over ambitiousness	The research performed in this project can become complicated and extensive quickly. Only things are essential for the functioning of the program should be done.
A.2	Miscommunication	Group members do not communicate well, causing the group to work inefficiently.
A.3	Time budget	The objective will not be achieved when deadlines are not met.
A.4	LaTeX editing	The risk of spending too much time converting text and correcting little mistakes in this program should be taken into account.

Table 10.2: (continued)

#	Risk	Description
		Scaling law risks
B.1	Superposition risks	When multiple scaling laws are used, the combined answer of the program might not be as accurate as when applying single scaling laws.
B.2	Incorrect allowable stresses used in calculations	The failure and allowable stresses that are used in structural calculations have direct influence on the mass of the aircraft. Incorrect stress values therefore lead to incorrect aircraft mass.
B.3	Simplification risks	In the derivation of scaling laws many simplifications have been made, these can lead to inaccurate scaling laws.
B.4	Limited scope scaling law risks	The scaling laws used in the computer program are only valid for scaling medium range mid size transport aircraft.
B.5	Loading case risk	The structural calculations take only into account one critical loading case. Which is the maximum loading factor taken from the flight envelope generated in the program, applied at MTOW.
B.6	Fuel weight inaccuracy	The fuel weight calculation is based on statistical data and the Breguet formulas. However those statistics may not be representable for the fuel consumption of the GE UDF engine.
B.7	Snowball effect on the weight estimation	When there is a mistake in the weight calculation of one part, this also influences the outcome of other correct weight calculations.
B.8	Scaling law parameter domain limitation risk	All the scaling laws are constrained by a domain over which parameters can be varied. If this domain is exceeded results might be obtained that are not accurate or even invalid.
B.9	Scaling law flight condition limitation risks	It can be possible a scaling law is applied for a flight condition, where it was not derived for.
B.10	Generating inconsistent scaling law risk	The developed computer program is able to perform numerical computations in order to create scaling laws. In order to get correct scaling laws the settings of the computer program have to be correct.
		Computer program risks
C.1	Program fails to converge to a design	The developed program is unable to produce a single design or gives errors because of divergent equations or characteristics.
C.2	Coding mistakes	Mistakes cause the program to malfunction.
C.3	Round-off errors	The program will round off the results. Which can be undesired and might lead to inaccurate results.
C.4	Program overlooks optimal options	Possibility that the programmed model does not include every optimization option.
C.5	Program user experience	The board of directors (and their technical advisors) of aircraft manufacturing companies need to be convinced by clear and realistic computer program output.
C.6	Inadequate Weight factors	Weight factors used to indicate the importance of optimization criteria should have the value corresponding to the customers needs. Such that the computer program arrives at the desired solution.
C.7	Invalid scaling laws	The scaling laws used are not applicable in the reality and thus the final model becomes incorrect.

Table 10.2: (continued)

#	Risk	Description
		Verification and validation risks
D.1	Program is not proved to be correct	The program might be rejected by experts, when it is not (or cannot quickly shown to be) sufficiently verified and validated.
D.2	Engine performance uncertainty	There is the possibility that the engine will not perform as well as expected. As the chosen engine has not been used commercially before.
D.3	Program sub-files not verified and validated	The computer program consists of many sub-files. It might be the case that mistakes in several sub-files cancel each other out, such that it looks as if the overall program gives good results in most cases. However in certain cases the overall program might return wrong results.
		Feasibility of the computer program
E.1	Limited amount of customers	The computer program has specificly been developed for a medium range, medium passenger capacity aircraft; which is only being designed by a very limited amount of companies.
E.2	Uncommon to use a scaling computer program	The scaling law design approach is still relatively uncommon to aircraft designing companies. The promotion of this design approach to aerospace engineers needs to be convincing.
		Feasibility of a typical scaled aircraft from the SCALAIR project
F.1	No engine production risk	Propfans are infrequently used engines. It might be that these engines will never be produced.
F.2	Risk of high engine development cost	Since the selected GE UDF engine was not certified yet, there are still a lot of development costs to come.
F.3	Public acceptance risks	The public might not like the open rotor technology.
F.4	Final aircraft design offers no improvement	If the program is not working correctly, the output might offer no improvement w.r.t. the A320.
F.5	Customer requirements are not met	There is a risk that the customer requirements will not be met by the computer program.
		Approval of a typical scaled aircraft from the SCALAIR project by the EASA
G.1	Bird/debris strike risk	The GE UDF engines have propellers such that they are vulnerable to bird/debris strikes from multiple directions. Whereas turbofans are almost only vulnerable to bird strikes from the front.
G.2	Blade separation risk	Separation of one blade causes the entire engine to malfunction since the c.o.g. of the propeller is not coincident with the rotation axis anymore. Moreover there is a chance that a seperated blade hits the cabin or the tail. This might even cause drastic failure of the aircraft.
G.3	Engine noise	The engine noise might be so loud that the aircraft is not allowed to land at many airports.
G.4	Thrust effect on the pitching moment	When mounting the engines above the c.o.g. of the aircraft, the thrust will have an influence on the pitching moment of the aircraft. In particular during take off and landing when the pilot varies the thrust to control the glide slope of the aircraft.

Table 10.3: Technical risk assessment matrix, consequences vs. probability

Catastrophic	**G.2**	**C.7, F.1, G.1**		
Critical	**C.1**	**A.3, B.1, B.4, B.8, C.4, C.6, F.4**	**A.1, B.9, B.10, C.2, C.5, C.6, D.1, D.3, E.1, E.2, G.1, G.3**	
Marginal	**A.4, C.3**	**B.2, C.2, D.2, F.3, F.5**	**A.2, B.3, B.5, B.6, B.7, F.2, G.4**	
Negligible				
	Very Unlikely	**Unlikely**	**Likely**	**Very Likely**

10.2 Risk Handling

The risks that were identified and analysed were placed in the risk map shown in 10.3. This subsection will describe how the risks were handled up till now and how they will be handled in post DSE phase. The way the risks were handled is described in Table 10.4.

Table 10.4: Risk Handling

Handling general design process risks		
#	Risk	Description
A.1	Over ambitiousness	The group and the group coordinators want to first create a program which is as simple as possible, and that can be extended later on.
A.2	Miscommunication	Will be prevented by organizing daily meetings and assigning a progress coordinator who keeps track of the status of the work.
A.3	Exceeding time budget	This is prevented by creating a relatively simple computer program first. Which can be extended later on in the project.
A.4	Much time spent on LaTeX editing	In order to prevent text editing delay, the "'LaTeX experts" of the group do the debugging and set up the structure for the rest of the group.
Handling scaling law risks		

Table 10.4: (continued)

#	Risk	Description
B.1	Superposition risks	One possibility of running the scaling program is by applying ceteris paribus on the parameter set. In that case the program has been verified and validated to deliver accurate results. During the project development there was looked into multi parameter scaling and applying superposition on the scaling laws. Some scaling laws were derived for varying one parameter, whilst other were derived for varying two parameters. To prove that superposition can be applied accurately on scaling laws, the group has compared the results of these scaling laws with the results of fully numerical program runs on the same design. A numerical run means that the program checks the performance of the resulting design by calculating all stresses in the structure, and running AVL on the design to calculate the aerodynamic performance. Furthermore the numerical calculation part of the program was validated by performing calculations on existing aircraft designs. These calculations were for example performed on reference aircraft such as the Airbus A320-200, Fokker 100, Boeing 737 and Boeing 747-400. Still the accuracy of superimposing scaling laws is expected to be lower than applying one scaling law. It is recommended to perform a numerical calculation as a check after performing multivariate scaling laws.
B.2	Incorrect allowable stresses used in calculations	Allowable stresses in aircraft designs are based upon tests, calculations and requirements form airworthiness authorities. However aircraft manufacturers know by experience which maximum allowable stress can be used in order to design for fatigue. Therefore the allowable stress values the group obtained by literature and calculations, were checked with expert opinions from the ASM TU Delft.
B.3	Simplification risks	The simplified scaling laws were checked in the validation phase, and only applied in the computer program after a successful validation.
B.4	Limited scope scaling law risks	In the verification and validation phase research has been done in which cases the scaling laws are valid. The computer program using the scaling laws will give messages to the user in case of inapplicable use of the scaling laws. Furthermore in the reports on the scaling laws and user manuals of the program the recommended range of application of the scaling laws will be indicated.
B.5	Loading case risks	The program might not take into account the critical loading cases for each particular aircraft that is used. However in the initial design stage the only important output of structural calculations is the weight. To guarantee the accuracy of the calculated weights, the structural weight calculations and the used scaling laws have been verificated and validated, see sections 5.5 and 5.5.1.
B.6	Fuel weight inaccuracy	The validation in chapter 6.3 shows that the fuel weight inaccuracy is always lower than 8%. Which is considered good enough for this phase of the project.
B.7	Snowball effect on the aircraft mass estimation	For each parameter set that is scaled by the computer program the mass is constantly updated. Therefore the snowball effect is taken into account.
B.8	Scaling law parameter domain limitation risk	The computer program will be written such that the user cannot give parameter input that is outside the allowable range. These allowable ranges were determined based on minimum chosen accuracy, as overall accuracy of the computer program might decrease when using ranges which are too large.

Table 10.4: (continued)

#	Risk	Description
B.9	Scaling law flight condition limitation risks	The flight condition limitations to which scaling laws can be applied are clearly indicated in the report. Additionally the computer program gives warnings when scaling laws are used for unsuitable flight conditions. For instance when the critical Mach number is exceeded.
B.10	Generating inconsistent scaling law risk	To ensure that the generated scaling laws are correct all settings of the computer program are checked before generating a scaling law. Specific attention will be paid to verify that the input parameters are consistent.
		Handling computer program risks
C.1	Program fails to converge to a design	The computer program is designed such that a design is always calculated. It works by starting with many different parameter sets. Each of those is scaled to the local optimum, which is always possible by applying scaling laws. Then the overall optimum design is chosen from all local optima.
C.2	Coding mistakes	These are prevented by a programming cordinator who provides base files in which other team members can program. Test runs will be performed on the modules to check if they are working correctly. Connecting the sub files of the program (and the debugging) is done by the programming coordinator.
C.3	Round-off errors	The SCALAIR program runs in MATLAB. Which uses floating point numbers with a mantissa of 15 numbers, as a standard setting. For the developed scaling program this accuracy is assumed to be surely high enough.
C.4	Program overlooks optimal options	This risk is handled in the same way as risk C.1.
C.5	Program user experience	To satisfy the user, attention is paid to the Graphical User Interface (GUI). Leading to a program which can be operated easily and quickly in terms of input from the user and output to the user. For expert users sufficient data will be provided, such that they can use their expertise to see if the program output is realistic.
C.6	Inadequate Weight factors	At the start of the project it was expected that weight factors would be needed to add weight to optimization criteria. However no weight factors are used at all, since there is only one optimization criterion. Which is to minimize fuel consumption. From this one optimization criterion all other sub optimizations can be guided as follows. The computer program tries to meet the requirements specified by the user. With an aircraft weight that is as low as possible. The aircraft with lowest weight that can meet the requirements also will have the lowest fuel consumption.
C.7	Invalid scaling laws	To prevent the final scaling laws from being incorrect, a verification and validation procedure will be performed.
		Handling verification and validation risks
D.1	Program is not proved to be correct	The project group will do effort in order to verify and validate the program. Furthermore the project group will be trained to present how the program was verified and validated.
D.2	Engine performance uncertainty	Engine data from NASA and GE was found. Which can be assumed to be accurate enough.

Table 10.4: (continued)

#	Risk	Description
D.3	Program sub files not verified and validated	Most sub files of the program are about subsystems of an aircraft. To validate such sub files, data on the subsystems of the aircraft is required. However such data is hard to find compared to data of an entire aircraft. So a number of the sub files still lack validation and verification. For now it is assumed that overall validation of the program and validation of sub files where possible is good enough. In the post DSE phase, contact with aircraft manufacturers would open access to more specific subcomponent data. That enables to perform better verification and validation of the sub files of the program.
	Handling risks on the feasibility of the computer program	
E.1	Limited amount of customers	The SCALAIR DSE project has been focussed on scaling a medium range, medium passenger capacity aircraft. In the post DSE phase, the SCALAIR computer program can be extended to different type of aircraft. The obtained experience will cause the extending process to be relatively easy compared to the first stage of the project. Moreover, the potential customers for the SCALAIR computer program include very large companies such as Airbus and Boeing. When only one of these customers buys the program, there will probably be enough money to fund the project.
E.2	Uncommon to use a scaling computer program	In the post DSE sufficient attention should be paid to promotion. For instance by providing the scaling program to aerospace students for free, and by offering free trial versions for companies.
	Handling scaled aircraft risks	
F.1	No engine production risk	Propfan engines are necessary for the aircraft designs are generated by the SCALAIR computer program. However propfan engines are still under development. However when large companies such as Airbus or Boeing will use the developed design approach, it is an option for them to ask engine manufacturers to produce propfan engines.
F.2	Risk of high engine development cost	Although prototypes of the GE UDF propfan have been tested successfully. Aircraft engine approval by airworthiness regulations requires many successful tests. Again as with point F.1 resources are the decisive factor here. Large aircraft companies have sufficient money to let engine manufacturers develop propfan engines.
F.3	Public acceptance risks	Propfans still are uncommon engines, and might not be accepted due to their noise and different appearance. On the other hand fuel prices are rising constantly, resulting in considerably lower prices for a flight with the more efficient propfan engines. When well known aircraft manufacturers such as Airbus and Boeing start using propfans, the public will probably be confident about the safety of propfans.
F.4	Final aircraft design offers no improvement	The goal of the project is surely not to keep all operational characteristics the same, and only to reduce the fuel consumption. That would be an A320 improvement. This goal of this project is more to trade between several operational performance parameters. For example a more fuel efficient aircraft can surely be achieved, by for example reducing airspeed, reducing sweep, increasing aspect ratio and using propfans.

Table 10.4: (continued)

#	Risk	Description
F.5	Customer requirements are not met	The project group did set up the requirements for the computer program that they would be developing. As there was no customer that gave them a list of requirements. Advice on how what the program should be doing was given by the tutors and coaches of our project group, who are experts in different fields of aircraft engineering from the TU Delft. Therefore the project group is confident that the developed program is useful for aircraft designing companies.
	Handling airworthiness approval risks	
G.1	Bird/debris strike risk	The risk that critical bird strikes occur with a propfan engine will always stay higher than with turbofan engines. Therefore sufficient research should be done into the vulnerability of a propfan to bird strikes. This risk will very probably stay critical and likely to occur at least a few times in the lifetime of an aircraft.
G.2	Blade separation risk	A careful engine design will have to be made to prevent blade separation. Still this will remain a risk with catastrophic consequences. Therefore it will be hard to get approval from airworthiness authorities.
G.3	Engine noise	This is a problem for crowded areas or nature reserves around airports. Nevertheless when considering fuel consumption and air pollution, propfans have large advantages compared to turbofans. This can be read in the Section 3.1. So a trade off will have to be made.
G.4	Thrust effect on the pitching moment	In the final aircraft design the engine is placed circa 3.5 meter above the c.o.g.. So thrust surely influences the pitching moment. This can be a risk when trying to control the aircraft, in particular during take off and landing.

Table 10.5: Technical risk assessment matrix, consequences vs. probability after Risk Handling

Catastrophic		**G.1, G.2**		
Critical	**B.8, C.4, C.7, F.5, G.4**	**B.9, B.10, C.2, D.1, E.1, F.1, G.4**		
Marginal	**B.3, B.4, C.1, F.4, G.3**	**A.1, A.2, A.3, B.6, C.5, D.2, D.3, E.2, F.3**	**B.1, B.5**	
Negligible	**A.4, B.7, C.3, C.6**	**B.2**	**F.2**	
	Very Unlikely	**Unlikely**	**Likely**	**Very Likely**

Chapter 11

Final Design

11.1 Trade-off Study

This section provides an overview of various trade-off processes that have been performed to arrive at an improved A320 design. First, the trade-off for the engine option is presented. It is a summary of the entire description of this process, presented in the MTR. The reader is referred to this document for a more thorough elaboration on this subject. The second part describes the trade-offs which are made with respect to aspect ratio, taper ratio, flight speed, sweep angle and their effects on DOC and other key aspects.

11.1.1 Engine Trade-off

To select the best propulsion system for the redesigned A320, an extensive trade-off has been performed. The first step in this process was to conduct a market analysis on available engines. Since the assignment dictated the implementation of propeller propulsion, the emphasis was put on this segment. For completeness, conventional turbofan engines were considered as well.

Many comparable aircraft and their propulsion system have been investigated to generate a relation between MTOM and thrust. In this comparison a distinction is made between turbofan and turboprop aircraft, because they have different performance characteristics. Relations were established for the required thrust or power as a function of MTOM. These two could not be compared directly, since the units are different. However, when assessed at a certain flight speed the two can be compared. This speed should be the take-off speed because in this stage of the flight maximum thrust is required. The relation between all the considered reference aircraft can be seen in Figure 11.1. For the scaled A320 the MTOM will be approximately the same as for the original A320. This indicates that the required thrust lies between 100kN and 110kN per engine.

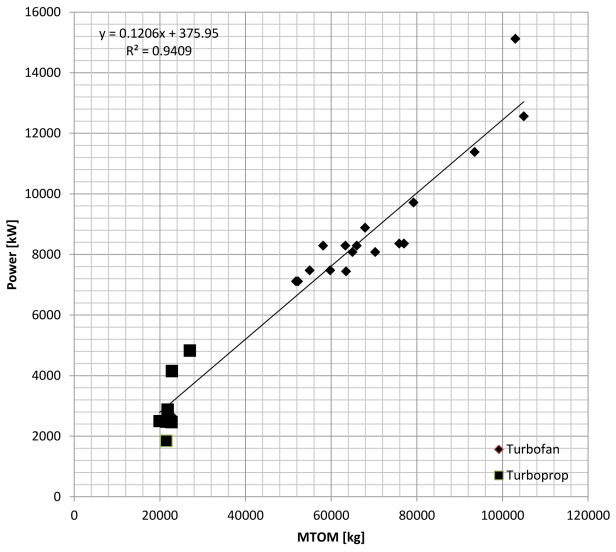

Figure 11.1: Power vs. MTOM of all reference aircraft

With the above information, possible engine options are selected. Several engines have been considered, on various locations. The various combinations of engines and locations gave a total of nine options to choose from. The possible engines were the TP400-D6, currently in use on the

A400M, the Progress D-27, currently in use on the Antonov-70, and the General Electric UDF. For a detailed description of the engine characteristics the reader is referred to Table 7.3 in the MTR. In short, the D-27 and the UDF both offer a fuel reduction of over 30 per cent, while the TP400 offers 12 per cent reduction. All three engines have typical cruise speeds around Mach 0.7. To compare the SFC of these engines with that of a turbofan engine, the same procedure was applied as with the required power determination. Next, the cruise speed was selected as reference, since the SFC in cruise is of importance.

For the location of the engine, two places have been considered. Wing mounted engines or fuselage mounted engines. Within these categories some subcategories have been created to distinguish some more possibilities. All the advantages and disadvantages of these options were considered with respect to many important aspects. For instance structural considerations, cabin noise, safety, maintenance issues, efficiency and many other aspects were taken into account. Some advantages for wing mounted engines were the good access in favour of maintenance, the undisturbed inlet flow and the counteracting of the wing bending moment by the engine weight. On the other hand, advantages of a fuselage mounted engine are a clean wing, less cabin noise and the engines being closer to the aircraft centre-line. For both configurations also many disadvantages existed. All engines located on the various possible positions were evaluated according to a large set of criteria. These criteria were weighted and their weight factors were determined using the Analytic Hierarchy Process (AHP), which is described in Chapter 6 in the MTR. Much effort was put in accurately judging the various options on all aspects. A sensitivity analysis has been performed on the outcome to see which options might face uncertainties in the eventual implementation. After careful consideration, the best option turned out to be a General Electric UDF mounted on the fuselage, with the tail remaining in the conventional configuration.

It is noted, that the choice for this option brings a decrease in fuel burn and hence DOC. The compromise is made to the prejudice of flight speed and noise, and hence passenger comfort. However, much research is currently put in the reduction of noise pollution, both inside and outside the aircraft. It is expected that the noise levels will be within acceptable limits in the future. For now, it is up to the airlines to decide if the reduction in DOC outweighs the reduction in passenger comfort.

The complete trade-off table and the scores for all considered options can be seen in Table 7.6 in the MTR. In Figure 11.2 the best engine location is visualised.

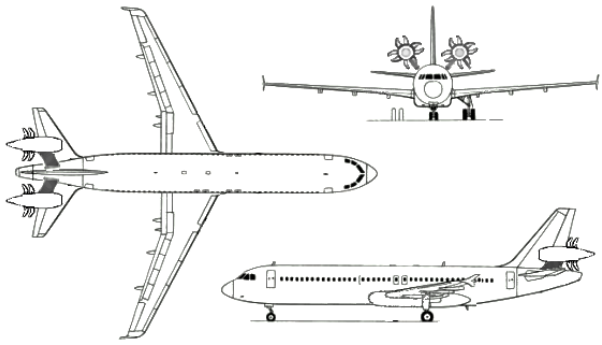

Figure 11.2: A320 with fuselage mounted UDF and low tail configuration

11.1.2 Airframe Trade-off

The changed layout which the Matlab program produces is based on trade-offs. When all the individual effects of changing parameters are assessed the positive and negative effects have to be traded off. Every change in input parameters, i.e. aspect ratio, taper ratio, sweep etc. can be expressed in a change in DOC, the driving parameter for this project. For the sake of simplicity and overview intermediate steps are used, such as lift over drag ratio, weight and fuel burn.

The influence of the aspect ratio on the aerodynamic wing efficiency is off course positive, since it reduces induced drag. This means the required thrust is lower and the engines have to burn less fuel. The required fuel weight is reduced, and the fuel consumption is even further reduced. In this way, a snowball effect is started, which works for practically all minor improvements. However, an increased aspect ratio increases the wing structural weight since the bending moment increases and the chord length and height becomes smaller, thus a thicker structure is required. This effect will start another snowball effect of increasing weight, and compensates for the increased aerodynamic

wing efficiency. In this way, it is very hard to say if increasing the aspect ratio is of any good use. This off course holds for more elements such as sweep, flight speed and other parameters. When the program calculates outputs belonging to a range of inputs, all their effects can be assessed. The effects on weight, efficiency and DOC can then be traded off. The effects which are not calculated, such as cabin noise, external noise, pollution etc. are also considered in the trade-off.

The Matlab program allows sweep and flight speed to be varied as an input, but this is not done in practice. The sweep angle is dictated by the critical Mach number of the airfoil. From calculations it became apparent that lowering the sweep angle more than the minimum required by the critical Mach number did not prove to be more efficient. The same holds for the flight speed which is dictated by the engine. To arrive at an improved design, it is therefore assumed that sweep and flight speed are constant inputs.

The parameters on which the trade-off is then based are the aspect ratio and taper ratio. The user is free to vary these parameters as wanted. Obviously, very large deviations from the values of the A320 will lead to invalid results and should be avoided. When an input is given, the program calculates the corresponding outputs. If a range of inputs is specified, the outputs can be compared and a trade-off can be made. This is done manually, since the program is not able to perform this due to time constraints.

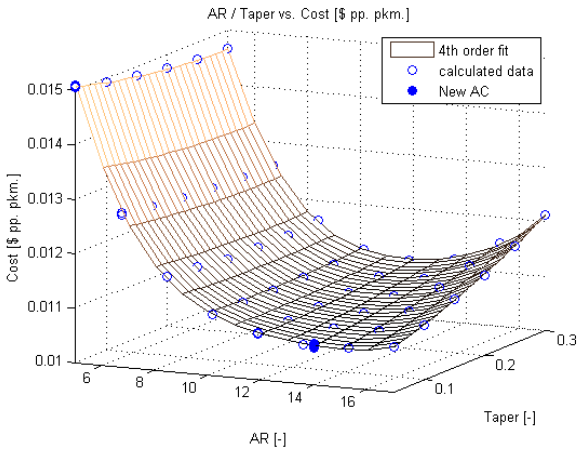

Figure 11.3: Cost per kilometre per passenger as a function of aspect ratio and taper ratio (Range=5000km, Λ=17$\circ$ and new engine configuration

Figure 11.3 shows the relation between the aspect ratio, taper ratio and fuel consumption. It can be seen that a low taper ratio and an aspect ratio of approximately fourteen are desired. This figure serves as an example of how the optimal values for several parameters are determined. As already mentioned, the iteration step in the program cannot be performed due to time constraints. Therefore, this is done by trial and error on the input parameters. The effects of changing inputs are assessed for fuel burn per passenger per kilometre. All the graphs which show the variation of lift over drag or weight with certain parameters can be translated to show the variation with the aforementioned driving factors. These are just intermediate steps and are done by the program. When the produced graphs are then reviewed, an updated estimation of the inputs can be made. In this way, many possible configurations were tested and the positive and negative effects could be assessed. Obviously, the negative effects were tried to be minimised and the positive influences increased to arrive at an optimum. When this process was finished, the optimal parameters, i.e. for the lowest DOC, were found to be as seen in Section 11.2.

11.2 Design Characteristics

The optimum configuration of the aircraft has an aspect ratio of 11.4 and a taper ratio of 0.25. The specifications of the final design have been calculated by the computer program. The specifications of the optimum scaled aircraft will be compared to the reference aircraft: the Airbus A320. This comparison will be performed with the actual A320, and also with the A320 data modelled by the developed computer program.

11.2.1 Specifications

The specifications are split into multiple categories: general specifications, mass breakdown, dimensions, performance and an improvement comparison. These specifications can be found in Table

11.1.

Table 11.1: Specifications for the final design, the modelled Airbus A320 and the actual A320

General Specifications				
Specification type	**Unit**	**Final Design**	**Modelled A320**	**A320**
Design passenger count	[pax]	150	150	150
Design range	[km]	5,000	5,000	5,000
Cruise speed	[M]	0.72	0.78	0.78
Aspect ratio	[/]	11.4	9.39	9.39
Taper ratio	[/]	0.25	0.24	0.24
Engine count	[/]	2	2	2
Wing / fuselage mounted	[/]	F	W	W
Mass breakdown				
Mass type	**Unit**	**Final Design**	**Modelled A320**	**A320**
MTOM	[kg]	62,304	72,803	73,500
OEM	[kg]	36,763	40,569	41,310
MEM	[kg]	33,613	37,419	38,160
Airframe mass	[kg]	28,899	31,817	32,558
Design fuel mass	[kg]	11,291	17,963	17,940
Design payload mass	[kg]	14,250	14,250	14,250
Dimensions				
Dimension type	**Unit**	**Final Design**	**Modelled A320**	**A320**
Surface area	$[m^2]$	97.33	122.1	122.4
Wing span	[m]	33.60	33.9	33.9
LE sweep	[°]	17	28	28
Fuselage length	[m]	37.37	37.37	37.37
Fuselage width	[m]	3.95	3.95	3.95
Fuselage height	[m]	4.24	4.24	4.24
Horizontal tail area	$[m^2]$	18.39	18.7	31
Horizontal LE sweep	[°]	21	32	32
Vertical tail area	$[m^2]$	18.26	21.5	21.5
Vertical LE sweep	[°]	29	40	40
Root chord length	[m]	5.04	6.76	6.77
Tip chord length	[m]	1.26	1.62	1.62
Performance				
Performance type	**Unit**	**Final Design**	**Modelled A320**	**A320**
Thrust per engine	[kN]	91.5	107	120
Specific fuel consumption	[g/kNs]	11.15	16.98	16.98
Fuel use design range	[kg/pax/km]	0.01107	0.0179	
Fuel use average range	[kg/pax/km]	0.01265	0.0197	
Fuel use cruise	[kg/hour]	1300	2105	2100
L/D		18.77	16.45	16.73

Table 11.1: (continued)

Improvements of the final design with respect to the A320

Improvement type	Unit	Improvement
Design fuel use	[%]	-38.16
Average fuel use	[%]	-35.79
Fuel use cruise	[%]	-38.10
Fuel weight	[%]	-37.06
TOC Drag	[%]	-26.17
L/D	[%]	+12.19
MTOM	[%]	-15.23
OEM	[%]	-11.01
Specific fuel consumption	[%]	-34.3
Cruise speed	[%]	-7.3

11.2.2 Design Drawings

A isometric view of the SCALAIR A320 is given in Figure 11.4 and the design drawings of the SCALAIR A320 compared to the Airbus A320 is given in Figure 11.5.

Figure 11.4: Design drawings with dimensions of the SCALAIR A320 (top left three) and Airbus A320 (yellow bottom right three) [64]

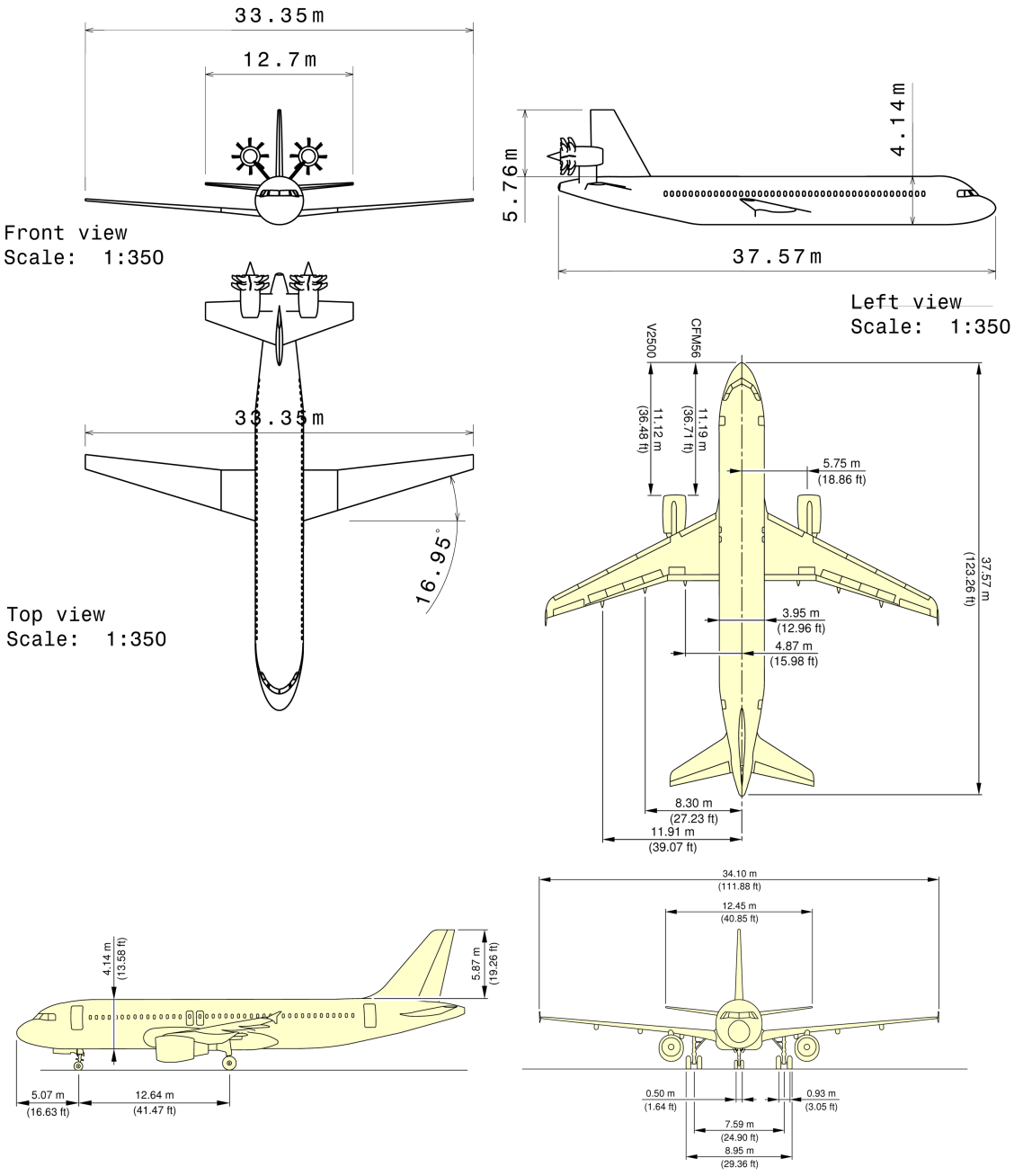

Figure 11.5: Design drawings with dimensions of the SCALAIR A320 (top left three) and Airbus A320 (yellow bottom right three) [64]

11.2.3 Validation results

With the final characteristics of the new design and the calculated characteristics of the A320 known, a final validation is still required. This is done by comparing the data in Table 11.1. More precisely, the data presented of the calculated and actual A320 data in these tables are compared.

When looking at the data presented in Table 11.1, it becomes clear that nearly all aspects are near identical between the actual and modelled A320. The only real differences can be seen between in the horizontal tail area calculations. However, this deviation is explained in more detail is Section 8.4. Due to the snowball effect, this results in some small changes for the rest of the model. However,

these changes remain below two per cent in all cases. Furthermore, the model calculated a thrust of 107 kN per engine instead of 120 kN. However, it can be noted that this is the required thrust. The engine used by the Airbus A320-200 is not specifically designed for the A320. As such, it generates more thrust than required. The required thrust is therefore difficult to compare.

It can be concluded that the model represents the A320 very accurately, which presents a final validation to the entire program.

11.2.4 Analysis Results

As the data of improvements in Table 11.1 show, the performance increase for the new model is very large with respect to the Airbus A320. The change in engine already improves the specific fuel consumption with 34%. However, the a more efficient wing design also leads to an improvement of lift over drag by 12% and a reduction in MTOM by 15%. In total, this leads to a reduction in design fuel consumption of over 38%. This value is considerably higher than the required reduction of 30%.

However, it can be noted that this increase in fuel efficiency does have a cost: namely an increase in noise production and a decrease of cruise speed by seven per cent.

11.3 Sustainability of the Final Design

Once a final design is presented, one of the main requirements of this design should be checked: how sustainable is this new design? For the most part, the sustainability approach of this project has already been discussed in Chapter 3. As such, this chapter will not discuss the details which have already been presented. It will focus strictly on the SCALAIR final design.

First of all, it can be noted that the change in propulsion also leads to a large reduction in fuel consumption and emission reduction. More detail with respect to the propulsion can be found in Chapter 3.

However, the change of propulsion is not the only change which leads to a reduction in emissions. As Table 11.1 shows, the SCALAIR design also offers a reduction in drag of 26.2 per cent, leading to a total fuel reduction of over 35 per cent for an average range of 3,500 km. Furthermore, a reduction as high as 38 per cent is achieved for the design range. A similar ratio of fuel reduction can be achieved for the emissions of greenhouse gasses. As such, the results in terms of fuel reduction and the reduction of CO_2 emissions can be found in Table 11.2 for 3,300 flight hours per year.

Table 11.2: Fuel and CO_2 reduction of the SCALAIR aircraft

	Unit	**Airbus A320**	**SCALAIR A320**	**Reduction**	**Reduction** [%]
Fuel burned	[kg/flight]	10,353	6,643	-3,895	-35.8%
Fuel burned	[kg/pax/km]	0.0197	0.01265	-0.00705	-35.8%
Fuel burned	[kg/year]	6,930,000	4,288,680	2,641,320	-38.11%
CO_2 emissions	[kg/flight]	32,301	20,726	11,575	-35.8%
CO_2 emissions	[kg/pax/km]	0.0615	0.0395	0.0220	-35.8%
CO_2 emissions	[kg/year]	21,621,600	13,380,682	8,240,918	-38.11%

As Table 11.2 shows, the SCALAIR design is more fuel efficient than the Airbus A320. Replacing a single Airbus A320 by the SCALAIR design leads to an impressive reduction of in carbon dioxide emissions of over 8,200,000 kg per year.

Furthermore, as is already explained Chapter 3, the use of scaling can significantly reduce the design time and the manufacturing cost. In this simple case, the model can be used to generate an initial design for nearly any configuration based on the Airbus A320. Furthermore, applying adjustments to all sub-models s.a. aerodynamics or structures, this method can be used to scale different aircraft types as well.

Moreover, it can be noted that the internal electrical design as well as nearly the entire design of the fuselage remain constant. As such, these require considerably less design. This means considerably less energy is used for production, reducing the ecological footprint.

11.4 Compliance matrix

This chapter presents the compliance matrix for this project. It presents all the initial requirements and shows if they are met by means of a check mark as shown in Table 11.3. All the top-level system requirements from the project guide are listed, and in the second column it is indicated with a check mark if the requirement is met. It can be seen that all the requirements are met. Subsection 11.2.3 provides a validation of the model by analysing the A320 with the developed program. The results of this also indicate that the requirements are met.

Table 11.3: Compliance matrix

Requirements	**Required value**		**Actual value**
Evaluate the effects of aircraft scaling	-	✓	-
Design a mathematical description of the vehicle	-	✓	-
Process is based on applying scaling laws for relevant aspects	-	✓	-
- Aerodynamics	-	✓	-
- Stability & Control	-	✓	-
- Structures	-	✓	-
- DOC	-	✓	-
Scaling laws should be limited for medium range	-	✓	-
Validation of the scaling model	-	✓	-
Develop new aircraft with large aspect ratio and propeller propulsion	-	✓	-
Lower fuel consumption	30%	✓	35.8%
Reduced DOC	-	✓	8.0%

11.5 Operations & Logistics

After manufacturing the design, it will be operated. Therefore, an operations and logistics concept is needed which will be described in this section. It will indicate the use of the system and also the support that is needed for the system. The design that has been obtained belongs to aircraft in the commercial medium size range. Hence, its operations and logistics are very comparable to other medium size jetliners. The basic operations are shown in a flow diagram in Figure 11.6.

First, the aircraft is taken out of the hangar and prepared for the pre-flight phase. It is a start-up phase so the flight initiation phase can begin. The flight initiation deals with the operations from the terminal gate to take-off. The key operations are catering, ramp service and airport service.

The catering makes sure that the consumables are loaded on the aircraft. The ramp service deals among others with ground handling of the aircraft, cargo loading and refuelling of the aircraft. The airport service takes care of the departure and boarding of the passengers. All these operations can be handled by the owner of the aircraft or it can be outsourced [65, 66].

After the flight initiation phase is finished, the aircraft can proceed to the actual flight. The aircraft starts then with the take-off. However, this is only possible after approval is given by Air Traffic Control (ATC). The take-off is then followed by the cruise. During cruise the aircraft is monitored by one or multiple ATC centres. Not complying to local or international rules can lead to

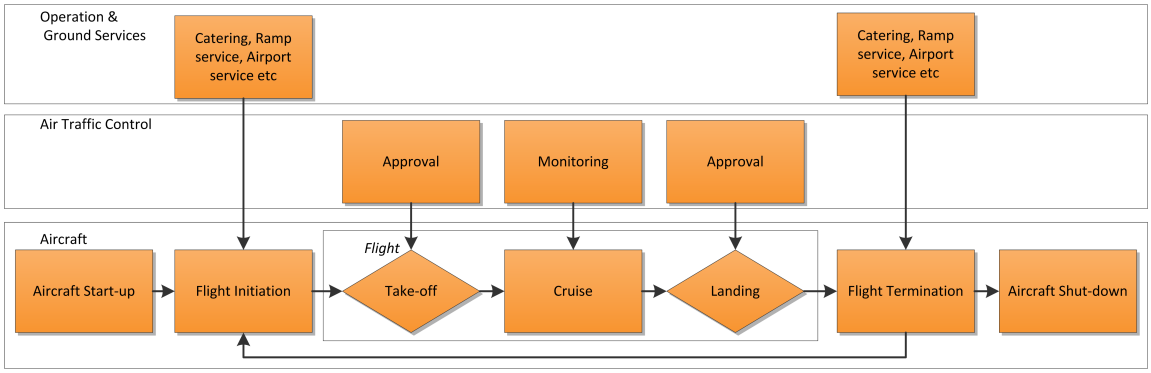

Figure 11.6: Operational Flow Diagram

a termination of the flight. After cruise, the landing phase is started which also needs an approval from the ATC.

The flight ends with the landing of the aircraft. Hereafter, the flight termination is started.

Depending on the next phase of the aircraft, the aircraft is prepared for another flight or shut-down. If the aircraft has to be prepared for another flight, then the aircraft will continue to the flight initiation phase after the termination is finished. During the termination the aircraft is being serviced again. The catering unloads the unused food. The ramp service takes care of the ground handling and unloading of the aircraft. Other jobs might include de-icing and de-fueling of the aircraft if necessary. The airport service takes care of the arrival and de-boarding of the passengers.

If the aircraft is not used for another flight, it will be shut-down and stored in a hangar.

Chapter 12

Direct Operating Costs

The total operating costs of an aircraft consist of the Indirect Operating Costs (IOC) and the Direct Operating Costs (DOC).The IOC concern expenditures which are passenger related and are independent of the type of aircraft that is used. These costs are operator related and thus will not be influenced by the scaling of the aircraft.

The DOC include all costs which are associated with and are dependent on the type of aircraft. Reducing these costs for the A320 is one of the main goals of the SCALAIR project and will be elaborated on in this chapter. The DOC can be split up in several segments, as can be seen in Figure 12.1.

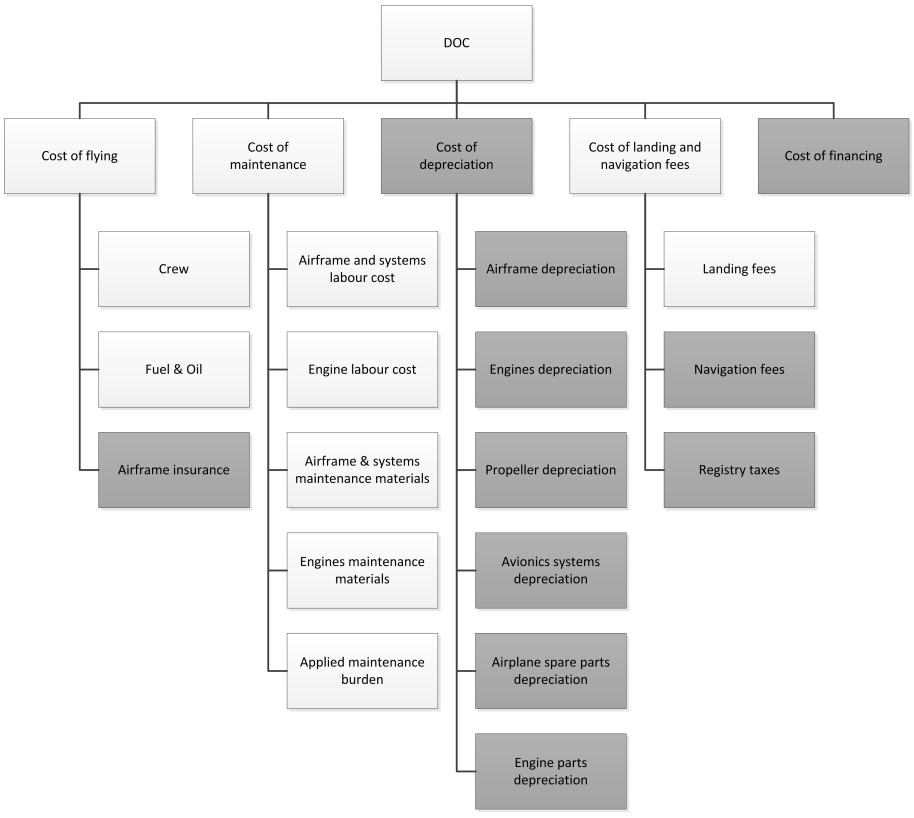

Figure 12.1: Breakdown of Direct Operating Cost [67]

The elements in Figure 12.1 which are coloured grey are not influenced by scaling the aircraft and thus remain constant.

In order to calculate the DOC the method presented in [68] is used, which is based on the work of Liebeck [1]. In this method the costs of flight and cabin crew, airframe and engine maintenance,

landing fee and finally of the ownership will be determined. The ownership costs consist of the depreciation, interest and insurance costs. These costs are calculated for the Airbus A320 and due to scaling these costs will not change and thus they are considered to be the same for the SCALAIR. However, this method has some limitations, which will be examined beforehand to account for its inaccuracies. These limitations are:

- Airframe maintenance cost depend only on airframe weight, this is not correct. It should also account for skin thickness. However, when looking at reference material [69] the values agree with each other. That the costs for the SCALAIR are smaller seems logical, since the wing span and wing area have smaller dimensions.

- Engine maintenance cost depend on thrust and are probably only intended for common jet engines and not for propeller engines. Replacing the engine of the A320 with a propeller engine will however increase the maintenance cost by **52%**, which is obtained from [69]

- Landing fees depend only on aircraft weight, which is correct, however, in Europe due to the noisy engine, these costs will probably increase compared to the conventional A320 engine. However, since the main driver is the aircraft weight and thus the relation between the SCALAIR and the Airbus A320 can be assumed to be correct

The results of the final DOC are presented in Table 12.1. Note that the time in hours which are used are for block hours, not for flight hours.

Table 12.1: Differences between the Airbus A320 and the SCALAIR A320

		Airbus A320	**SCALAIR A320**
Design range	[km]	5,000	5,000
Average range	[km]	3,500	3,500
Speed	[m/s]	230.5	221.8
Block hour duration	[h]	5.1256	5.3071
Flight hours	[h/year]	3,300	3,300
Fuel Price	[$/kg]	0.99	0.99
Fuel Consumption	[kg/h]	2,019.8	1,279.8
Fuel Cost	[$/h]	2,000.85	1267.81
Crew Cost	[$/h]	966.61	953.28
Airframe maintenance cost	[$/h]	304.56	291.96
Engine maintenance cost	[$/h]	464.27	705.69
Landing fees	[$/h]	109.58	99.59
Ownership costs	[$/h]	3,638.89	3,638.89
Total DOC	[$/h]	7,484.76	6,889.76

The final breakdown of the DOC, expressed in percentages, are shown in Figures 12.2 and 12.3 for the Airbus A320 and the final design respectively.

The costs calculations for the Airbus A320 agree with the costs from *Fourth Meeting of the ALLPIRG/Advisory Group* [70]. Further validation can be found from [71, 72], which show a similar DOC breakdown as the Airbus A320, such as values of 27% for the fuel costs and 54% for the ownership costs.

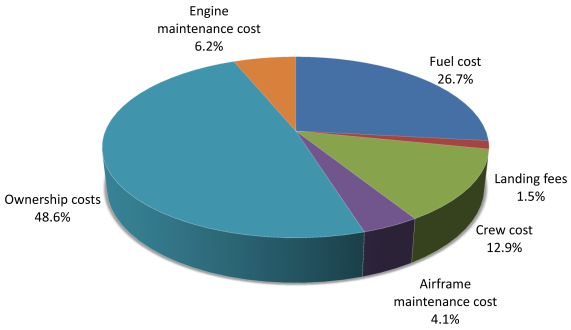

Figure 12.2: DOC breakdown for the Airbus A320

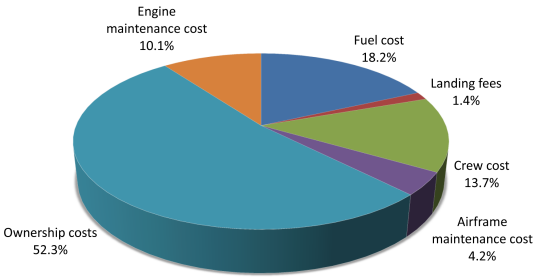

Figure 12.3: DOC breakdown for the SCALAIR A320

The dramatic increase in jet fuel costs has a major influence on the DOC, as can be seen in Figure 12.4 [73]. This can also be observed from the results. The SCALAIR has a reduction of fuel consumption of 740 kg/h with respect to the Airbus A320. While the fuel costs influence the DOC of the Airbus A320 by 27% the fuel costs for the SCALAIR only represents 18.2%. The reduction in DOC of the SCALAIR are **8%** w.r.t. to the Airbus A320 and account for a reduction of **595 $/h**.

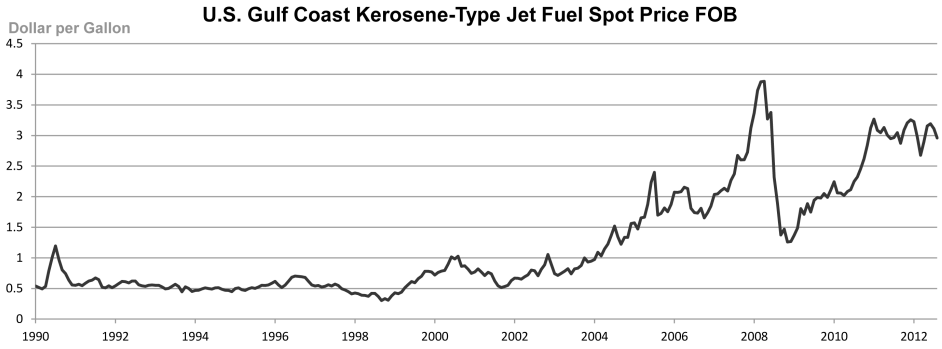

Figure 12.4: Historical trend of the fuel price over the last 22 years [73]

12.1 Economic effects of lower cruise speed

In order to assess the effects of a changing cruise speed on the revenues for an airline, the operations of Qatar Airways are considered. Since the available information on this topic is limited, there is only one airline taken into account. The fleet of this airline consists of a total of 95 aircraft from various types. Among this are 23 A320s, which are considered for this analysis. According to Qatar Airways their fleet of A320s is slightly underused. Qatar Airways is operating in the Middle East, from where their A320s fly to destinations in Europe, Africa, India and off course the Middle East itself. The operational characteristics of the 23 A320s can be seen in Table 12.2 [74].

Table 12.2: A320 operational characteristics

A320 Operational characteristics		
Total weekly utilization	min	117035
Fleet size		23
Average daily utilization	min	727
Average daily utilization	hours	**12:07**
Total weekly cycles		672
Average cycle length	min	174
Average cycle length	hours	**02:54**

The most important fact that follows from this table is that an aircraft flies an average of 4.18 cycles per day. This can be seen when the total weekly cycles are divided by the fleet size and converted to a daily basis. If the flight speed is decreased, the time for a complete cycle will increase. This means that on average, less cycles can be flown during a day. With a new cruise mach number of 0.72, the distance covered per hour decreases to 656 kilometer. This is calculated using the moethod for the average flight speed for a given cruise Mach number. It is now assumed that the average daily utilization remains constant, since this number is determined by the airlines operation schedule and strategy. Also airport and ATC capacities play a role in the utilization. The average cycle distance for the Qatar Airways operated A320 is 2059km. This is determined from the average cycle length and the cruise speed (Mach 0.78). Assuming this remains constant, the amount of cycles which can be flown during a day with a cruise Mach number of 0.72 has then decreased to 3.86.

When the amount of cycles per day is known, the distance covered per plane per day can be determined. Multiplied with the available seats in an A320 (144 seats [75]) this yields the Available Seat Kilometer (ASK). The ASK for Qatar Airways is 1239644 per plane per day. It is obvious that when the amount of cycles on a day is reduced, so does the ASK.

The load factor of Qatar Airways was 83% in 2012, according to IATA [76]. The load factor is the ratio between the RPK and the ASK. RPK is a measure for the amount of passengers that actually travel along a certain route, but is not important in this analysis. When the ASK decreases, the load factor increases. This is not a problem, up to the point where the load factor would exceed 100%. Above this point, the capacity of the airline is lower than the demand from passengers and the revenues will decrease. Therefore, the Mach number associated with a load factor of 100% will be the lowest allowed Mach number for the design. From Table 12.3 it can be seen that this is a Mach number of 0.65. This number serves as a guideline, since data from individual airlines may vary.

Table 12.3: Load factor as a function of cruise Mach number

Cruise Mach number	**km/h**	**# of cycles**	**ASK**	**Load factor**
0.78	710	4.18	1239644	0.83
0.72	656	3.86	1144287	0.90
0.65	592	3.48	1033037	1.00

Chapter 13

Post DSE

The project aims at creating a scalable aircraft model. The second goal is to use this model to redesign an aircraft. This aircraft is to compete with the Airbus A320 and to excel in fuel consumption and DOC. Requirements set for the project are changing the propulsion system to a turboprop and using a higher aspect ratio. When the project is concluded, the post-DSE phase is started. Therefore, a post-DSE project plan has been set up with recommended activities that could be done in the future.

This chapter will present possibilities for when the DSE period of ten weeks is over. First, Section 13.1 will discuss the post-DSE time planning. Next, Section 13.2 presents a cost breakdown of any future activities.

13.1 Gantt Chart

The Post DSE activities consist of numerous elements, which are rather time consuming. A Gantt chart of these activities has been created to estimate the time needed. As this is still an initial estimation, it will be subject to changes. For this estimation it is assumed that the same resources are available as during the DSE-phase except for the time. An initial estimation is set at about 5 weeks while the DSE is spanned over 10 weeks. The Gantt chart of the Post-DSE in shown in Figure 13.1.

ID	Task Name	Duration	Start	Finish
1	**Post-DSE Activities**	**40 days**	**Mon 11-2-13**	**Fri 5-4-13**
2	**Pre-Design**	**5 days**	**Mon 11-2-13**	**Fri 15-2-13**
3	**Planning**	**3 days**	**Mon 11-2-13**	**Wed 13-2-13**
4	Organizational Bre	4 hrs	Mon 11-2-13	Mon 11-2-13
5	Work Flow Diagran	1 day	Mon 11-2-13	Mon 11-2-13
6	Work Breakdown S	8 hrs	Tue 12-2-13	Tue 12-2-13
7	Gantt Chart	8 hrs	Wed 13-2-13	Wed 13-2-13
8	Literature Study	16 hrs	Thu 14-2-13	Fri 15-2-13
9	**Model Development**	**27 days**	**Mon 18-2-13**	**Tue 26-3-13**
10	Data Acquisition	48 hrs	Mon 18-2-13	Mon 25-2-13
11	New Module Development	88 hrs	Tue 26-2-13	Tue 12-3-13
12	Test and Evaluation	48 hrs	Wed 13-3-13	Wed 20-3-13
13	Runtime Enhancemer	32 hrs	Thu 21-3-13	Tue 26-3-13
14	**Reporting**	**8 days**	**Wed 27-3-13**	**Fri 5-4-13**
15	Trade-off	24 hrs	Wed 27-3-13	Fri 29-3-13
16	Final Design	16 hrs	Mon 1-4-13	Tue 2-4-13
17	Documentation	24 hrs	Wed 3-4-13	Fri 5-4-13

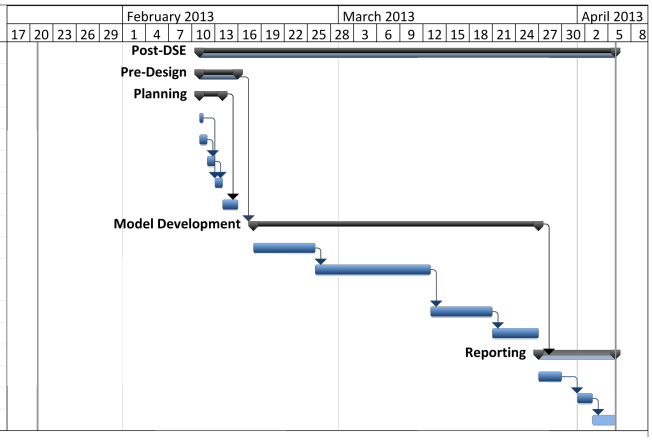

Figure 13.1: Gantt Chart for the Post-DSE

13.2 Cost Break-down Structure

The Cost Break-down Structure (CBS) contains the cost elements of the post-DSE project activities. These costs originate from various sources which are time consumption, tooling, documentation or others. A diagram of these cost elements is shown in Figure 13.2.

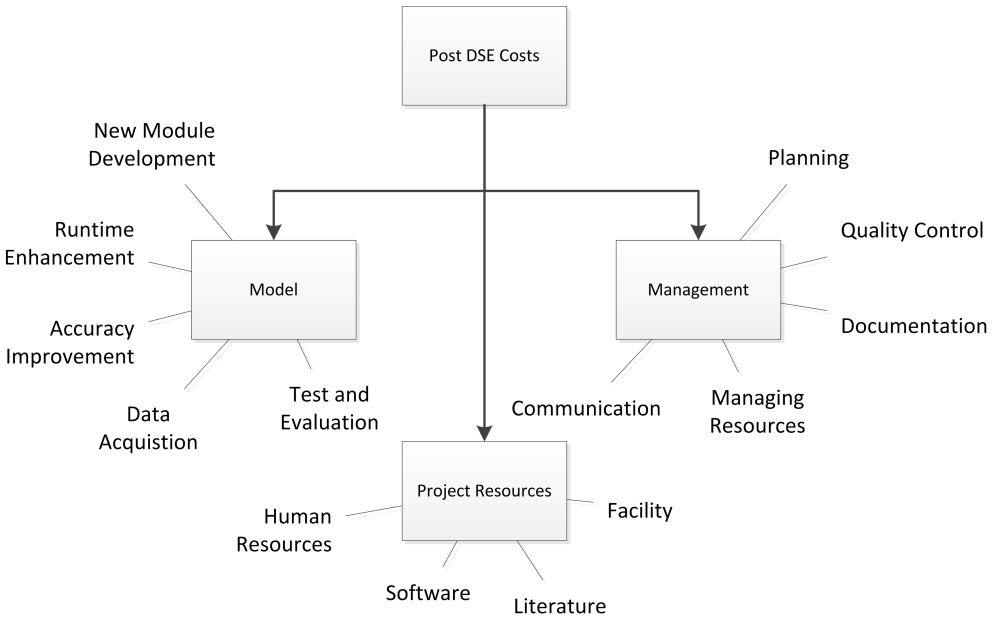

Figure 13.2: Cost Break-down Structure of the Post-DSE phase

As can be seen, the numerous cost elements have been attributed to three major sources. These sources are identified as model related costs, costs on the resources and the management of the project.

The costs that are linked to management can be subdivided into communication, managing resources, documentation, quality control and planning. The management is necessary to maintain the quality and a high efficiency throughout the project. This is not only done through planning and quality control but also documentation and communication. Meetings are effective to keep track on planning and improve the communication between the workers. A good management is a necessity for a successful project.

Another type of costs are the resources needed for the project. These costs are affiliated with facility costs, literature, software and human resources. All of these costs are key elements for the project. Human resources are needed for the further development of the model but also for the management. Software costs are related to licenses of the program for the model. Also (extra) programming training for the model can be attributed to these costs. The literature and facility costs are necessities that come along with human resources. Facility costs will increase proportional to an increase in human resources.

The costs related to the model can be broken up into new module development, runtime enhancement, accuracy improvement, data acquisition and test and evaluation. These parts are rather time and resource consuming. Therefore they can increase the cost of the project considerably.

Chapter 14

Conclusion and Recommendations

When the geometrical lay-outs of modern transport aircraft are compared, a large degree of resemblance can be found. Most of these aircraft are designed bottom-up, starting nearly from scratch. As an alternative design method, scaling can be applied which could lead to a more time and cost efficient design process. This chapter will conclude the results of the *SCALAIR - Scalable Aircraft Model* project and afterwards recommendations will be given to indicate which improvements can still be made.

14.1 Conclusion

The mission of the SCALAIR project was to develop a more time and cost efficient aircraft design method for medium-size, medium-range passenger aircraft. The second goal was to use this method to redesign an existing medium-size, medium range transport aircraft into a more efficient aircraft with lower Direct Operating Costs due to the reduction in fuel consumption of at least 30 %. This was to be achieved by utilising high aspect ratio wings and propeller propulsion.

The purpose of the final report was to state the results of the whole project, obtained during the last nine weeks. The results consist of scaling laws, the optimal design parameters for the most efficient aircraft model and further recommendations on how to improve the model in the future.

From the performed market analysis it was concluded that the demand for narrow-body aircraft is on the rise. A growth rate of 4.7-5 % in air traffic demand is expected with narrow-body aircraft taking a market share of 68-70%.

Furthermore, the sustainable development strategy combined with the engine analysis showed that the use of propfan propulsion could result in significant sustainable improvements. First of all, it was concluded that using the General Electric Unducted Fan engine leads to a decrease in specific fuel consumption of 34 %, as well as a dramatic reduction in pollutant emissions. However, it was also concluded that more research is still to be conducted regarding propfan propulsion. On top of this, the use of propfan propulsion also poses problems with respect to noise and vibrations.

Moreover, the sustainable development strategy can also be used to draw conclusions with respect to scaling. As it was found that using a scalable model reduces the design time and presents options for a more modular manufacturing process. As such, the resource and manufacturing costs can also be reduced.

From a more detailed analysis it was deducted that it is possible to develop a scalable aircraft model. Thereby the first goal of the mission was achieved. The model was created based on aerodynamics, structures, performance, propulsion and stability and control. It was shown that this model can be used to quickly develop an initial estimate for a wide range of medium-size aircraft. Furthermore, it was found that this model can not only be used for medium-range aircraft but also for the initial sizing of a medium size aircraft with any range. Finally, it was concluded that this model can be used to find scaling laws which could then be incorporated or which can be used in other applications.

The next goal of the SCALAIR project was to use this model to redesign an existing aircraft with similar requirements, but with lower DOC through higher fuel efficiency with respect to the reference aircraft, Airbus A320. By using the scalable aircraft model to optimise the design it was shown that it was possible to increase the fuel consumption (kg/pax/km) of the A320 by as much as 35.8% for the design range, significantly surpassing the required 30%. This reduction was a result of using fuselage mounted GE UDF engines, increasing the aspect ratio to 11.4, slightly increasing the taper ratio to 0.25 and reducing the flight velocity to Mach 0.72. The latter also resulted in a lower sweep angle of 17 degrees. Consequently, the lift over drag increased by 12% and the MTOM reduced by 15%.

A final analysis with respect to the sustainability characteristics has shown that if this design is implemented, as much as 8,241,000 kg of CO_2 emissions could be saved each year by replacing a single Airbus A320 by the SCALAIR design. Last but not least, it was also concluded that replacing the A320 by the SCALAIR design would lead to a reduction in Direct Operating Costs of 8%.

14.2 Recommendations

The model can be further improved in the post-DSE phase. Several notable recommendations to improve the model are mentioned below. These recommendations can be attributed to different aspects of the model. Implementing these recommendations will affect the model in multiple ways. First of all, the accuracy of the model will be improved. Next, the runtime of the program can be reduced. Furthermore, the model can be made more widely applicable and more use friendly. Finally, recommendations are also presented from a design perspective.

14.2.1 Aerodynamics

Revisions can be made to the aerodynamics part of the program. In particular to the data which has been used for the spanwise wing twist and spanwise aerofoil profile. If such data was available on the A320 itself, then the reference data would be more accurate. As such, the model would have a closer defined reference aircraft and should thus lead to preciser scaling laws.

Also, the effect of spanwise twist distribution can be investigated in more detail. This is an important feature as the Oswald factor depends heavily on it. These changes will greatly increase the accuracy of the program.

Next, the scaling laws can also be improved, both in interdependency and in quantity of inputs. As has already been stated, scaling laws for spanwise twist and spanwise aerofoil selection should be incorporated. Furthermore, scaling laws for speed and air density are also interesting to consider. Ideally, scaling laws are made which incorporate the interdependency for all scalable parameters together. Implementing these scaling laws would greatly reduce the runtime of the program without affecting the accuracy significantly.

For even more accuracy, an improved estimation or calculation of the C_{D_0} can be made. In the current calculations, this number is assumed to be constant because it is beyond the scope of the project to vary this number. Also, estimations on wave drag can be made for improvements at higher speeds. For this, a CFD analysis would be required and therefore also far beyond the scope of this project.

Finally, from a design perspective, it is also interesting to optimise the aerofoil selection and the wing twist. Currently, the aerofoil selection has not been considered for the SCALAIR design, nor the kink twist. Additional selection on these matters could further improve the model.

14.2.2 Structural Design

Next, a number of recommendations can be made based on structural design.

First of all, a number of recommendations can be made with respect to the wing module. Currently, the wing module still uses the analytical wing module. This is very time consuming. The

scaling laws that have been found should be incorporated into the model, where the user should be given the choice to either run the analytical module or to incorporate scaling laws.

However, it can be noted that these scaling laws are not yet perfect. In order to make the scaling laws more accurate, a larger number of variables, such as air density, should be considered. Furthermore, in the ideal case, all variables would be combined in multi-dimensional scaling laws. Currently, there are already three dimensional scaling laws. However, these dimensions could be increased even further.

In addition, the accuracy of the wing module can be improved even further by increasing the amount of failure modes that are considered and by modelling the load distribution more accurately. However, it can be noted that the accuracy of the wing module is already high.

Besides the wing module, there are also additions that can be made to the tail module. First of all, it is useful to incorporate the detailed scaling laws in the tail module. They should present a more accurate result than the current calculations. Furthermore, as these scaling laws are known, incorporating these laws should not be too difficult.

However, it can also be noted that these scaling laws are not yet perfect. Currently, these detailed scaling laws are based on scaling laws that have been generated for the main wing. In order to improve the accuracy of the model, these same scaling laws should be made by running an analytical tail wing module, which can be done by adjusting the analytical wing structure module slightly. Increasing the accuracy and applicability even further can be done in a manner as has been described for the wing module.

Furthermore, changes can also be made to the fuselage module. Similar to the wing module, the amount of detail and the amount of scaling laws should be increased. Furthermore, in order to make the model more widely applicable, the fuselage dimensions and internal loadings should adaptable.

Finally, the landing gear can be modelled much more accurately. In the current model the weight of the landing gear is being scaled with the MTOW. It can be further developed by using more data points which are used to describe the trend to increase the accuracy.

It can also be noted that for the final design, the landing gear is kept equal in length. However, as the engine is moved to the fuselage, the spacing between the ground and the engines is reduced significantly. As such, it might be possible to reduce the landing gear length. This should be investigated further.

14.2.3 Performance and Propulsion

Currently, a restriction of the model is that it is unreliable for varying speed. This is due to the effects of speed on the engine performance, to be more specific, on the SFC of the engine. In the model the SFC is set fixed. This is due to the lack of available data. If the SFC is described as a function of speed, the engine would be modelled with higher accuracy.

Furthermore, there are numerous performance characteristics which are currently not outputs of the model. These include for example the take-off length of the aircraft. A module can be added which calculates additional performance characteristics.

Finally, the accuracy of the fuel module can be improved. Using a more detailed analysis of the flight profile presents the possibility to model the fuel consumption even more accurately. Furthermore, it could present more detailed information on the duration of each indivdual component of the flight which could be used to calculate the DOC more accurately.

14.2.4 Stability and Control

The preliminary analysis performed for the stability and control can be improved on several accounts, this leads to the following recommendations.

For the current tail module the interaction between the engine and the tail surfaces are not taken into account. The engine does, however, have a large influence on the behaviour of the flow over the horizontal stabiliser. As the inflow reduces the pressure and thereby increases the lift coefficient quite significantly. This is visualised in a simplified manner in Figures 14.1 and 14.2. These figures were created by means of a flat plate, vortex sheet analysis for incompressible, inviscid flow with

also two vortices emanating from respectively the top and bottom of the engine to show an initial estimate of the effect for 0 kN and 110 kN of thrust. As can be seen, the change in lift coefficient is significant. Therefore it is advisable to consider the interaction when computing the required tail areas.

Also, the presence of the engine near the vertical stabiliser surfaces induces changes in the directional stability and control that will have to be investigated on e.g. shielding effects and pressure effects.

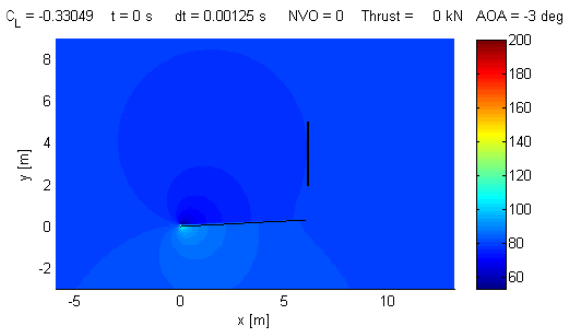

Figure 14.1: Incompressible, inviscid velocity field over the horizontal tail surface without engine effects

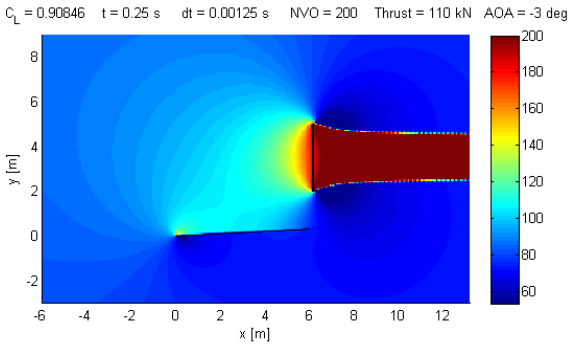

Figure 14.2: Incompressible, inviscid velocity field over the horizontal tail surface with engine effects

In order to obtain a loading diagram and a total CG position of the aircraft every single component's CG position needs to be obtained. It is extremely important that the CG position of each component is variable if the configuration changes and components are scaled. This part is not fully incorporated into the current program and should be improved to obtain more accurate results.

Furthermore, the used method for finding the optimum horizontal tail size and its corresponding wing position does not include a variable elevator surface which changes the tail's characteristics. Most obtained lift and moment coefficients and the aerodynamic centre locations are taken from semi-empirical formulae and might show inaccuracies or inconsistencies for scaled components (the stability subprogram should be further connected with the aerodynamic model in order to obtain more accurate results). Additionally, effects like aeroelastic bending, iced tail surfaces and most importantly the effect of the engine placement at the rear are not incorporated.

Finally, the eigenmotions were not taken into account in the current program. This part should be added using for example AVL in order to obtain the stability derivatives and ensure stable eigenmotions which could otherwise lead to fatal consequences. The eigenmotion characteristics can be added as an additional constraint during scaling.

14.2.5 General Model

The model has multiple inputs which can be varied. To add other inputs to the model, modules can be added to the program. This leads to an increase in its functionality. For example a fuselage module could be added. The current model has a fixed fuselage. Hence, adding a module to adjust the fuselage size opens other possibilities for scaling in aspects like the amount of passengers. Other modules which can be included are for example electrical and hydraulic modules.

Further advancements can also be achieved on integration between the modules. Effects between modules can then be incorporated even better. This could for example be done for the engine and tail. The effects of varying the engine's position on the tail can then be taken into account for the aircraft.

The model uses iterations to generate designs. Hence, inefficient structured codes and unnecessary calculations should be avoided in order to keep the runtime of the program low. Currently, the model needs a considerable amount of time to run. Altering the MATLAB code, can shorten

the runtime of the program. In particular for the wing module a reduction in runtime would be beneficial. The calculation time in the wing module is about ten seconds per iteration. Since it is iterated multiple times, the run time of the wing module has a large influence on the total runtime. Also, in order to reduce the amount of iterations, the program could start iterating from a design which has been found quickly using general scaling laws, rather than starting at the Airbus A320.

A next aspect which could be improved is the user interface. First of all, the GUI can be improved. At this point, it is not yet possible to stop the program at certain points from the GUI itself. If this is to be done, the program will have to be stopped from within the code itself. Furthermore, showing intermediate output should also be possible from the GUI. Also, the output variables can be presented in a more structured manner. Finally, the amount of input and output variables can be changed to widen the usability of the program without affecting the user interface.

14.2.6 Market Analysis

To have a better overview of the expected demand for scalable aircraft it would be worthwhile to analyse the developments with respect to new generation aircraft. Because, such a change in aircraft designs might jeopardise the equivalent topology strategy that is applied for the current scaling design methodology. Given that scalable aircraft models might evolve over the years as well, a complete analysis taking into account both the generality of the design methodology versus innovative new technology should be conducted.

Bibliography

[1] R. H. Liebeck, D. A. Andrastek, J. Chau, R. Girvin, R. Lyon, B. K. Rawdon, P. W. Scott, and R. A. Wright, "Advanced subsonic airplane design and economic studies," tech. rep., NASA, 1995.

[2] L. Veldhuis, "Project guide design synthesis exercise - scalair scalable aircraft model," tech. rep., TU Delft, 2012.

[3] Airbus, *Navigating the Future - Global Market Forecast*. Airbus, 2012.

[4] Boeing, "Current market outlook 2012-2031," tech. rep., Boeing, 2012.

[5] J. Leahy, "Global market forecast 2012-2031." Promotion Lecture, 2012.

[6] Embraer, "Market outlook 2012-2031," tech. rep., Embraer, 2012.

[7] S. J. Karam, "Boeing vs. airbus: Orders and profits," 2012. `http://seekingalpha.com/article/592001-boeing-vs-airbus-orders-and-profits`.

[8] C. Lewis, "Commercial fleet forecast global:2011-2030 h-2." Summary, 2011.

[9] G. J. Harrison, "Challenge to the boeing-airbus duopoly in civil aircraft: issues for competitiveness," tech. rep., Congressial Research Service, 2011.

[10] J. Gamble and A. Thompson Jr., *Essentials of Strategic Management*. McGraw-Hill Education, 2nd ed., 2011.

[11] S. Storm and C. Naastepad, *Macroeconimics beyond the NAIRU*. Harvard University Press, 2011.

[12] J. A. D. Corporation, "Worldwide market forecast for commercial air transport 2010-2029," tech. rep., Japan Aircraft Development Corporation, 2010.

[13] D. Schwamborn, T. Gerhold, and R. Meinrich, "The dlr tau code: recent applications in research and industry," in *ECCOMAS CFD 2006*, 2006.

[14] R. A. Brealey, S. C. Myers, and F. Allen, *Principles of Corporate Finance, Concise Edition*. s, 2010.

[15] IEA, *Transport Energy and CO2: Moving towrds sustainability*. International Energy Agency, 2009.

[16] J. J. Lee, S. P. Lukachko, I. A. Waitz, and A. Schafer, "Historical and future trends in aircraft performance, cost and emissions," tech. rep., Department of Aeronautics and Astronautics and Center for Technology, 2001.

[17] D. G. 10, "Midterm report - scalair scalable aircraft model," tech. rep., TU Delft, 2012.

[18] R. Hager and D. Vrabel, *Advanced Turboprop Project*. NASA Scientific and Technical Information Division, 1988.

[19] *AGARD- CP - 366 - Aerodynamics and Acoustics of Propellers*, 1984.

[20] M. Prather and R. Sausen, "Ipcc special report on climate change," 1999. `http://www.grida.no/publications/other/ipcc_sr/?src=/climate/ipcc/aviation/064.htm`.

[21] G. Ruijgrok and D. van Paassen, *Elements of Aircraft Pollution*. Delft University Press, 2005.

[22] M. D. Guynn, J. J. Berton, E. S. Hendricks, M. T. Tong, W. J. Haller, and D. R. Thurman, "Initial assessment of open rotor propulsion applied to an advanced single-aisle aircraft," tech. rep., AIAA 2011-7058, 2011.

[23] S. Hartjes, "Ae3502 - aircraft noise." Lecture Slides, 2012.

[24] NASA, "Green aviation: A better way to treat the planet," tech. rep., Aeronautics Research Mission Directorate, 2009.

[25] WHO, "Environmental health inequalities in europe. assessment report," tech. rep., World Health Organization, 2012.

[26] Bombardier, "Q400 and sustainable development." Presentation slides, 2007.
[27] A. Stuermer and J. Yin, "Dlr-as cror & propeller noise prediction," tech. rep., Institute of Aviation Warsaw, 2010.
[28] R. Akkermans, O. Brodersen, J. Delfs, A. Stuermer, and J. Yin, "Progress in aerodynamic and aeroacoustic integration of cror propulsion systems," 2012.
[29] H. Brouwer, "Analytic description of the noise radiation from single- andcontra-rotating propellers," tech. rep., NLR, 2011.
[30] M. D. Guynn, J. J. Berton, E. S. Hendricks, M. T. Tong, W. J. Haller, and D. R. Thurman, "Performance and environmental assessment of an advanced aircraft with open rotor propulsion," tech. rep., NASA, 2012.
[31] D. G. 10, "Baseline report - scalair scalable aircraft model," tech. rep., TU Delft, 2012.
[32] I. Applied Aerodynamics Group, "Uiud airfoil coordinates database." `http://www.ae.illinois.edu/m-selig/ads/coord_database.html`.
[33] D. P. Raymer, *Aircraft Design: A Conceptual Approach*. American Institue of Aeronautics and Astronautics, Inc., 1992.
[34] E. Torenbeek, *Synthesis of Subsonic Airplane Design*. Kluwer Academic Publishers and Delft University Press, 1982.
[35] G. La Rocca, "Ae3201 - systems engineering and aerospace design." Lecture Slides, 2012.
[36] A. Filippone, *Flight Performance of Fixed and Rotary Wing Aircraft*. Elsevier Ltd., 2006.
[37] E. Obert, "Aerodynamic design of transport aircraft," tech. rep., TU Delft, Faculty of Aerospace Engineering, 2009.
[38] A. M. T. Association, "Faces behind amt's," 2010. `http://www.amtausa.com/awa.html`.
[39] E. in System Engineering and Development, "Exxpertsystems gmbh," 2010. `http://www.exxpertsystems.de/portfolio.htm`.
[40] L. Jenkinson, "Southampton data sheets," 2005. `http://www.southampton.ac.uk/~jps7/Aircraft%20Design%20Resources/Lloyd%20Jenkinson%20data/Aircraft%20data/`.
[41] K. Seywald, "Wingbox mass prediction considering quasi-static nonlinear aeroelasticity," Master's thesis, Royal Institute of Technology, 2011.
[42] J. Ostrower, *Airbus looks to Sharklet structure to lay A320neo groundwork*. Flightglobal, November 2011. `http://www.flightglobal.com/blogs/flightblogger/2011/11/airbus-looks-to-sharklet-struc.html`.
[43] T. Canuck, "747-200 cruise speed," 2012. `http://www.airliners.net/aviation-forums/tech_ops/read.main/313226/`.
[44] M. D. Ardema and M. C. C. et al., "Analytical fuselage and wing weight estimation of transport aircraft," tech. rep., NASA, 1996.
[45] EASA, "Certification specification for large aeroplanes, cs-25." Regulation, 2007.
[46] G. La Rocca, "Ae3021 - aircraft design." Lecture Slides, 2011.
[47] EASA, *Certification Specifications for Large Airplanes*, amendment 5 ed., September 2008.
[48] Airbus, *A320 Family Instructor Support*, 2001.
[49] J. Roskam, *Airplane Design: Part I: Preliminary Sizing of Airplans*. DAR Corporation, 1997. Page 10 Figure 2.3.
[50] D. P. Raymer, "An approximate method of deriving loiter time from range," tech. rep., Conceptual Research Corporation, 2003.
[51] Airbus, "Airbus specifications," 2012. `http://www.airbus.com/fileadmin/media_gallery/files/tech_data/AC/Airbus-AC-A320-Jun2012.pdf`.
[52] Boeing, *737 Airport Characteristics for Airport Planning*, 2005.
[53] G. A. Engines, "Full scale technology demonstration of a modern counterrotating unducted fan engine concept - design report," tech. rep., NASA, 1987.
[54] U. Government, "Cfr, title 14, part 36, noise standards: Aircraft type and airworthiness certification."
[55] ICAO, "Environmental protection, chapter 4, annex 16, noise." Regulation, 2008.
[56] G. H. et al., "Experimental performance and acoustic investigation of modern, counterrotating blade concepts," tech. rep., NASA CR-185158, 1990.
[57] Y. M. Gisin, "Wing-nacelle assembly multidisciplinary performance optimization," Master's

thesis, California Polytechnic State University, 2006.
[58] L. Jenkinson, P. Simpkin, and D. Rhodes, "Russian aircraft data," 2005. http://www.elsevierdirect.com/companions/9780340741528/appendices/data-a/table-7/default.htm.
[59] Airbus, *A318/A319/A320/A321 Performance Training Manual*.
[60] Boeing, "Design groups," 2011. http://www.boeing.com/commercial/airports/faqs/aircraftdesigngroup.pdf.
[61] Boeing, "Design groups," 2010. http://www.boeing.com/commercial/aeromagazine/articles/2010_q3/3/.
[62] A. A. Trani, "Aircraft classifications." http://128.173.204.63/courses/cee5614/cee5614_pub/acft_classifications.pdf.
[63] FAA, "Faa airport standards," 2012. http://www.faa.gov/documentLibrary/media/Advisory_Circular/150_5300_13a.pdf.
[64] Airbus, *A320 Aircraft Characteristics Airport and Maintenance Planning*, 2012.
[65] Jetex, "Jetex flight support," 2005. http://www.jetex.com.
[66] Jetwash, "Jetwash aviation services," 2013. http://www.jetwash.ca/.
[67] W. Gnarowski, W. Zdrojewski, and M. Pokorski, "D4.2 Operating Cost Analysis," tech. rep., EPATS and Institute of Aviation, 2008.
[68] J. Scanlan, "AAE 451 Spring 2004 - Method for Calculating Direct Operating Cost," 2004. http://www.southampton.ac.uk/~jps7/Aircraft%20Design%20Resources/Cost%20data/aircraft%20operating%20cost%20equations.pdf.
[69] I. M. Goldsmith, "Nasa contractor report 166138: A study to define the research and technology requirements for advanced turbo/propfan transport aircraft," tech. rep., NASA, 1981.
[70] ALLPIRG, "Fourth Meeting of the ALLPIRG/Advisory Group - ALLPIRG/4-WP/28 Appendix - Cost Tables for CNS/ATM Planning and Evaluation Tools," tech. rep., ICAO, 2001.
[71] W. Mason, "Cost (and other issues)." Lecture Slides, 1997. http://www.southampton.ac.uk/~jps7/Aircraft%20Design%20Resources/Cost%20data/commercial%20aircraft%20costs%20and%20design.pdf.
[72] D. Visser, "Ae3501 - air transportation." Lecture 4: Airline costs (& revenues), 2011.
[73] U. E. I. Administration, "U.S. Gulf Coast Kerosene-Type Jet Fuel Spot Proce FOB." http://www.eia.gov/dnav/pet/hist/LeafHandler.ashx?n=PET&s=EER_EPJK_PF4_RGC_DPG&f=D.
[74] Sky4all and K. L. Swartz, "Qatar airways: ultimate operational analysis (part ii)," 2011. http://sky4all.wordpress.com/2011/10/31/qatar-airways-ultimate-operational-analysis-part-ii/.
[75] SeatGuru, "Qatar airways airbus a320 (320)," 2009. http://www.seatguru.com/airlines/Qatar_Airways/Qatar_Airways_Airbus_A320_B.php.
[76] A. Gazette and M. Khawaja, "Middle east airlines register strong july growth iata," 2012. http://arabiangazette.com/middle-east-airlines-july-iata/.
[77] M. Drela, "Avl." http://web.mit.edu/drela/Public/web/avl/.
[78] J. Anderson, *Fundamentals of Aerodynamics, Fourth Edition*. Mc Graw Hill, 2007.
[79] J. Moran, *An introduction to theoretical and computational aerodynamics*. John Wiley & Sons, 1984.
[80] J. Katz and A. Plotkin, *Low-Speed Aerodynamics, Second Edition*. Cambridge University Press, 2001.
[81] S. Hulshoff, "Ae4930 - aeroelasticity," 2011. Lecture Notes for Aeroelasticity AE4930.

Appendix A

Aerodynamics

While the flow would be most accurately described by the Navier-Stokes equations, it is unfortunately not a trivial case to solve these in a practical manner. Therefore, simplifications will have to be made. In this project the Athena Vortex Lattice (AVL) [77] program is used for the initial analysis of the aerodynamic characteristics, such as lift distribution and induced drag. The simplifications of this program are described in section A.1. Consequently, section A.2 briefly reviews the Vortex Lattice Method (VLM).

A.1 Flow Simplifications

The simplifications made in the AVL program are as follows:

- **Quasi-steady flow**

  The unsteady shedding of vorticity is not taken into account. Basically only slow oscillatory motions are allowed.
- **Inviscid flow**

  Neglecting the viscous terms in the Navier-Stokes equations means that the flow will not have any friction, thermal conduction or diffusion effects.
- **Incompressible flow**

  For incompressible flow the density remains perfectly constant.

  Since the aircraft operates at Mach 0.72 the encounters highly non-linear transonic flow regimes. Therefore compressibility effects are actually not to be neglected. In AVL these are accounted for by means of the (linear) Prandtl-Glauert transformation.
  Note that for an unswept wing this would be highly discutable due to the likely occurrence of transonic flow phenomena. Since the design should be such that high-transonic conditions are avoided, this risk is already minimised by using swept wings, as it decreases the perpendicular Mach number. For perpendicular Mach numbers up to 0.7, the AVL results will be valid as initial estimates (given the phase of the project) [77]. Therefore, with the cruising Mach number of 0.72 for the GE UDF engine, the computations of AVL will indeed be valid.
- **Irrotational flow**

  The Prandtl-Glauert transformation is derived from the linearised perturbation velocity potential equation (with transformed variables equivalent to Laplace's equation in equation A.2).Note that if there is a velocity potential, the flow has to be irrotational. By assuming the flow to be irrotational, the curl of the velocity vector will be zero, as indicated in equation A.1. Or in other words, the vorticity at any point in the flow is zero.

$$\nabla \times \mathbf{V} = 0 \tag{A.1}$$
$$\Delta\phi = 0 \tag{A.2}$$

With as boundary conditions:

$$u_{x=\infty} = \frac{\delta\phi}{\delta x} = V_\infty \tag{A.3}$$
$$v_{y=\infty} = \frac{\delta\phi}{\delta y} = 0 \tag{A.4}$$
$$\mathbf{V} \cdot \mathbf{n} = \left(\frac{\delta\phi}{\delta n}\right)_{y_{wall}} = 0 \tag{A.5}$$

- **Small angle of attack**

  For a small angle of attack: $sin\alpha \approx \alpha$, $cos\alpha \approx 1$ and $tan\alpha \approx \alpha$. Note that in AVL the trailing vortices are aligned with the X axis, so a small angle of attack is important with respect to e.g. the induced drag computation.

- **Thin airfoil**

  Assuming a thin airfoil, the camber line can be described by a vortex sheet of strength $\gamma(s)$. Then to make the camberline a streamline of the flow the *fundamental equation of thin airfoil theory* in equation A.6 has to be solved for the vortex strength $\gamma(\xi)$ [78]. Note that the equation needs to satisfy the Kutta condition at the trailing edge, i.e. $\gamma_{TE} = 0$.

$$\frac{1}{2\pi}\int_0^c \frac{\gamma(\xi)d\xi}{x-\xi} = V_\infty\left(\alpha - \frac{dz}{dx}\right) \tag{A.6}$$

The most well-known result of this theory is the lift slope $\frac{dc_l}{d\alpha} = 2\pi$, which is linear and constant for low-to-moderate angles of attack for any type of airfoil. Furthermore, the lift and quarter chord moment coefficient are approximated by [78]:

$$c_l = \frac{dc_l}{d\alpha}(\alpha - \alpha_{L=0}) \tag{A.7}$$

Where,

$$\alpha_{L=0} = \frac{1}{\pi}\int_0^\pi \frac{dz}{dx}(cos\theta_0 - 1)d\theta_0 \tag{A.8}$$

And

$$c_{m,\frac{c}{4}} = \frac{\pi}{4}(A_2 - A_1) \tag{A.9}$$

Where,

$$A_n = \frac{2}{\pi}\int_0^\pi \frac{dz}{dx} cosn\theta_0 d\theta_0 \tag{A.10}$$

A.2 Vortex Lattice Method

The Vortex Lattice Method (VLM) is essentially a method that breaks down a surface into several quadrilateral panels with one discrete horseshoe vortex for each panel. Let the horseshoe vortex be defined as the combination of a bound vortex filament and two free vortices trailing downstream, with the bound vortex 'replacing' a discrete part of the wing span. The bound vortex here represents the circulation eventually leading to a lift distribution. This 'threefold' definition of the vortex follows Helmholtz's vortex theorems. For further reference, see chapter 5 in Anderson [78].

The strengths of the vortices are then to be determined by imposing the flow-tangency condition (equation A.12) at the mid-points of the panel's three-quarter chord. [79] To solve for the vortex strength, the normal velocity components induced by the bound vortices and the freestream should thus add up to zero (equation A.11). Note that the quadrilateral panels are parallel to the streamwise direction. Thereby allowing for swept wings.

Since the VLM also allows for the use of separate systems of panels it is possible to model the wing's different sections in partitions (e.g. flaps, cranked wings). This is a huge advantage in comparison with, for example, lifting line theory. The possibilities of the VLM also stretch beyond the planform surface itself. The trailing vortices in the wake can be modelled by equating them with the strength of the vortex at the trailing edge.

$$V_\infty sin\alpha - \sum_{i,j} \Gamma_{ij} w_{ij}(x_{cp}, y_{cp}) = 0 \tag{A.11}$$

$$\mathbf{V} \cdot \mathbf{n} = (\nabla \phi) \cdot \mathbf{n} = 0 \tag{A.12}$$

Then using the Kutta-Joukowski theorem, or in other words the *circulation theory of lift*, the lift per panel can be computed as for example(discretely) stated in equations A.13 (at the leading edge, $i = 1$) and A.14 ($i > 1$) [78], [79], [80].

$$\Delta L_{ij} = \rho V_\infty \Gamma_{i,j} \Delta y_{ij} \tag{A.13}$$

$$\Delta L_{ij} = \rho V_\infty (\Gamma_{i,j} - \Gamma_{i-1,j}) \Delta y_{ij} \tag{A.14}$$

For the total lift this then yields [80], where the matrix size is given bij M and N.

$$L = \sum_{i=1}^{M} \sum_{j=1}^{N} \Delta L_{ij} \tag{A.15}$$

The pressure difference across the panel is then defined by equation A.16 for panel area ΔS_{ij} [80].

$$\Delta p_{ij} = \frac{\Delta L_{ij}}{\Delta S_{ij}} \tag{A.16}$$

The computation of the induced drag then becomes, similarly to the segment-wise lift, respectively for $i = 1$ and $i > 1$ [80]

$$\Delta D_{ij} = -\rho w_{ind_{i,j}} \Gamma_{i,j} \Delta y_{ij} \tag{A.17}$$

$$\Delta D_{ij} = -\rho w_{ind_{i,j}} (\Gamma_{i,j} - \Gamma_{i-1,j}) \Delta y_{ij} \tag{A.18}$$

For the total drag this then yields [80]

$$D = \sum_{i=1}^{M} \sum_{j=1}^{N} \Delta D_{ij} \tag{A.19}$$

The induced drag can also be calculated by using a 'far field analysis' in the two-dimensional Trefftz plane [80]. Infinitely far downstream the main contribution to the drag comes from the cross-flow kinetic energy.This ultimately results in the following equation, for k is 1 to the total number of trailing vortices N_W.

$$D = -\frac{\rho}{2} \sum_{k=1}^{N_W} w_{ind_k} \Gamma_k \Delta y_k \tag{A.20}$$

Appendix B

Structural Design

B.1 Weight Elements

The method described in Subsection 5.1.1 leads to estimating the weights of the A320. The data has been taken from two different sources [37, 40]. The results are displayed in Figure B.1.

				Fixed fuselage weight	Variable fuselage weight	Fixed wing weight	Variable wing weight	Fixed Horizontal	Variable Horizontal	Fixed Vertical	Variable Vertical	Fixed Engine	Variable Engine	Summation	
Ratio	*1,03215651*			26164,96	7207,14	1605,05	28992,13	103,76	669,79	103,76	502,58	6503,05	1647,79	73500	
Structural Fixed Percentage				*30%*		*0%*		*0%*		*0%*		*90%*			
Structural weight				9225,41		9084,01		645,10		477,89		0,00			
	Sub element	**Complete weight**	**Total**	**Fuselage percentage**	**Fuselage weight**	**Wing percentage**	**Wing weight**	**Horizontal percentage**	**Horizontal weight**	**Vertical percentage**	**Vertical weight**	**Engine percentage**	**Engine weight**		
Non Scaled Parts	Hydraulic generation (50%)	282,29	100%	40%	112,92	50%	141,15	0%	0,00	0%	0,00	10%	28,23		
	Hydraulic distribution (50%)	164,63	100%	30%	49,39	40%	65,85	15%	24,69	15%	24,69	0%	0,00		
	Bleed Air System	257,01	100%	30%	77,10	30%	77,10	0%	0,00	0%	0,00	40%	102,80		
	Air conditioning	685,35	100%	100%	685,35	0%	0,00	0	0,00	0%	0,00	0%	0,00		
	Fire protection	87,73	100%	30%	26,32	50%	43,87	5%	4,39	5%	4,39	10%	8,77		
	Flight controls	796,82	100%	35%	278,89	65%	517,94	0%	0,00	0%	0,00	0%	0,00		
	Fuel System	308,61	100%	0%	0,00	100%	308,61	0%	0,00	0%	0,00	0%	0,00		
	Instruments	73,28	100%	80%	58,63	20%	14,66	0%	0,00	0%	0,00	0%	0,00		
	Maximum payload weight	14250,00	100%	100%	14250,00	0%	0,00	0%	0,00	0%	0,00	0%	0,00		
	Auto-flight system	104,25	100%	100%	104,25	0%	0,00	0%	0,00	0%	0,00	0%	0,00		
	Navigation	428,34	100%	70%	299,84	20%	85,67	5%	21,42	5%	21,42	0%	0,00		
	APU	230,17	100%	100%	230,17	0%	0,00	0%	0,00	0%	0,00	0%	0,00		
	Communication	191,98	100%	100%	191,98	0%	0,00	0%	0,00	0%	0,00	0%	0,00		
	Electric generation	354,03	100%	40%	141,61	30%	106,21	0%	0,00	0%	0,00	30%	106,21		
	Electric distribution	1065,19	100%	60%	639,11	20%	213,04	5%	53,26	5%	53,26	10%	106,52		
	Furnishing	2509,17	100%	100%	2509,17	0%	0,00	0%	0,00	0%	0,00	0%	0,00		
	Oxygen	106,31	100%	100%	106,31	0%	0,00	0%	0,00	0%	0,00	0%	0,00		
	Lighting	206,43	100%	100%	206,43	0%	0,00	0%	0,00	0%	0,00	0%	0,00		
	Equipped engine	6150,52	100%	0%	0,00	0%	0,00	0%	0,00	0%	0,00	100%	6150,52		
	Engine Controls	29,93	100%	100%	29,93	0%	0,00	0%	0,00	0%	0,00	0%	0,00		
	Anti Icing	30,96	100%	0%	0,00	100%	30,96	0%	0,00	0%	0,00	0%	0,00		
	Water installation	81,54	100%	100%	81,54	0%	0,00	0%	0,00	0%	0,00	0%	0,00		
	Standard and Operational items	3318,38	100%	100%	3318,38	0%	0,00	0%	0,00	0%	0,00	0%	0,00		
	Summation of non scaled parts	31712,95			23397,33		1605,05		103,76		103,76		6503,05		
Scaled Parts	Maximum fuel weight	17940,00	100%	0%	0,00	100%	17940,00	0%	0,00	0%	0,00	0%	0,00		
	Hydraulic generation (50%)	282,29	100%	40%	112,92	50%	141,15	0%	0,00	0%	0,00	10%	28,23		
	Hydraulic distribution (50%)	164,63	100%	30%	49,39	40%	65,85	15%	24,69	15%	24,69	0%	0,00		
	Equipped engine	683,39	100%	0%	0,00	0%	0,00	0%	0,00	0%	0,00	100%	683,39		
	Pylons	936,17	100%	0%	0,00	0%	0,00	0%	0,00	0%	0,00	100%	936,17		
	Landing gear	2348,16	100%	25%	587,04	75%	1761,12	0%	0,00	0%	0,00	0%	0,00		
	Summation of scaled parts	22354,64			749,35		19908,12		24,69		24,69		1647,79		
	Summation of scaled and non scaled	54067,59			33372,09		30597,18		773,55		606,34		8150,84	73500	*MTOW*
	Summation of all parts and structural	73500										*MTOW - Payload - Fuel =*		41310	*OEW*

Figure B.1: Variable and Fixed Weight of the A320

Appendix C

Model Description

In this appendix the Communication Flow Diagram (COMFD) and the Function Flow Diagram (FFD) for the MATLAB model can be found.

C.1 Communication Flow Diagram

Aside from understanding how information flows, it is also important in what order the communication occurs. This can be found in Figure C.1. Since the model is very Modular, this diagram will actually have a lot in common with the Data flow diagram in Figure 9.1. As can be seen, each parameter set will go through one module at the time, namely the Wing, Tail, Fuselage and Engine module. after each iteration, the Main class decides if the iteration is done. It calculates how big the difference in MTOM was with the last iteration. if this is smaller then a certain percentage, the parameter set is done iterating. Also, if the amount of iterations is larger then a certain amount, the program also decides the iteration is finished.

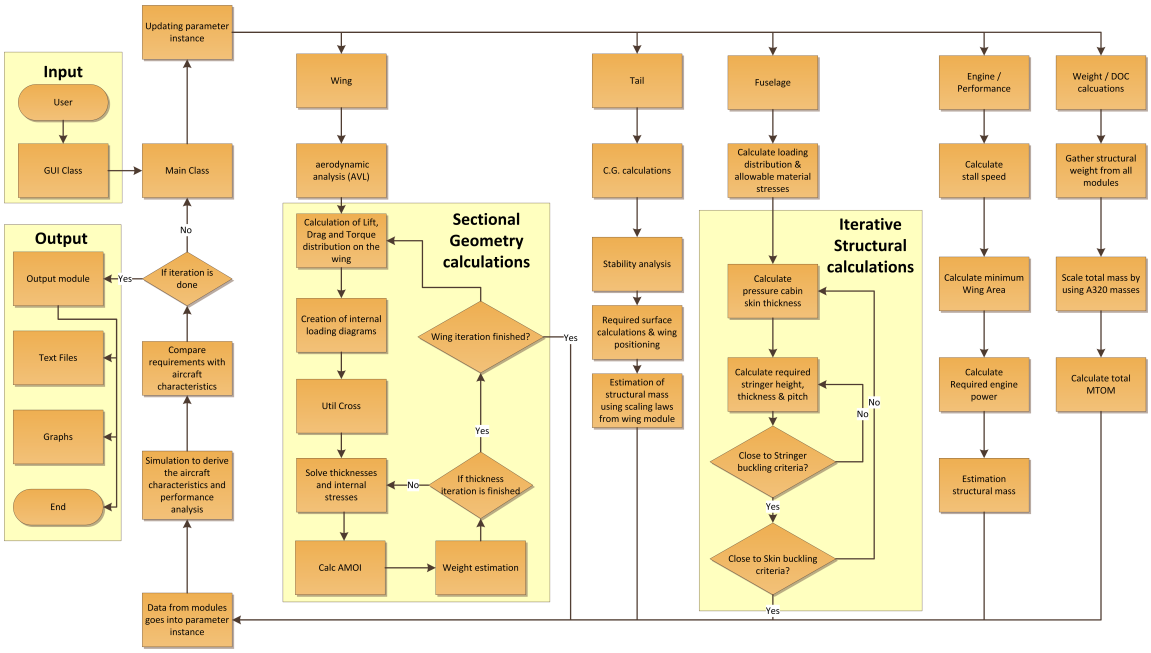

Figure C.1: Communicational Flow Diagram

C.2 Functional Flow Diagram

The last diagram which can offer a good overview of the program is the Functional Flow Diagram. This diagram shows all different functions the program has to perform, in the order in which they are performed.

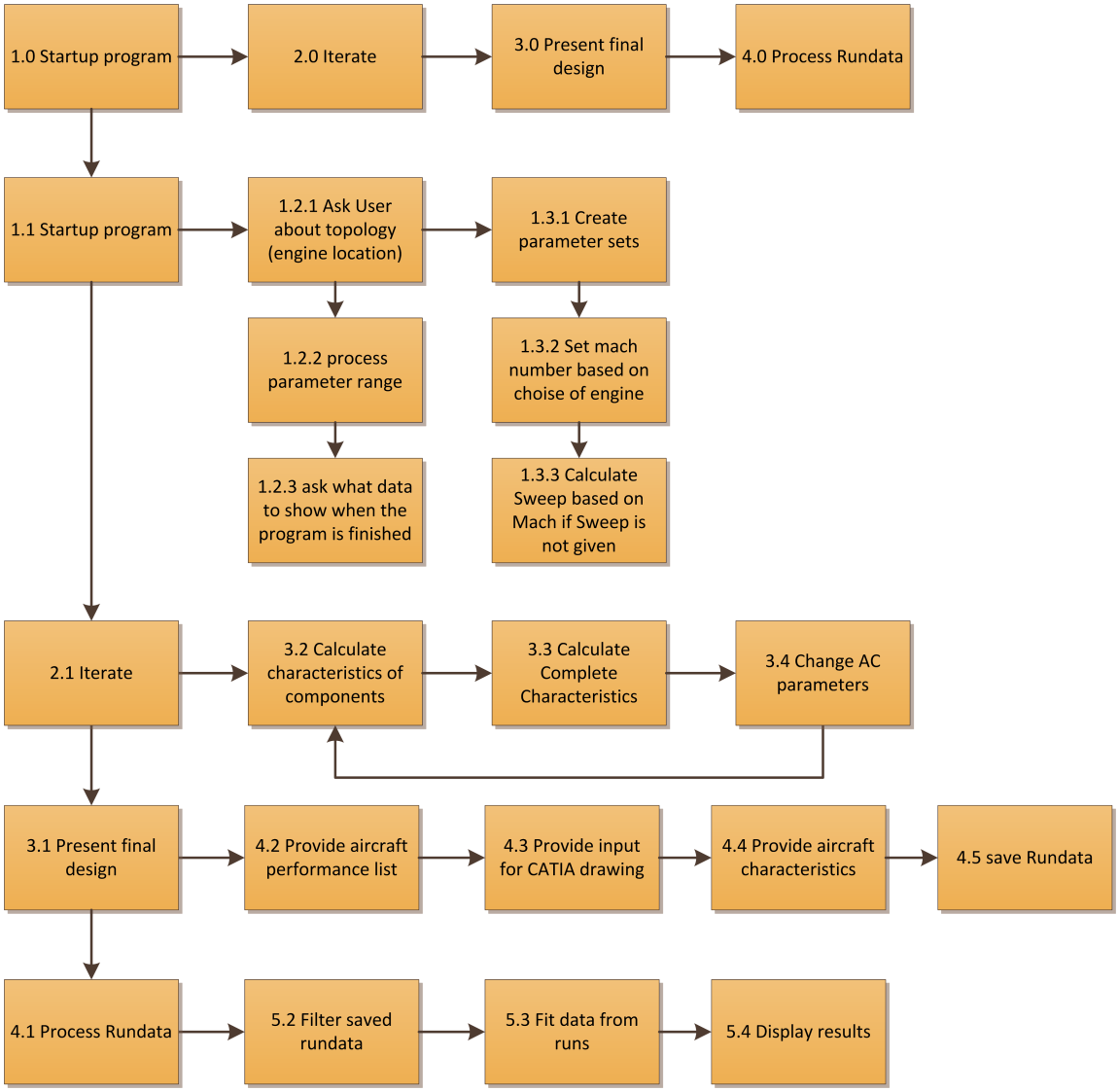

Figure C.2: Functional Flow Diagram

Appendix D

Aeroelasticity

The current appendix on aeroelasticity combines both isolated structural and aerodynamic considerations and describes the effects of their interaction. Fluid-structure interactions are of particular importance for aircraft designs with high aspect ratio wings. It should also be noted that the engines will be placed on the fuselage due to the engine choice described in this report. Because of this, the local centre of gravity (CG) of the wing section is shifted aft considerably. Besides that, the damping effect of the engine on the wing will also vanish. This shift in CG and the lack of damping might make the wings significantly more prone to flutter.

Note, however, that this appendix mainly serves as an initial endeavour into the world of aeroelasticity. Solving for flutter boundaries can be considered highly non-trivial. Therefore, the possiblities of computing these boundaries might be limited in this project. The goal of this chapter is to figure out the opportunies with respect to using aeroelastic approximations. Therefore, the basics are explained first with the aerodynamic model and the equations of motion. Subsequently, section D.3 goes into more detail and defines what is possible for our project.

D.1 Low-frequency Aerodynamic Model

As a first simplification the aerodynamic model is described as a low-frequency model. This model concerns the typical airfoil section (taken around 66 to 75 percent of the span). The angle of attack includes the vertical translation speed $\dot{h}$. The lift and moment are then given by equation D.2 [81].

$$L(t) = qSC_{L_\alpha}\left(\alpha(t) + \frac{\dot{h}(t)}{V_\infty}\right) \tag{D.1}$$

$$M_{EA}(t) = qSecC_{L_\alpha}\left(\alpha(t) + \frac{\dot{h}(t)}{V_\infty}\right) \tag{D.2}$$

D.2 Equations of Motion

The equations of motion for an uncambered typical section (two degrees of freedom; θ,h) with a low-frequency aerodynamic model, and without control surfaces, are expressed in equation D.3[81].

$$\left[M\right]\left\{\ddot{x}\right\} - \frac{q}{V_\infty}\left[A_1\right]\left\{\dot{x}\right\} + (\left[K\right] - q\left[A_0\right])\left\{x\right\} \tag{D.3}$$

where

$$\left[M\right] = \begin{bmatrix} m & S_\theta \\ S_\theta & I_\theta \end{bmatrix}, \left[K\right] = \begin{bmatrix} K_h & 0 \\ 0 & K_\theta \end{bmatrix} \tag{D.4}$$

$$\left[A_0\right] = \begin{bmatrix} 0 & -SC_{L_\alpha} \\ 0 & 2SebC_{L_\alpha} \end{bmatrix}, \left[A_1\right] = \begin{bmatrix} -SC_{L_\alpha} & 0 \\ SecC_{L_\alpha} & 0 \end{bmatrix} \tag{D.5}$$

Note that the stiffness matrix does not have any coupling terms. The structural coupling might have to be taken into account given that the wing to be designed probably will have a certain camber. Also note that the mass matrix includes the coupling term S_θ. This term takes into account that the total displacement field depends on both the plunging and the pitching.

D.3 Instability Boundary Problems

Instability boundary problems are solved to find out where the division is between the stable and unstable fluid-structure interactions. This can be approached both in a static and in a dynamic manner. For the static boundary the time gradients are negligible and the divergence is analysed (i.e. the "tearing off of the wing", indicated by the real part of the eigenvalue). For the dynamic approach, the oscillatory behaviour will also have to be analysed. Ergo, both the imaginary part and the real part of the eigenvalues play a role. The latter problem is also known as flutter.

The possibility of using either of these approaches is addressed in sections D.3.1 and D.3.2.

D.3.1 Torsional Divergence

For the torsional divergence problems, the equations of motion can be simplified by neglecting all of the time derivatives, as it involves a static problem. Also, the bending deflection θ is assumed to be small.

The static problem basically describes the relation between the aerodynamic forces and the structural forces. If the dynamic pressure increases such that the spring stiffness is exceeded, the wing will tear off or, as stated in the aeroelasticity lecture notes [81]: *"Beyond this speed θ increases without bound in response to a perturbation"*. The operating dynamic pressure is limited to prevent divergence for a single degree of freedom (θ) as is seen in equation D.6.

$$q \leq \frac{K_\theta}{C_{L_\alpha} ecS} \tag{D.6}$$

Because of the static nature of the divergence problem, it is a feasible option as a first aeroelastic analysis. However, given that the wings are expected to be swept backwards (even by a small amount), torsional divergence is highly unlikely to occur due to e.g. the reduced lift resulting from the twist that accompanies the wing bending. Therefore, the static problem is not addressed any further in this project.

D.3.2 Flutter

Flutter is an instability phenomenon where the interaction of the structural and aerodynamic forces results in self-sustained oscillatory behaviour. The risk in this type of behaviour is that the oscillations might increase in amplitude if the airfoil motion (plunging and pitching) is in phase and aligned with the lift force, thereby displaying divergent behaviour. To analyse the shift from stable to unstable regimes, it is easiest to describe the flutter points on the flutter boundary (i.e. at constant amplitude, thus possible to assume harmonic motion) encompassing the flutter envelope. From airworthiness requirements the flutter envelope should be at least at 115 per cent of the flight envelope.

Using the equations of motion (equation D.3) and the aforementioned harmonic motion for the pitching and plunging, the characteristic equation can be written and solved for its roots (real, imaginary or complex). Then, several types of motions exist based on the form of the respective roots. Through the dynamic pressure, q, these are related to the flutter speed. Note that for flutter only the oscillatory converging and diverging motions are of interest and that negative frequencies are deemed non-physical, which then leads to their dismissal.

A solution of the form presented in equation D.7 can then be assumed.

$$\left\{x\right\} = \left\{\hat{x}\right\} e^{pt} \tag{D.7}$$

For the low-frequency model this yields the characteristic equation as is presented in equation D.8 [81].

$$a_4 p^4 + a_3 p^3 + a_2 p^2 + a_1 p + a_0 = 0 \tag{D.8}$$

where the coefficients are

$$a_4 = mI_\theta - S_\theta^2 \tag{D.9}$$

$$a_3 = \frac{q}{V_\infty} SC_{L_\alpha}(2ebS_\theta + I_\theta) \tag{D.10}$$

$$a_2 = mK_\theta + I_\theta K_h - (2meb + S_\theta)qsC_{L_\alpha} \tag{D.11}$$

$$a_1 = m\frac{q}{V_\infty} SC_{L_\alpha} K_\theta \tag{D.12}$$

$$a_0 = K_h(K_\theta - 2ebqSC_{L_\alpha}) \tag{D.13}$$

Then, the characteristic equation can be solved for p for increasing V_∞. To simplify the analysis all other structural, inertial or aerodynamic terms in these coefficients are to remain constant throughout the computation. Consequently, if it is assumed that the roots are of the form $p = \sigma + i\omega$, the flutter diagrams can be plotted for the real and imaginary eigenvalues versus the dynamic pressure, thereby displaying the damping σ (indicating the amplification) and the frequencies ω (indicating the oscillatory behaviour).

Given the fact that the problem can be simplified into a two-dimensional problem by using a typical section (and thus equivalent stiffnesses etc.), the low-frequency flutter analysis, by means of flutter diagrams, is accomplishable. To assess whether there are any flutter modes within the vicinity of the flight envelope, these diagrams can be compared with the various flight conditions from the performance analysis. Future projects dealing with a similar topic are advised to use the approach that is laid out in this appendix.